THE CONTROL OF NORMAL AND TUMOR CELL BEHAVIOR USING NOVEL MATERIALS

By

JIYEON LEE

A DISSERTATION PRESENTED TO THE GRADUATE SCHOOL
OF THE UNIVERSITY OF FLORIDA IN PARTIAL FULFILLMENT
OF THE REQUIREMENTS FOR THE DEGREE OF
DOCTOR OF PHILOSOPHY

UNIVERSITY OF FLORIDA

2010

To my dear husband, Choon, and my baby

ACKNOWLEDGMENTS

I acknowledge the support and guidance of my doctoral advisor, Dr. Tanmay Lele. He was helpful throughout my time at the University of Florida, encouraging me to study challenging research topics with the right path. I would like to thank my other doctoral committee members for their time and patience spent with me. I appreciate the material science knowledge Dr. Fan Ren has given me. In collaboration with his lab, I could study nanostructure for designing novel biomaterials. In addition, I must thank Dr. Peng Jiang and Dr. Stephen Pearton for their willingness to participate in my doctoral review process. I thank Dr. Yiider Tseng for the opportunity to serve as a teaching assistant and his helpful discussion of my research. I thank Dr. Richard Dickinson and Dr. Kirk Ziegler for their insightful viewpoints in my research. I appreciate Dr. Jason Weaver's help for allowing me to learn his lab work.

I greatly appreciate a valuable discussion with Dr. Shamik Sen and Dr. Sanjay Kumar in the Department of Bioengineering at University of California, Berkeley. Dr. Anand Gupte in the Department of Medicine at University of Florida, gave me an opportunity to study tumor cells which I am extremely grateful. Also, I must thank many colleagues working with me in Dr. Lele's lab. Dr. Hengyi xiao taught me many important lab procedures during my first days in the lab. TJ Chancellor, Bob Russell, and Jun Wu were always helpful to work together in the lab. Nicole Clarke was my co-worker in the lab and she was very helpful for me to perform the experiment. David Lovett was supportive during my last days in the lab. Additionally, I appreciate a great deal of support from Dr. Ren's group colleagues, Byung Hwan Chu and Dr. Byoung Sam Kang.

I thank my family for their support and understanding. My parents always encourage me with their constant trust. My sisters and brothers-in-law have always

helped me. I must thank my father-in-law and mother-in-law for their support to my husband and me during our stay in USA. I really appreciate patient understanding of my dear husband, Choon Jae Ryu. He has always inspired me and been helpful. With his broad knowledge of computer knowledge and mechanical engineering, he is also my good discussion partner. I thank him for his constant love and support. Lastly, I thank my precious baby.

TABLE OF CONTENTS

page

LIST OF TABLES

Table page

LIST OF FIGURES

Figure page

LIST OF ABBREVIATIONS

AFM	Atomic force microscopy
APS	Ammonium persulfate
APTMS	(3-aminopropyl)trimethoxysilane
BCE	Bovine capillary endothelial cell
BrdU	5-bromo-2-deoxyuridine
BS	Blebbistatin
CPD	Critical point drying
DAPI	4'-6-diamidino-2-phenylindole
DBS	Donor bovine serum
DMEM	Dulbecco/Vogt modified Eagle's minimal essential medium
ECM	Extracellular matrix
EthD-1	Ethidium homodimer-1
FBS	Fetal bovine serum
FCS	Fetal calf serum
FITC	Fluorescein isothiocyanate
FN	Fibronectin
FTIR	Fourier transform infrared spectroscopy
GAPDH	Glyceraldehyde-3-phosphate dehydrogenase
GFP	Green fluorescent protein
HCl	Hydrochloride
Het1A	Human esophageal epithelial cells
HUVEC	Human umbilical cord vein endothelial cells
LINC	Linker of nucleoskeleton to the cytoskeleton
MEM	Minimum essential medium eagle

MSC	Naïve mesenchymal stem cell
MSD	Mean square displacement
NaOH	Sodium hydroxide
NKHUVEC	Nesprin-1 knockdown siRNA transfected HUVEC
NMR	Nuclear magnetic resonance
PAAm	Polyacrylamide
PBS	Phosphate buffered saline
PCL	Poly(*ε*-caprolactone)
PCU	Poly(carbonate urethane)
PDMS	Poly(dimethyl)siloxane
PECVD	Plasma enhanced chemical vapor deposition
PR	Photoresist
PU	Pellethane
PVDF	Polyvinylidene fluoride
RGD	Arginine-Glycine-Aspartic acid
SD	Standard deviation
SDS	Sodium dodecyl sulfate
SEM	Scanning electron microscopy
SEM	Standard error of the mean
SHUVEC	Control smartpool siRNAs transfected HUVEC
SiO_2	Silicon dioxide
TBST	Tris buffered saline with Tween 20
TEM	Transmission electron microscopy
TEMED	Tetramethylethylenediamine
TiO_2	Titanium dioxide

TIRF	Total internal reflectance fluorescence
UV	Ultraviolet
ZnO	Zinc oxide

Abstract of Dissertation Presented to the Graduate School
of the University of Florida in Partial Fulfillment of the
Requirements for the Degree of Doctor of Philosophy

THE CONTROL OF NORMAL AND TUMOR CELL BEHAVIOR USING NOVEL MATERIALS

By

Jiyeon Lee

May 2010

Chair: Tanmay P. Lele
Major: Chemical Engineering

Cell interactions with nanostructured biomaterials are of broad interest because of applications in controlling tissue response to biomedical implants. In particular, mammalian cell adhesion to and proliferation on implanted devices is desirable for preventing the blockage of cardiovascular stents and tumor stents. Current methods to prevent stent blockage include coating with slow-release chemicals, but these have a finite lifetime requiring stent removal which causes clinical complications.

The potential of densely coated nanorod monolayers for controlling normal mammalian cell adhesion involved in cardiovascular stent blockage was first explored. Densely packed nanorods were fabricated with a solution-based technique. NIH 3T3 fibroblasts and vascular endothelial cells were unable to adhere on dense nanorods. Cells could not assemble focal adhesions, and were poorly spread. Cell survival in adherent cells was reduced by more than 100-fold on nanorods. This reduction was not due to changes in protein adsorption nor due to toxicity of unknown dissolving material into the solution.

The adhesion of tumor epithelial cells on nanorods was investigated. The morphology of tumor epithelial cells cultured on nanorods was rounded compared to flat surfaces and was associated with decreased cellular stiffness and non-muscle myosin II phosphorylation. Tumor cell number was decreased by nearly 50%, although proliferation and survival in adherent cells was unaltered. Single tumor cell motility was significantly increased on nanorods compared to flat surfaces coupled with a decrease in cell adhesion.

Collectively, the results appear to support a model in which nanorods interfere with integrin clustering at the nano-scale, preventing cell adhesion and spreading and resulting in decreased cell survival. Nanostructured surfaces may be a promising approach to decrease cell adhesion.

The role of nuclear-cytoskeletal connections in mediating cell mechanosensitivity was investigated. Endothelial cell adhesion and motility was found to be significantly perturbed in the absence of nesprin-1, a nuclear-cytoskeletal linker. Cells lacking nesprin-1 were observed to lose the ability to sense substrate rigidity. The results suggest a new role for nesprin-1 in mediating cell mechanosensing.

A new method for studying wound healing under realistic conditions *in vitro* was developed. The method involves creating defined patterns of damaged, necrotic cells with PDMS stamping. This novel assay permitted the quantification of wound healing rates in the presence of cell debris. Experimental results with this assay suggest that cell migration in the presence of cell debris is a two step process requiring migration and myosin dependent phagocytosis.

CHAPTER 1
INTRODUCTION

An important application of tailoring the surface of biomedical implants is preventing mammalian cell adhesion to the implant surface. An example of this is anti-fouling tumor stents. Tumor stents are used to prevent the collapse of gastrointestinal, pancreatic and biliary ducts that have tumors surgically removed from them. However, a persistent problem that interferes with normal stent function is the adhesion and growth of tumor cells on the stent surface [1, 2]. As the stent blockage increases morbidity and mortality in patients, there is a critical need for strategies for preventing tumor cell adhesion to the stent surface. Similarly, preventing macrophage adhesion to titanium surfaces is crucial for the success of bone prosthesis [3]. Platelet adhesion and subsequent clogging of cardiovascular stents is another problem that needs anti-fouling materials [4, 5].

Anchorage-dependent cells (typically involved in the blockage of stents) require adhesion to the solid extracellular matrix (ECM) for normal function [6-9]. The ECM consists of fibrous networks composed of proteins like fibronectin, laminin, vitronectin, collagen and elastin [10]. These structures provide physical and chemical signals at the nanometer length scale that control cell functions such as migration, proliferation, and apoptosis [8, 11, 12]. The ECM in the body can be mimicked *in vitro* by fabricating materials that present defined chemical and physical signals to the cell [13-17]. In particular, manipulating cell adhesion by fabricating material surfaces with nano-scale structures has emerged as a promising approach to control cell function both *in vivo* [18, 19] and *in vitro* [20-24]. Hence, fabricating biomedical implants with nanostructured

surfaces can allow the selective control of cellular interactions with the implant. The mechanisms of cell adhesion at the nano-scale to solid substrates are discussed below.

Cell-Substrate Adhesion

Cell adhesion to the solid substrate occurs through specific binding interactions between transmembrane receptors called integrins and their ligands (e.g. fibronectin, collagen, laminin and vitronectin) which are adsorbed on the substrate [25-27]. The integrin receptor is a heterodimer consisting of and subunits. In mammals, 18 subunits and 8 subunits have been so far discovered [28]. The different subunits make it possible to form different types of integrin heterodimers which bind selectively to specific ligands. Many integrin receptors recognize Arginine-Glycine-Aspartic acid (RGD) motifs which are present in ECM ligands such as fibronectin and vitronectin.

The ligation of integrin receptors causes a change in their conformation. This triggers the binding of cytoplasmic proteins such as talin to the cytoplasmic tails of integrins. Talin binding is thought to cross-link neighboring integrin receptors, giving rise to spatial clustering of ligated integrins [29]. The clustering of integrins causes the recruitment of several different types of proteins including enzymes like focal adhesion kinase and src kinase [30], adaptor molecules like paxillin [31] that are known to bind to several other proteins and α-actinin-1 [32], that directly link integrins and the actin cytoskeleton [27, 33]. The resulting multimolecular assembly of proteins is collectively called the focal adhesion. Focal adhesions measure roughly ~60 nanometers in thickness [34], and extend out a few square micrometers in the plane of the cell membrane (Figure 1-1). Tension generated through the action of the motor protein myosin as it walks along actin filaments is transmitted through connector proteins like α-

actinin to integrins, and hence to the substrate-adsorbed ligands [35-38]. This connection between tensed actomyosin filaments (that are crosslinked further into tensed structures called stress fibers, see Figure 1-1) and focal adhesion proteins allows a continuous mechanical link between the inside of the cell and the external substrate. In this manner, the focal adhesion establishes a physical path for mechanical force transfer between the cell and the substrate. Importantly, focal adhesions are not static structures but dynamic multi-molecular assemblies that start out as dot-like focal complexes at the leading edge of the motile cell, and eventually mature into focal adhesions [39-41].

In addition to acting as locations where cellular tensile forces are in balance with compressive forces in the substrate, focal adhesions are also signaling complexes. For example, integrin ligation can trigger signaling cascades that control gene expression, differentiation and apoptosis [42]. Interfering with focal adhesion assembly controls the degree of cell spreading, cell shape as well as cell fate [43]. In fact, control of focal adhesion assembly at the nano-scale is a key mechanism by which nanostructured surfaces control cell function.

Nanostructured Surfaces for Anti-fouling Applications

A class of nanostructures that have shown promise for reducing mammalian cell adhesion is a surface covered with upright nano-scale cylinders, variously referred to as nanorods, nanoposts and nanoislands [44-48] A recent paper showed that fibroblast numbers were reduced to approximately 30% on needle-like silicon nanoposts compared to the smooth substrate [44]. Cells on nanoposts extended filopodia structure along the sharp tips, and spread much less than cells on the smooth surface. The authors of this study also suggest that upright nanoposts may be useful as an anti-

fouling surface [44]. Other studies have demonstrated that nano-scale island structures can reduce cell adhesion [47-49]. These studies have showed that the dimension of the nanoisland plays an important role in modulating cell adhesion. Similarly, in osteoblasts, cell numbers on nanoislands with height 85 nm were reduced by ~80% compared to cells on the flat surface [49]. Aligned and densely packed carbon nanotubes have also been reported as an excellent anti-fouling surface toward platelet adhesion [4]. Few platelets could adhere on fluorinated poly(carbonate urethane) (PCU) treated carbon nanotubes (these are superhydrophobic films which potentially interfere with ECM protein adsorption). Moreover, activation of platelets was decreased by 50% on nanotubes.

The above studies offer strong support to the hypothesis that upright cylindrical structures with nano-scale dimensions can be used to decrease cell adhesion. The mechanisms of how this may occur at the molecular level are less clear. As discussed in the reported literatures [9, 17, 18, 50], altered matrix protein adsorption may be an important factor in determining cell response. Other possibilities include the disruption of the molecular processes that participate in cell adhesion to surfaces, such as clustering integrins (see Chapter 2).

This dissertation explores the potential of upright nanorods for achieving a significant reduction in cell adhesion. We show that nanorods covered surface can be used as effective anti-fouling surface (see Chapter 3 and Chapter 4) toward fibroblasts and vascular endothelial cells. We also show that the adhesion of malignant human tumor cells can be modulated with nanorod monolayers (see Chapter 5). We suggest that the decrease in adhesion is not due to altered protein adsorption, but rather due to

a disruption of integrin clustering at the nano-scale. Together, our results suggest a novel, promising approach that could be potentially used to prevent blockage of stents.

Organization of this Document

In Chapter 2, current literature on the nano-scale control of cell-substrate adhesion is reviewed. In Chapter 3, the potential of zinc oxide (ZnO) nanorods grown on substrates to reduce cell-substrate adhesion is investigated. Because of the potential toxicity of ZnO to some cell types, silicon dioxide (SiO_2) coated nanorods are investigated in Chapter 4. Finally, in Chapter 5, tumor cell interactions with SiO_2 coated nanorod surfaces are studied. In Chapter 6, the role of nuclear-cytoskeletal connections in mediating cell mechanosensitivity is explored. In Chapter 7, a new wound healing assay is presented to study coupled cell peeling and migration under realistic conditions *in vitro*.

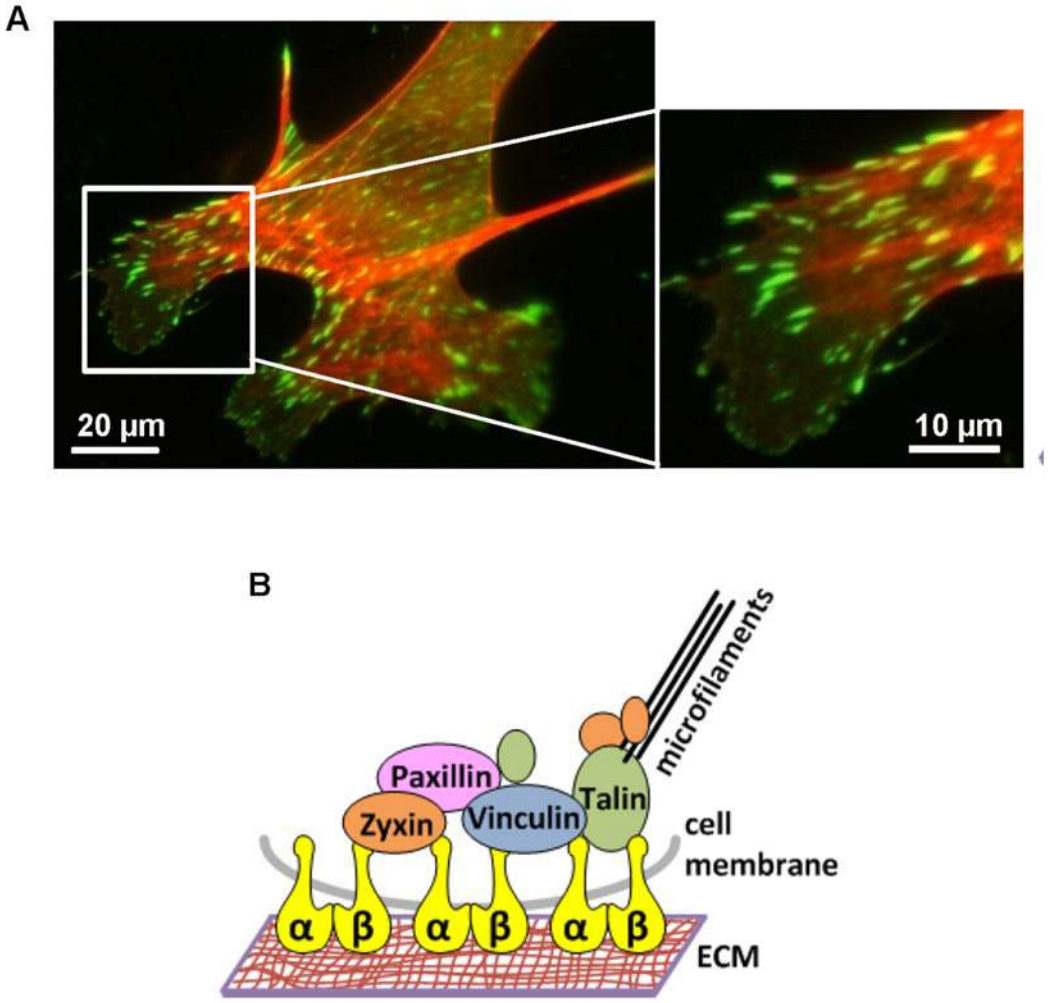

Figure 1-1. Cell-substrate adhesion. A) Fluorescent microscope image of a single bovine capillary endothelial cell cultured on a smooth glass substrate. Cell was stained for vinculin (green) and F-actin (red). Focal adhesions (green) are located at the tips of stress fibers (inset image). B) A simplified diagram of a focal adhesion that shows α and β integrins ligated to the ECM and intracellular proteins that link integrins to the cytoskeleton.

CHAPTER 2
NANO-SCALE CONTROL OF CELL-SUBSTRATE ADHESION

Introduction

At the nano-scale, cells have been found to be sensitive to a variety of surface topologies, include nanopits [51], nanoposts [52], nanocracks [53], nanotubes [54] and nanoislands [55]. While it is clear that cells are exquisitely sensitive to nanostructured surfaces, the molecular mechanisms that determine this sensitivity are less clear. This chapter focuses on current understanding of the mechanism of nano-scale control of cell-substrate adhesion.

Control of Cell Adhesion by Intermolecular Spacing

Evidence that focal adhesion assembly can be directly controlled at the nanometer scale has come from recent studies with gold nanodot arrays [8, 56-60]. The approach relies on fabricating ordered arrays of nanodots, each with diameter comparable to the size of a single integrin receptor (an integrin cylinder is ~ 160 Å long and ~ 20 Å in diameter [61], a head of an integrin is roughly 5.6~7.2 nm in diameter [62]) and the nanodots are 5~8 nm in diameter [56]. The nanodots are fabricated with dibock copolymer nanolithography, which allows precise control between nanodot spacing. An RGD peptide is conjugated to an organic molecule containing a thiol group that is bonded to the gold nanodot. Areas between the nanodots are passivated with adsorption of the linear poly(ethylene glycol) mPEG2000-urea polymer which prevents any protein adsorption from serum. Owing to the size of the nanodot (5~8 nm), only one RGD peptide is presented per nanodot, and only one integrin receptor can be conjugated per nanodot. Therefore, the systematic variation of nanodot spacing at the

nano-scale results in a control of the spacing between ligated integrins at the nano-scale.

This model system has been used to understand some key features of cell adhesion at the nano-scale. An important finding is that spacings larger than 70 nm cause a significant decrease in cell adhesion [56]. The number of attached osteoblasts on 73 nm nanodots was decreased by 80% compared with that on 28 nm nanodots. Cells were unable to assemble focal adhesions and stress fibers on 73 nm spaced nanodots. The dynamic turnover of focal adhesions was observed to be significantly higher on nanodots with spacing of 108 nm [59]. The levels of the adhesion protein paxillin were found to be significantly decreased, and stress fiber formation and cell adhesion were decreased on the nanodots with spacing 108 nm. These studies provide clear evidence that nano-scale presentation of ligands alters focal adhesion assembly. It is hypothesized [59] that forcing ligated integrins to be more than 70 nm apart potentially prevents crosslinking on the cytoplasmic side and prevents adequate coupling between the actomyosin cytoskeleton and the substrate. This results in decreased adhesive forces on the substrate, a lack of cell spreading and altered cell signaling.

The nano-scale topography of the surface can also profoundly control cell adhesion and cell migration, a process called contact guidance. The molecular mechanisms of how nanotopographical features alter cell adhesion are less clear. Multiple possibilities exist which are discussed below.

Protein Adsorption on Nanostructures

The ECM protein adsorption can be substantially different on nano-rough materials compared to smooth materials. Materials which are rough at the nano-scale display

large changes in their surface hydrophilicity or hydrophobicity [63], which can potentially influence not only the amount of matrix protein adsorption, but also the conformation of the adsorbed protein. Interestingly, nano-rough materials exhibit an increase in hydrophilicity if the corresponding smooth material is hydrophilic and an increase in hydrophobicity if the corresponding smooth material is hydrophobic [63-66].

Webster et al. [67] have shown that vitronectin adsorption is significantly enhanced on nano-scale alumina compared to conventional alumina. Vitronectin on nano-scale alumina was observed to be in a more unfolded structure, suggesting that binding motifs in the ligand may be more easily available on nano-scale alumina. The mechanism for increased vitronectin adsorption is less clear, but is attributable either to increased hydrophilicity of nano-scale alumina or increased adsorption of other molecules (such as calcium) that promote vitronectin adsorption [67]. The adsorption of fibronectin has similarly been shown to increase with increased nano-scale roughness on composites made of carbon nanotubes and PCU [68]. The increased adsorption was shown to correlate with increased surface energy of the nano-scale structures. Fibronectin adsorption has also been shown to increase on titanium surfaces with increasing roughness at the nano-scale which is attributable to increased surface energy [69].

Increasing hydrophobicity by creating nano-rough surfaces has been proposed as an approach to create anti-fouling protein surfaces [4, 70]. For example, Fe-Co-Ni metal alloy nanowires are more hydrophobic than the corresponding smooth surface [70]. Bovine serum albumin adsorption on these nanowires decreased significantly compared to the flat surface. Superhydrophobic surfaces have also been created by

grafting aligned carbon nanotubes with fluorinated PCU [4] and abnormal platelet adhesion to these structures has been attributed to altered protein adsorption.

While these studies clearly indicate the importance of protein adsorption in cell-nano-scale interactions, considerable more work remains to be done for obtaining a clear atomic-level understanding of how protein adsorption is influenced by nanostructure.

Alterations in Focal Adhesions Assembly by Nano-scale Topography

As discussed in Chapter 1, the assembly of focal adhesions and the transfer of intracellular tension to the nanostructured material can be altered by nano-scale presentation of ligand molecules. In a similar manner, nano-scale topography could alter the assembly of focal adhesions. It has been shown, for example, that epithelial cells align parallel along nano-scale ridges of width 70 nm created on silicon substrates [71]. Focal adhesions and stress fibers aligned parallel to the nano-scale ridges and the width of focal adhesions was observed to be controlled by the ridge width [71]. Interestingly, cell and focal adhesion alignment could be made perpendicular to the nano-scale ridges by changing soluble factors in the culture medium, indicating an interplay between soluble signaling pathways and adhesion assembly at the nano-scale [24]. Similarly, fibroblasts have been shown to align on the surface that presents nano-scale grooves [72, 73]. Alignment was observed only when the depth of patterns was over 35 nm and the ridge widths were bigger than 100 nm [72, 73].

Electrospun nanofibers have been examined for creating cell aligning scaffolds [74, 75]. Human schwann cells cultured on aligned poly(*ε*-caprolactone) (PCL) fibers had aligned nuclei and stress fibers along the fiber axes [74]. On random PCL fibers, cells were randomly oriented but still aligned along the random fiber axes. Similarly,

human ligament fibroblasts have been observed to align along electrospun pellethane (PU) nanofibers [75]. These results clearly show that nano-scale topography guides cell alignment and elongation.

Conclusions

Cells are sensitive to the nanostructure on the surface of the substrate. The mechanisms of how cells sense nanostructure are less clear. ECM ligands on a nano-rough material could influence the degree of integrin clustering by virtue of their three-dimensional presentation. This could feedback to regulate cell tension, cell shape and hence cell fate. Such effects in combination with altered matrix protein conformation or local surface concentration on nano-rough materials could alter adhesion assembly. Parsing out the degree to which these factors influence cell adhesion remains a formidable challenge, but it is the key to a clear understanding of cell sensing of nanostructure. Such understanding can greatly promote the rational design of nanostructured biomedical implants for applications such as the development of anti-fouling stents.

CHAPTER 3
THE CONTROL OF CELL ADHESION AND VIABILITY BY ZINC OXIDE NANORODS

Introduction

The success of implanted devices such as orthopedic implants, cardiovascular prosthesis and neural electrodes is affected by the ability of cells to interact with the exposed device material. Because properties such as surface topology are stable features of the surface, compared to chemical modifications which may be degraded over time, there has been immense interest in directing cell behavior by controlling the topology of materials [24, 52, 76-78]. Cells have been found to respond differently to smooth surfaces compared to materials with micro or nano-scale roughness in a cell type dependent manner [78-81].

One class of nano-structures that has received recent attention in the literature is a surface covered with upright slender cylinders, variously referred to as nanoposts, nanorods and nanocolumns [51, 52, 76, 82]. A recent study showed that cell numbers and proliferation in fibroblasts are greatly reduced on needle-like silicon nanoposts [52]. This study suggests that nanoposts may be useful as anti-fouling materials. Such surfaces could potentially be used for modulating the fibrotic response around implanted biomaterials.

We developed a strategy to reduce cell adhesion and survival on surfaces by culturing cells of three different cell types on a monolayer of upright ZnO nanorods of 50 nm diameter and 500 nm height in this chapter. A large number of nanorods were exposed to the cell (~ 60,000 to 150,000 per cell). Owing to the uniform distribution of the nanorod monolayer, the cells were not able to attach to any flat portion of the substrate. Our results indicate that initial adhesion, lamellipodia formation, dynamic cell

spreading and cell survival at 24 hours is greatly reduced on nanorod covered substrates in three different cell types.

Materials and Methods

Fabrication of ZnO Nanorods

ZnO nanorods were made by a solution-based hydrothermal growth method [83]. First, ZnO nanoparticles were prepared by mixing 10 mM zinc acetate dehydrate (Sigma Aldrich, St. Louis, MO) with 30 mM of sodium hydroxide (NaOH) (Sigma Aldrich, St. Louis, MO) at 58 ˚C for 2 h. Next, ZnO nanoparticles were spin-coated onto the substrate several times and then post-baked on a hot plate at 150˚C for better adhesion. The substrate with these ‘seeds’ was then suspended upside down in a Pyrex glass dish filled with an aqueous nutrient solution. The growth rate was approximately 1 µm per hour with 100 ml aqueous solution containing 20 mM zinc nitrate hexahydrate and 20 mM hexamethylenetriamine (Sigma Aldrich, St. Louis, MO). To arrest the nanorod growth, the substrates were removed from solution, rinsed with de-ionized water and dried in air at room temperature.

Preparation of Substrates for Cell Culture

For control substrate, we used 22 mm square glass cover slips (Corning, Inc., Lowell, MA) and ZnO flat substrates (Cermet Inc., Atlanta, GA). Before use, each substrate was sterilized with ultraviolet (UV) for 5 min and cleaned in 70% ethanol and de-ionized water. After drying substrates in air at room temperature, they were treated with 5 µg/ml human fibronectin (FN) (BD biosciences, Bedford, MA). After overnight incubation with FN at 4˚C, the substrates were washed twice with phosphate buffered saline (PBS). Cell suspensions of the same concentration and volume (i.e. same number of cells) were then seeded on each substrate.

Cell Culture and Adhesion

Cells of three different types were seeded on FN-coated substrates. NIH 3T3 fibroblasts were cultured in Dulbecco/Vogt modified Eagle's minimal essential medium (DMEM) (Mediatech, Inc., Herndon, VA) supplemented with 10% fetal bovine serum (FBS) (Hyclone, Logan, UT). Human umbilical cord vein endothelial cells (HUVECs) were cultured in EBM-2 Basal Medium and EGM-2 SingleQuot Kit (Lonza, Walkersville, MD). Bovine capillary endothelial cells (BCEs) were cultured in low-glucose DMEM supplemented with 10% fetal calf serum (FCS) (Hyclone, Logan, UT).

Immunostaining

After 24 hours of cell seeding, non-adherent cells were removed with two gentle washes with PBS. The samples were fixed with 4% paraformaldehyde for 20 min and washed several times with PBS. Fixed cells were immuno-stained for vinculin and stained for actin using our previously reported methods [84, 85]. Briefly, cells were fixed with 4% paraformaldehyde, permeabilized with 0.2% Triton X-100, and treated with mouse monoclonal anti-vinculin antibody (Sigma Aldrich, St. Louis, MO), followed by goat anti-mouse secondary antibody conjugated with Alexa Fluor 488 (Invitrogen, Eugene, OR). Actin was stained with phalloidin conjugated with Alexa Fluor 594 (Invitrogen, Eugene, OR). Cells were then imaged on a Nikon TE 2000 epifluorescence microscope using fluorescein isothiocyanate (FITC) and Texas Red filters. All images were collected using the NIS-Elements program (Nikon).

Cell Viability Assay

The live/dead viability/cytotoxicity kit for mammalian cells (Invitrogen, Eugene, OR) was used for quantifying adherent cell viability on each substrate. Cells were incubated at 30-45 minutes with calcein AM (2 μM for fibroblast, 5 μM for endothelial cells) and

ethidium homodimer-1 (EthD-1) (4 µM for fibroblast, 1.5 µM for endothelial cells) [86]. Next, epifluorescence images of five random fields were collected on a Nikon TE 2000 inverted microscope using a 10 X lens. The average number of cells adherent on each substrate, the number of adherent live cells (stained green with calcein AM) and adherent dead cells (stained red with EthD-1) were quantified from these images using the NIS-Elements program (Nikon). The experimental data was pooled and used for statistical comparisons using the Student's T-test.

Scanning Electron Microscopy (SEM)

Cells were prepared for SEM by fixation with 2% glutaraldehyde buffered in PBS and post-fixed in 1% osmium tetroxide. Samples were next dehydrated in graded ethanol concentrations. Critical point drying (CPD) was performed on a Bal-Tec 030 instrument (ICBR Electron Microscopy Core Lab, University of Florida) followed by e-beam metal deposition (Ti/Au, 10/50 Å). SEM was performed on a Hitachi S-4000 FE-SEM (ICBR Electron Microscopy Core Lab, University of Florida). Images of samples were taken at 1.8 -8.0 kX magnifications.

Time-Lapse Imaging

Cells which had been cultured as mentioned above were trypsinized and re-suspended in bicarbonate-free optically clear medium containing Hank's balanced salts (Sigma Aldrich, St. Louis, MO), L-glutamine (2.0 mM), 4-(2-hydroxyethyl)-1-piperazineethanesulfonic acid (HEPES) (20.0 mM), minimum essential medium eagle (MEM) and non-essential amino acids (Sigma Aldrich, St. Louis, MO), and 10% FCS [87]. Cells were passed onto FN-coated glass or ZnO nanorods, and phase contrast imaging performed overnight for 10 hours on the Nikon TE 2000 microscope. Images were collected every 1 minute, using a 20 X objective.

Results

Formation of Uniform ZnO Nanorod Monolayers

Shown in Figure 3-1A are SEM images of <001> vertically-aligned ZnO nanorod arrays. Such nanorods could be grown over areas on the order of 1 cm^2 and thus ZnO nanorods could be grown in uniform monolayers over very long distances compared to cellular length scales. The nanorods were approximately 50 nm in diameter, 500 nm in height and the density of nanorods was approximately 126 rods per square micron. Based on measured cell spreading areas, this number corresponds to approximately 60,000 nanorods per fibroblast and approximately 75,000-150,000 nanorods per endothelial cell.

Because of our focus on the effect of topology on cells, it was important to choose an appropriate control for statistically comparing effects of nanorods on cells. As the material itself can have effects on protein adsorption and cell adhesion, we chose a topologically smooth substrate made of ZnO, which is a thin film commercially available from Cermet Inc. An AFM image of this substrate is shown in Figure 3-1B. The flat substrate is smooth over long length scales with an average roughness of 1.33 nm. Interestingly, similar results were obtained for glass (average roughness of 1.34 nm, not shown), which allowed us to compare the performance of the ZnO flat substrate and ZnO nanorods with glass, a well-established substrate for cell culture.

Decreased Cell Spreading and Focal Adhesion Formation on ZnO Nanorods

We next investigated the influence of ZnO nanorods on cell spreading. Cells *in vitro* spread by assembling focal adhesions and stress fibers. Figure 3-2 shows fluorescence images of three different cell types- NIH 3T3s, HUVECs, and BCEs on glass, ZnO flat substrate, and ZnO nanorods. Cells on ZnO flat substrates and glass

cover slips assembled clear focal adhesions and stress fibers. Focal adhesions and stress fibers were not visible in cells on nanorods. The average area of cell spreading was decreased significantly on nanorods compared with ZnO flat substrates (a reduction of 60-70%, Table 3-1). These trends were observed in each of the three cell types.

Lack of Lamellipodia and Filopodia Formation on ZnO Nanorods

A recent study showed that cells on needle-like nanostructures only assemble filopodia [52]. To investigate this possibility for ZnO nanorods, we performed SEM studies on NIH 3T3 fibroblasts cultured on ZnO nanorods (Figure 3-4). Most cells on ZnO nanorods were rounded (Figure 3-4A). Instead of flat sheet-like lamellipodia, some cells formed thin processes (black arrow in Figure 3-4B) and thin filopodia-like structures (white arrows in Figure 3-4B) that appeared to attach to the ZnO nanorods. Therefore, while cells can attach to the ZnO nanorods using filopodia-like structures, they are not able to spread on the nanorods.

Decreased Initial Cell Spreading on ZnO Nanorods

In our studies, a large number of nanorods were exposed to cells. The results of Kim and co-workers showed that Si nanowires with diameter similar to our nanorods are engulfed by cells [82]. This raises the possibility that cells may spread initially on the nanorods but undergo apoptosis due to engulfment of nanorods at longer times. To clarify this, we performed time-lapse imaging for studying dynamic cell spreading on nanorods (Figure 3-5). After seeding, initial adhesion of HUVECs on glass occurred in the first hour (Figure 3-5A). Lamellipodia formation could be seen from 2 hours onward followed by complete spreading at approximately 5 hours (white arrows in Figure 3-5A). Conversely, on nanorods, little initial spreading occurred and cells remained rounded

over several hours (Figure 3-5B). No lamellipodia formation was visible. These results show that nanorods did not support initial cell spreading. While these results alone do not rule out long-term toxicity of nanorods due to engulfment, they provide evidence that cells are not able to initially spread on nanorods, which may contribute to decreased survival at long times.

Discussion

ZnO nanorods, nanowires, and nanotubes have attracted considerable attention for biosensing applications owing to their chemical stability, high specific surface area, and electrochemical activity [88-90]. ZnO nanoplaforms have been developed for highly sensitive and specific detection of biological samples [91, 92]. It is easy to control the aspect ratio and spacing of ZnO nanorods which is desirable for engineered materials [93]. However, before the promise of ZnO nanostructures for *in vivo* applications can be realized, it is crucial to prevent cell adhesion to these structures.

In this chapter, we found that the adhesion and viability of fibroblasts, umbilical vein endothelial cells, and capillary endothelial cells are greatly altered on ZnO nanorods. Cells adhered less and spread less on ZnO nanorods than the corresponding ZnO flat substrate. Scanning electron microscopy indicated that cells were not able to assemble lamellipodia on nanorods. Time-lapse phase contrast imaging showed that cells initially adherent to nanorods are unable to spread. This suggests that the lack of initial spreading on ZnO nanorods may cause cell death.

Our results indicate a lack of focal adhesion assembly in cells cultured on ZnO nanorods. The spacing between the ZnO nanorods is approximately 100 nm. Recent work by Arnold et al. showed that focal adhesion assembly requires that the spacing between ligated integrins be less than 70 nm [94]. Local integrin clustering probably can

occur on single nanorods as their diameter is on the order of 50 nm. However, focal adhesions extend over several microns. It is possible that integrin clustering does not occur over contiguous lengths of micron length scales, preventing focal adhesion assembly. Cells on nanorods also have no visible lamellipodia. As initial adhesion is required to polymerize actin filaments [95], the lack of lamellipodia is probably due to an inability of cells to establish strong initial adhesion to the substrate, thereby altering the dynamics of cell spreading. Our observations of altered cell spreading dynamics are consistent with observations by Cavalcanti-Adam et al. who observed similar behavior on RGD (Arginine-Glycine-Aspartic acid) nanopatterned substrates [59]. Our results can therefore be explained by a mechanism in which abnormal assembly of focal adhesions due to an inability to cluster integrins contributes to decreased cell spreading on nanorods. Because a lack of cell spreading can cause cell death in each of the cell types studied here [9, 17], decreased spreading may explain the observed decrease in cell survival on nanorods.

It is interesting to contrast our results with the work of Kim et al. [82]. They found that nanowires are engulfed by cells, but do not induce apoptosis. Because the nanowires were sparse in this study (20-30 nanowires exposed to each cell), it is likely that cells attach to the flat portions of the substrate and therefore survived. In our experiments, each cell was exposed to ~60,000 to 150,000 nanorods. Thus, we cannot rule out the possibility that a large number of nanorods are engulfed by our cells. If this is the case, then toxicity due to nanorod engulfment may cause cell death. Indeed, phagocytosed ZnO nanoparticles have been reported to be cytotoxic in vascular endothelial cells [96]. More detailed studies are needed to investigate this possibility. If

ZnO nanorods are engulfed by cells, then an interesting avenue for future investigation is the delivery of toxic material into cells. For example, the work by Kim et al showed that DNA immobilized on Si nanowires could be delivered into cells [88]. Thus, the efficiency of ZnO nanorods in preventing cell survival may be further enhanced by chemically conjugating toxins to the surface, and delivering these into the cell through penetration and subsequent cleavage.

The nanorod aspect ratio probably plays an important role in the observed response. For example, Curtis and coworkers do not report a large decrease in cell survival, although they also observed decreased cell spreading on nanoposts [88]. The diameter in these studies was 100 nm and the height was 160 nm. Curtis et al. report that nanocolumns are not engulfed by cells. As our aspect ratio is more similar to Kim and co-workers [82] where the nanowires were engulfed by cells, this could be another reason for the decreased cell survival in our experiments. Additionally, our observations of reduced cell adhesion and survival on nanorods are consistent with at least one recent study which employed an aspect ratio similar to the one used in this chapter [52].

Conclusions

Collectively, cell adhesion and viability were greatly decreased on ZnO nanorods. Our results indicate that ZnO nanorods can be used as an adhesion-resistant biomaterial capable of inducing death in anchorage-dependent cells. A better understanding of the mechanisms for the observed effects will be a key for designing optimal nanorod based substrates for minimizing cell adhesion and survival.

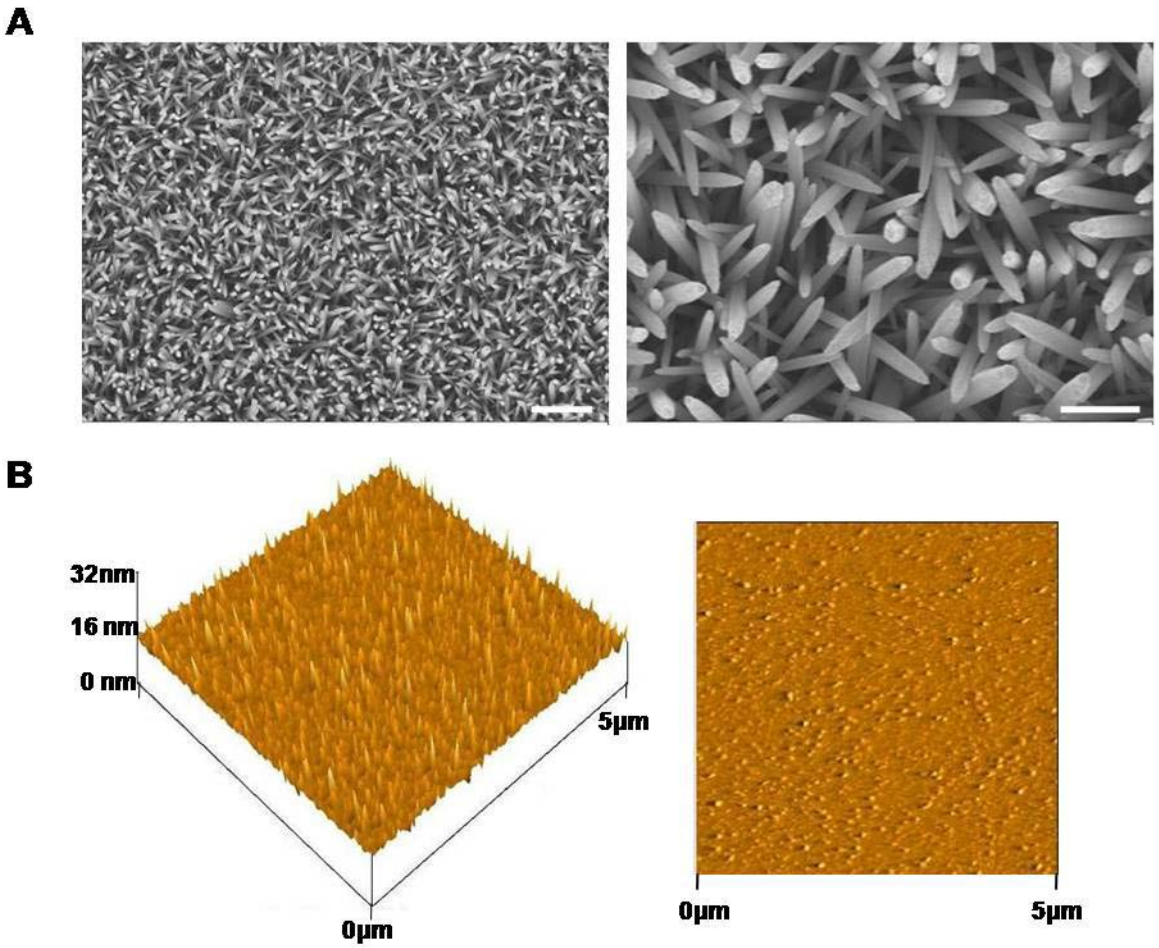

Figure 3-1. The morphology of ZnO nanorods and flat substrate. A) SEM images of ZnO nanorods indicating a uniform monolayer of ZnO (left, scale bar is 2 µm), and the upright growth of nanorods (right, scale bar is 500 nm). The diameter of nanorods was ~50 nm and the height was ~500 nm. B) AFM image of ZnO flat substrate. The surface roughness was approximately 1.33 nm indicating that this substrate is much smoother than the nanorods and can be used for comparisons of cell behavior between nanorods and smooth surfaces.

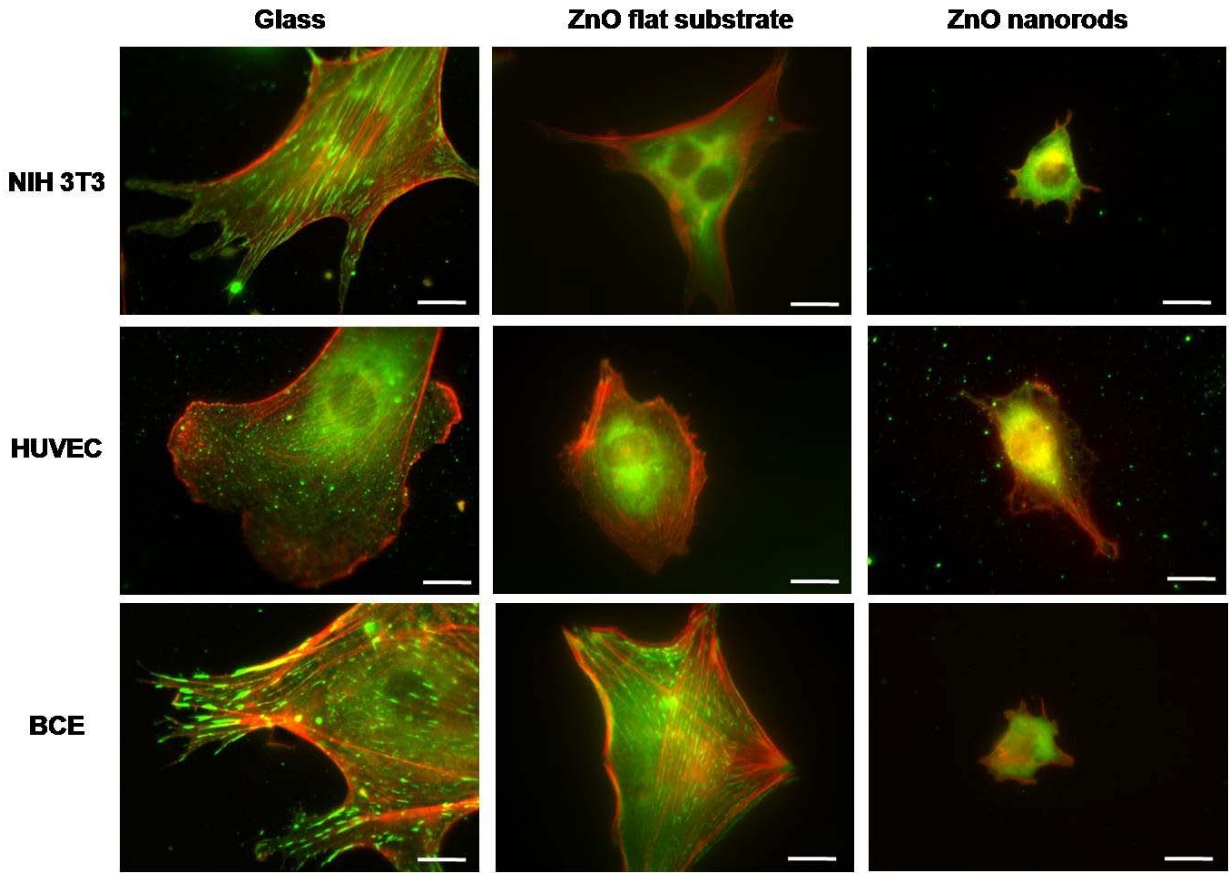

Figure 3-2. Cells do not assemble stress fibers or focal adhesions on nanorods. Fluorescent micrographs of NIH 3T3, HUVEC, and BCE cells stained for vinculin (green) and F-actin (red) on glass, ZnO flat substrate and ZnO nanorods. The cell spreading area is greatly reduced, and focal adhesions and stress fibers are not visible in cells cultured on the nanorods. Scale bar is 20 µm.

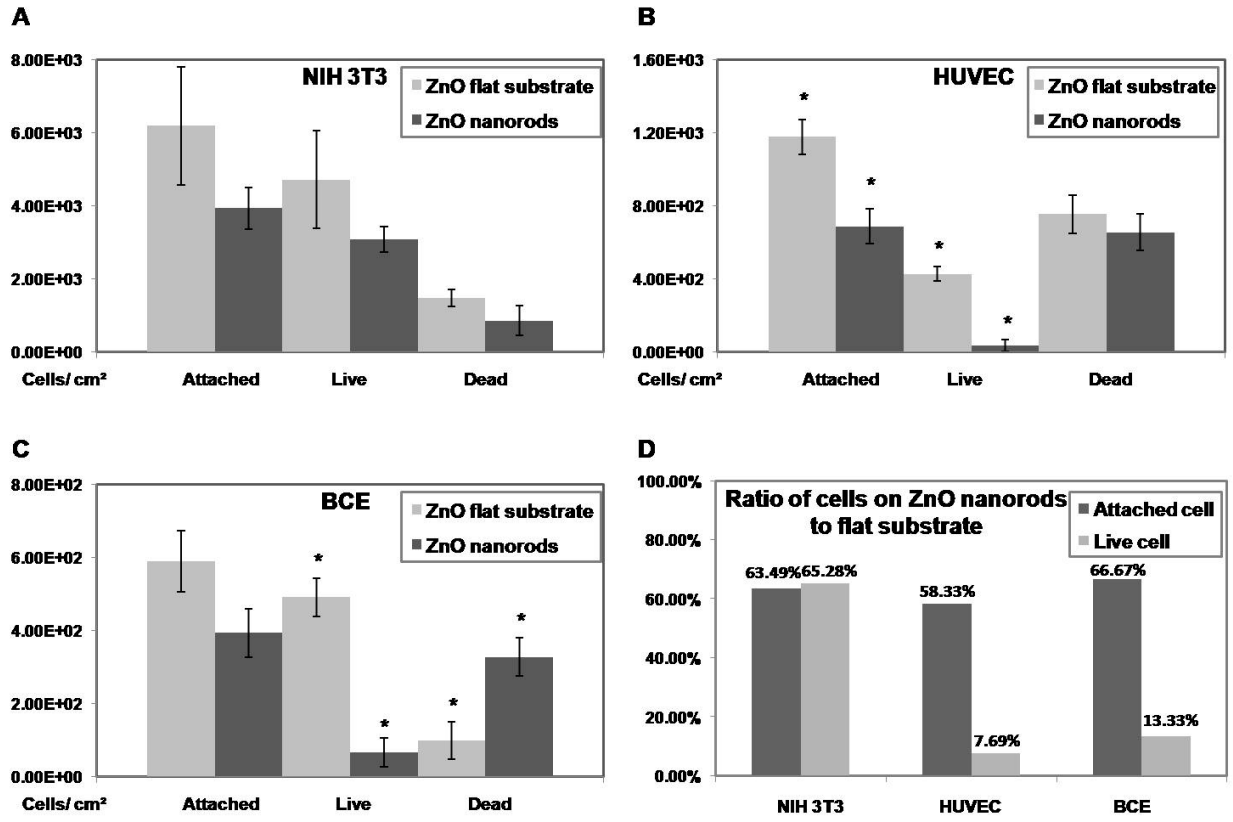

Figure 3-3. Total cell number and number of live adherent cells are reduced on nanorods. The average number of cells adherent on each substrate, the number of adherent live cells (stained with calcein AM) and adherent dead cells (stained with EthD-1) were quantified in three cell types A-C) by pooling data from five different images per cell type and condition. Bars indicate standard error of the mean (SEM). * indicates statistically significant differences with $p<0.01$ between the number of cells on ZnO nanorods and ZnO flat substrates ($n>50$ for HUVEC, $n>30$ for BCE, $n>300$ for fibroblasts, where n is total number of cells). D) The number of attached and live cells on ZnO nanorods normalized by the number of attached and live cells on ZnO flat substrates respectively. The results show that the ratio of attached cells on ZnO nanorods to that on ZnO flat substrates is approximately same for all three types of cells. The decrease in the number of live adherent cells on the nanorods is robust across three different cell types, with a larger effect demonstrated in endothelial cells (HUVEC, BCE) than fibroblasts (NIH 3T3).

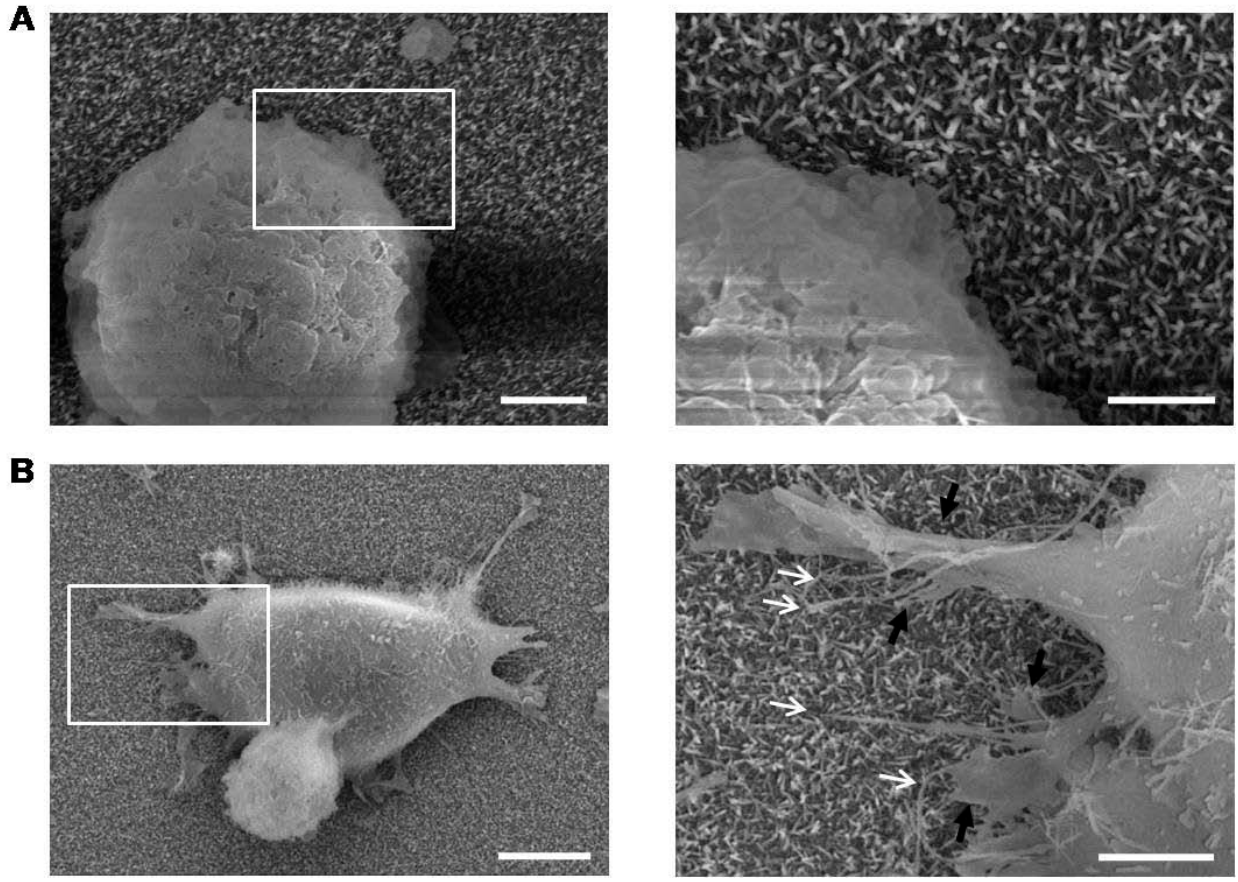

Figure 3-4. Cells cannot assemble lamellipodia on nanorods. Representative SEM images of NIH 3T3 fibroblasts on ZnO nanorods. A) Most of cells on ZnO nanorods were round and they did not form lamellipodia. Scale bars in left image and inset are 3 µm and 1 µm respectively. B) Filopodia-like structures were observed in some cells on nanorods (white arrows in inset) along with thin processes (black arrows). Scale bars in left image and inset are 5 µm and 2 µm respectively.

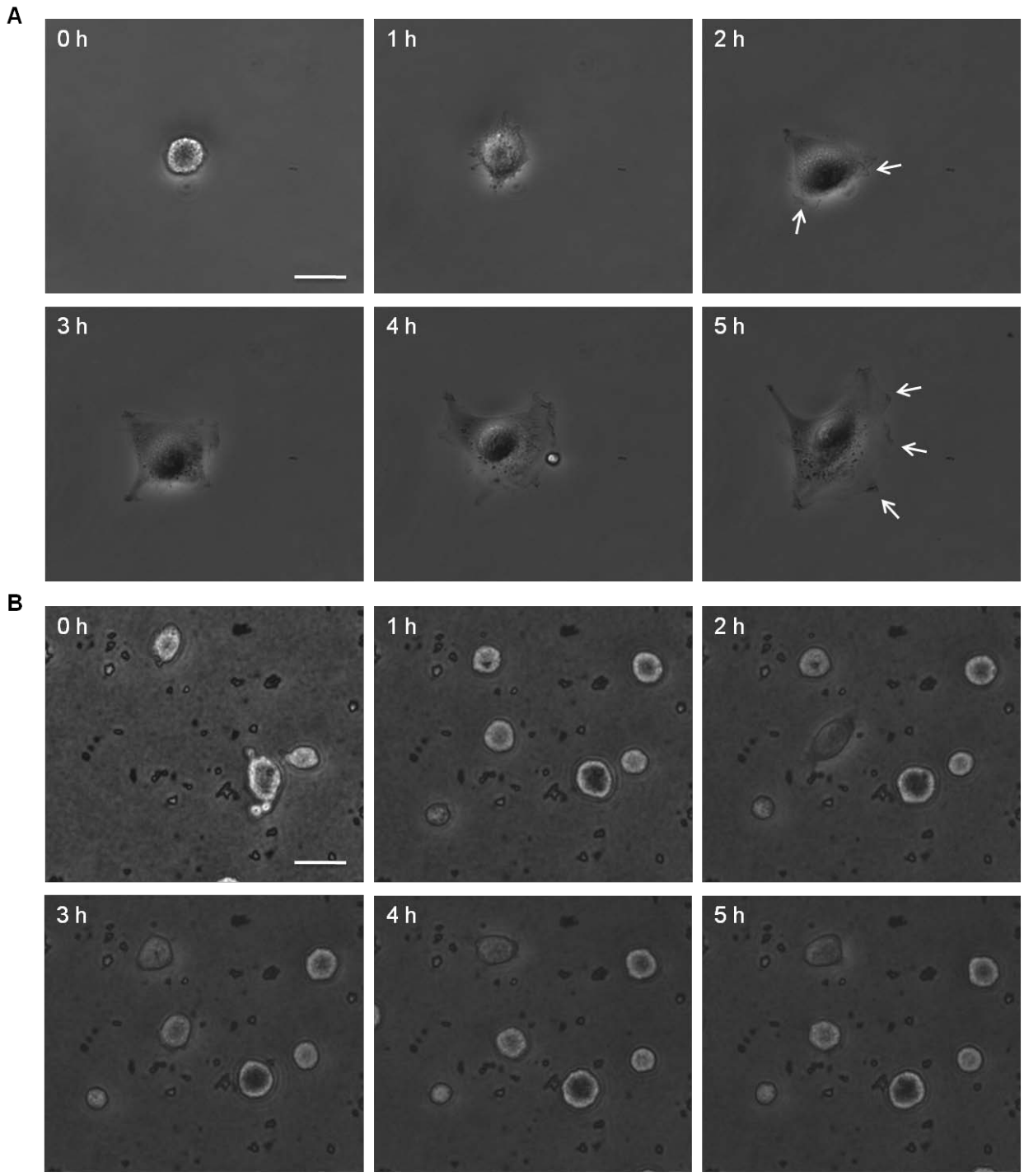

Figure 3-5. Dynamic cell spreading is altered on nanorods. Phase contrast imaging of HUVECs spreading on glass and ZnO nanorods. A) Cell spreading HUVECs is accompanied by lamellipodia formation (white arrows) and is complete in approximately five hours. B) Cells on nanorods do not spread, and do not develop any lamellipodia. Scale bar is 20 μm.

Table 3-1. Average area of cell spreading on ZnO flat substrate and ZnO nanorods.
(Average area ± Standard Error of the Mean (μm²))

Section name	NIH 3T3	HUVEC	BCE
ZnO flat substrate	(1.44E+03) ±(2.76E+02)	(1.73E+03) ±(2.35E+02)	(4.18E+03) ±(7.49E+02)
ZnO nanorods	(4.73E+02) ±(7.44E+01)	(6.02E+02) ±(6.94E+01)	(1.22E+03) ±(1.17E+02)

The differences of cell spreading area on ZnO flat substrate versus ZnO nanorods were statistically significant. (n=10, for NIH 3T3 and BCE, $p<0.005$ and for HUVEC $p<0.0005$)

CHAPTER 4
RANDOMLY ORIENTED, UPRIGHT SiO_2 COATED NANORODS FOR REDUCED ADHESION OF MAMMALIAN CELLS

Introduction

In the previous chapter, we have shown that endothelial cells and fibroblasts are unable to adhere and survive on ZnO nanorods compared to flat ZnO substrates. The advantage of ZnO nanorods is that they can be grown with solution based crystallization techniques at low temperature. Thus, the nanorods can be coated on surfaces of irregular geometries, and temperature sensitive materials such as stents. However, it is unclear if the dramatic decrease in cell adhesion and survival observed on ZnO nanorods is reproducible with similar nanorods but of a different material. The chemical nature of the nanorod surface is clearly important given that it can potentially influence protein adsorption. In addition, ZnO has the potential for having long-term toxicity to cells due to leaching into solution [97-99].

SiO_2 based nanowires and nanoneedles have received recent attention for modulating cell adhesion [44, 82]. Previous studies have shown that stem cells can survive for long periods of time on surfaces sparsely coated with SiO_2 nanowires [82]. Conversely, on comparatively denser SiO_2 nanoneedles, cell adhesion is decreased, suggesting their potential for anti-fouling surfaces [44]. However, the decrease in cell adhesion on nanoneedles was not observed to be as dramatic [44] as previously reported with ZnO nanorods (see Chapter 3).

Therefore, in this chapter, we explored if SiO_2 nanorods with similar morphologies as the previously used ZnO nanorods can result in a similar dramatic decrease in mammalian cell adhesion and survival. Our observations provide further evidence that

densely packed upright nanorods can be used to develop surfaces resistive to mammalian cell adhesion.

Materials and Methods

Fabrication of Nanorods

ZnO nanorods were made by a solution-based hydrothermal growth method [83]. First, ZnO nanocrystal seed solutions were prepared by mixing 15 mM zinc acetate dihydrate (Sigma Aldrich, St. Louis, MO) with 30 mM of NaOH (Sigma Aldrich, St. Louis, MO) at 60ºC for 2 h. Next, ZnO nanocrystals were spin-coated onto the substrate and then post-baked on a hot plate at 200ºC for better adhesion. The substrate with these seeds was then suspended upside down in a Pyrex glass dish filled with an aqueous nutrient solution. The growth rate was approximately 1 µm per hour with 100 ml aqueous solution containing 20 mM zinc nitrate hexahydrate and 20 mM hexamethylenetriamine (Sigma Aldrich, St. Louis, MO). To arrest the nanorod growth, the substrates were removed from solution, rinsed with de-ionized water and dried in air at room temperature. SiO_2 was deposited with a Unaxis 790 plasma enhanced chemical vapor deposition (PECVD) system at 50ºC using N_2O and 2% SiH_4 balanced by nitrogen as the precursors as reported before [100]. Patterned nanorods were fabricated by conventional photoresist (PR) lithography [83]. A glass cover slide was processed with negative PR (SU-8 2007, Microchem) so that a pattern with 50 micron circles was formed on the surface. The substrate was then post-baked at 110ºC for 30 min. The processed substrate was spin-coated with ZnO nanocrystals as seed materials and nanorods were grown on the substrate with an aqueous nutrient solution. The negative PR was removed by PG remover in a warm bath at 60ºC for 30 min.

Contact Angle Measurements

The contact angle of deionized water with surfaces was measured with a Ramé-Hart Goniometer and Ramé-Hart DROPimage Advanced Software using the sessile drop technique.

Cell Culture

For control substrate, we used 22 mm square glass cover slips (Corning, Inc., Lowell, MA). Before use, each substrate was sterilized with UV for 5 min and cleaned in 70% ethanol and de-ionized water. After drying substrates in air at room temperature, they were treated with 5 µg/ml human fibronectin (FN) (BD biosciences, Bedford, MA). After overnight incubation with FN at 4ºC, the substrates were washed twice with PBS. NIH 3T3 fibroblasts were cultured in DMEM (Mediatech, Inc., Herndon, VA) supplemented with 10% donor bovine serum (DBS) (Hyclone, Logan, UT). Human umbilical cord vein endothelial cells (HUVECs) were cultured in EBM-2 Basal Medium and EGM-2 Single Quot Kit (Lonza, Walkersville, MD). Cell suspensions of the same concentration and volume (i.e. same number of cells) were then seeded on each substrate.

Immunostaining and Cell Viability Assay

After 24 hours of cell seeding, non-adherent cells were removed with two gentle washes with PBS. The samples were fixed with 4% paraformaldehyde for 20 min and washed several times with PBS. Fixed cells were immuno-stained for vinculin and stained for actin and nucleus using our previously reported methods [46]. Briefly, cells were fixed with 4% paraformaldehyde, permeabilized with 0.2% Triton X-100, and treated with mouse monoclonal anti-vinculin antibody (Sigma Aldrich, St. Louis, MO), followed by goat anti-mouse secondary antibody conjugated with Alexa Fluor 488

(Invitrogen, Eugene, OR). Actin was stained with phalloidin conjugated with Alexa Fluor 594 (Invitrogen, Eugene, OR) and nucleus was stained with 4'-6-diamidino-2-phenylindole (DAPI) (Sigma Aldrich, St. Louis, MO). Cells were then imaged on a Nikon TE 2000 epifluorescence microscope using green fluorescent protein (GFP), Texas Red and DAPI filters. All images were collected using the NIS-Elements program (Nikon).

The live/dead viability/cytotoxicity kit for mammalian cells (Invitrogen, Eugene, OR) was used for quantifying adherent cell viability on each substrate. Cells were incubated at 30-45 minutes with calcein AM (2 µM for fibroblast and 4 µM for endothelial cells) and ethidium homodimer-1 (EthD-1) (4 µM for all types of the cells). Next, epifluorescence images of six to ten random fields were collected on a Nikon TE 2000 inverted microscope using a 10 X lens for NIH 3T3 and HUVEC. The average number of cells adherent on each substrate, the number of adherent live cells (stained green with calcein AM) and adherent dead cells (stained red with EthD-1) were quantified from these images using the NIS-Elements program (Nikon). Three independent experiments of cell viability were performed and the data were pooled. The average area of cell spreading was determined from three independent experiments with statistical comparison using the Student's T-test.

Time-Lapse Imaging

Cells were pre-cultured on the patterned nanorods for 24 hours as mentioned above. Before taking a movie, non-adherent cells were removed with two gentle washes with PBS and new media was added to the dish. Phase contrast imaging was performed for 6 hours on the Nikon TE 2000 microscope with humidified incubator (In Vivo Scientific, St. Louis, MO). Images were collected every 5 minutes using a 10 X objective.

Protein Adsorption on Nanorods and Glass

Sterilized SiO_2 coated nanorod and glass substrates were prepared as outlined above. Both of the substrates were incubated with 10 μg/ml rhodamine fibronection (Cytoskeleton, CO) diluted in PBS overnight, and these dishes were washed with PBS several times. Five randomly taken 20 X fluorescent images were collected with identical illumination and exposure time, and the fluorescent intensity was analyzed by the NIS-Element program (Nikon).

Results and Discussion

Fabrication of SiO_2 Coated Nanorods

Many biomedical implants are made of temperature-sensitive materials such as plastic. Hence, it is necessary to grow nanorods with techniques that do not require high temperature. Densely packed ZnO nanorods were fabricated with a low-temperature (95ºC) hydrothermal, solution-based growth method [83]. We next deposited nano-thin films of SiO_2 with controlled thickness, 50 Å, using PECVD at 50 ºC according to our previously published methods [100]. Transmission electron microscopy (TEM) images of the resulting nanorods with 50 Å thickness of SiO_2 nano-films deposited are shown in Figure 4-1A. The nanorods were randomly oriented in the upright direction, approximately 40~50 nm in diameter, 500 nm in height. The average spacing between nanorods was approximately 80 to 100 nm (Figure 4-1B, white arrows). Importantly, the SiO_2 coatings were deposited uniformly on each nanorod free of any local defects, which was confirmed with TEM, local electrical conductance measurements, chemical wet-etching and photoluminescence intensity measurements [100]. Our technique thus resulted in randomly oriented, upright SiO_2 deposited nanorods that cover the surface

with densely packed monolayers without any defects over cm length scales (Figure 4-1C).

Decreased Cell Adhesion on SiO_2 Coated Nanorods

As mentioned in Chapter 1 and Chapter 2, cell adhesion and spreading occurs by the ligation of trans-membrane integrins to ligands (such as fibronectin) immobilized on the surface. This is followed by clustering of the integrins at the nano-scale, and subsequent formation of multi-protein, micron-scale assemblies called focal adhesions [101]. Focal adhesions allow force transfer from the contractile acto-myosin cytoskeleton inside the cell to the outside surface, and this allows cells to adhere to and spread on the surface. If focal adhesions are not allowed to assemble in cells that depend on anchorage for survival, this leads to weak attachment to the surface, lack of cell spreading and subsequent apoptosis [9, 17]. Therefore, the assembly of focal adhesions was next studied using immunofluorescence microscopy.

Human umbilical vein endothelial cells (HUVECs) and NIH 3T3 fibroblasts were cultured on SiO_2 nanorods which were pre-incubated with fibronectin overnight. Cells were fixed with paraformaldehyde and stained for vinculin, actin stress fibers and the nucleus. Both HUVECs and NIH 3T3 fibroblasts assembled vinculin-labeled focal adhesions on glass (Figure 4-2). On the nanorod-coated surfaces, focal adhesions were not visible and cells were rounded and poorly spread (Figure 4-2). Cells on nanorods were also unable to assemble contractile stress fibers. Consequently, the average area of cell spreading on nanorods was significantly decreased (Figure 4-3) with a lack of focal adhesion and stress fiber formation. This result suggests that cells are unable to spread and assemble focal adhesions on nanorods, which may cause apoptosis in these adhesion-dependent cells [9, 17].

Protein Adsorption on Nanorods

Recent work by Spatz and co-workers showed that focal adhesion assembly requires the spacing between ligated integrins to be less than 70 nm [8, 56]. A spacing of more than 73 nm between ligated integrins limits attachment, spreading, and actin stress fiber formation in fibroblasts. As the diameter of the SiO_2 nanorods is approximately 40~50 nm, local integrin clustering may occur but to a very limited extent given the vertical nature and small length (500 nm) of the nanorods. Due to the spacing of 80~100 nm, integrin clustering may not occur over multiple nanorods, preventing the assembly of contiguous focal adhesions on the micron length scale (Figure 4-2).

Other possible explanations for the fact that cells cannot spread on nanorods are the super-hydrophobic nature of nanostructured surfaces such as ZnO nanorods [4, 102]. Protein adsorption is decreased on super-hydrophobic surfaces which potentially can explain decreased adhesion. To address this question, we first measured contact angles of SiO_2 coated nanorods and compared the contact angle with glass. We found that SiO_2 coated nanorods were hydrophilic (Figure 4-4: contact angle of 6.93+/-1.27^o compared to glass of 42.1+/-1.14^o). As fibronectin is known to adsorb successfully on hydrophilic surfaces [103], this result suggests that reduced matrix protein adsorption is likely not the reason for decreased adhesion.

To confirm this, we next measured the extent of fibronectin adsorption on nanorods (Figure 4-5). Rhodamine-labeled fibronectin was deposited overnight on SiO_2 coated nanorods and flat glass substrates. Fluorescent images of the rhodamine fibronectin adsorbed surface were captured and analyzed for differences in intensity. Interestingly, we found that fibronectin adsorption as measured by fluorescence intensity was increased two-fold on SiO_2 coated nanorods compared to glass. An

increase in protein adsorption is to be expected given the increased surface area of the nanorods. The increase in fibronectin adsorption argues against large decreases in protein adsorption as being responsible for the observed reduction in cell adhesion. Importantly, fibronectin is known to adsorb in an active conformation on hydrophilic surfaces [103]. Given that all our experiments were carried out in 10% serum which allows the adsorption of other matrix proteins on the hydrophilic surface, and also promotes the secretion of fibronectin by the cells themselves, it is unlikely that decreased or abnormal matrix protein adsorption plays a significant role in the observed response.

Spatial Patterning of Cell Adhesion with Nanorods

To investigate if it is feasible to pattern cell adhesion with nanorods, we spatially patterned nanorods using a low-temperature, and patterned growth method [83]. This method results in patterned nanorods that are not present inside circles, and are present outside in dense monolayers (Figure 4-6). The diameter of circles was 50 μm and spacing between the circles was 40~60 μm. Nanorods were 50 nm in diameter and 500 nm in height. Similar patterning was also observed with ZnO nanorods without SiO_2 coating (Figure 4-8). Moreover, while the cells were confined to the circular regions on average, cells were frequently able to migrate from circle to circle by spanning the intervening nanorods (Figure 4-9). This result suggests that spatially patterned nanorods provide a new way of dynamically patterning cells and therefore creating complex tissues.

Decreased Cell Survival on Nanorods

The number of cells adherent on SiO_2 coated nanorods was significantly reduced (a reduction of 98% in fibroblasts, 82% in HUVECs) compared to cells on glass (Figure

4-10A) after 24 hour culture. Next, a live/dead viability/cytotoxicity kit for mammalian cells was used for quantifying adherent cell viability. The decrease in viability in cells on nanorods compared to that on glass was dramatic (Figure 4-10B) with only one or two cells surviving on the SiO_2 nanorods for every 100 viable cells on glass. By culturing cells on glass in media that was incubated for 1 day, 3 days and 7 days with the nanorods, we confirmed that the cell death was not due to toxicity of unknown dissolving material from the nanorods (Figure 4-11). Therefore, these results suggest that densely packed nanorods have excellent anti-fouling potential by virtue of their topology.

Conclusions

In this chapter, we showed that cell adhesion was significantly decreased on SiO_2 coated nanorods. None of the cells were able to assemble vinculin-marked focal adhesions. When cultured on a patterned surface where flat circular areas were surrounded by nanorods, cells were able to migrate to adjacent flat areas by spanning the nanorods. Taken together, the results of this chapter indicated again that nanorods can be an anti-fouling surface to reduce anchorage cell adhesion as shown in Chapter3. Regardless of material composition of nanorods or protein adsorption, topology of nanorods plays an important role for reducing cell adhesion.

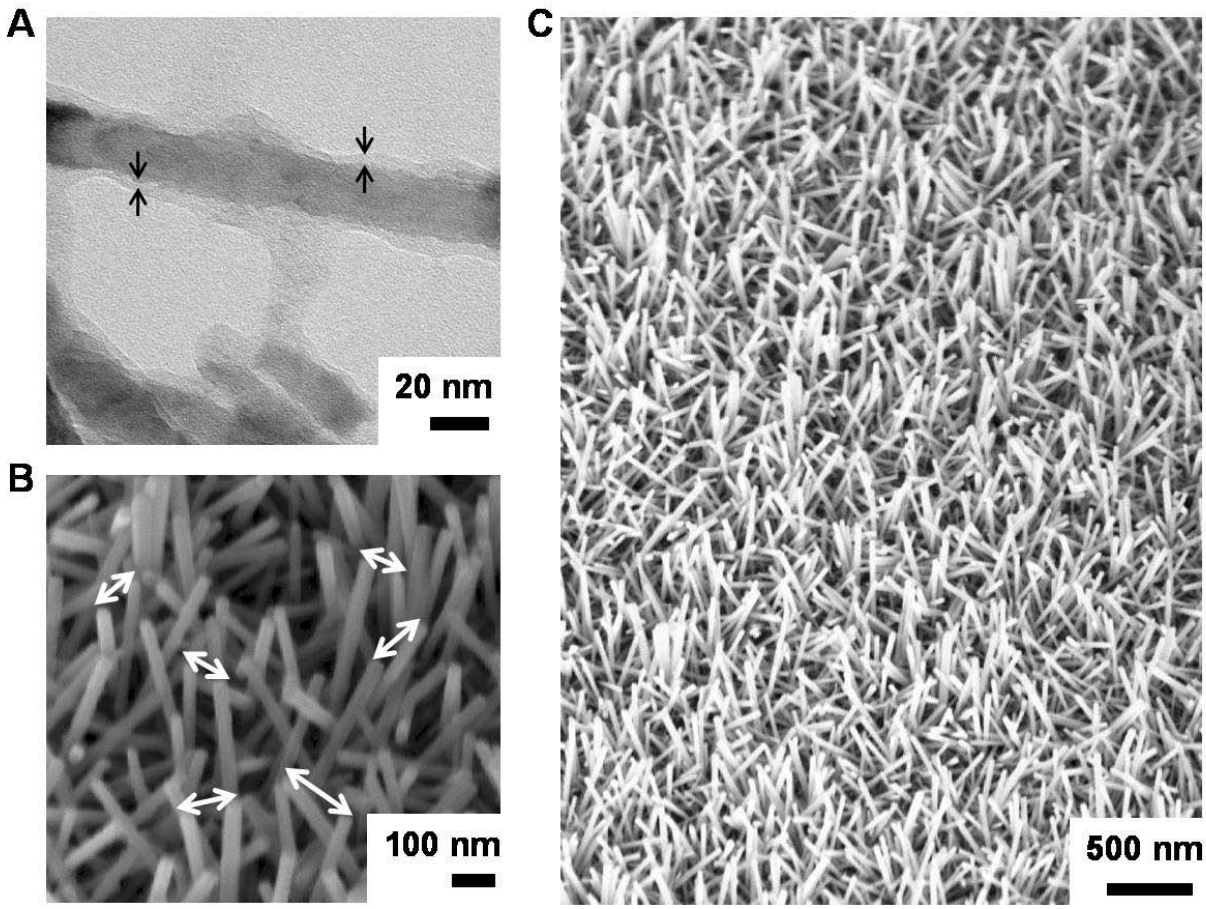

Figure 4-1. The morphology of nanorods. A) TEM image of SiO_2 deposited ZnO nanorods. Black arrows indicate SiO_2 thin film with a 50 Å thickness. ZnO nanorods are encapsulated by SiO_2. B) SEM image of nanorods on glass. White arrows indicate the spacing between nanorods. The spacing between nanorods ranges from 80 to 100 nm. C) SEM image of a monolayer of nanorods. Upright nanorods were covered on the underlying glass substrate uniformly.

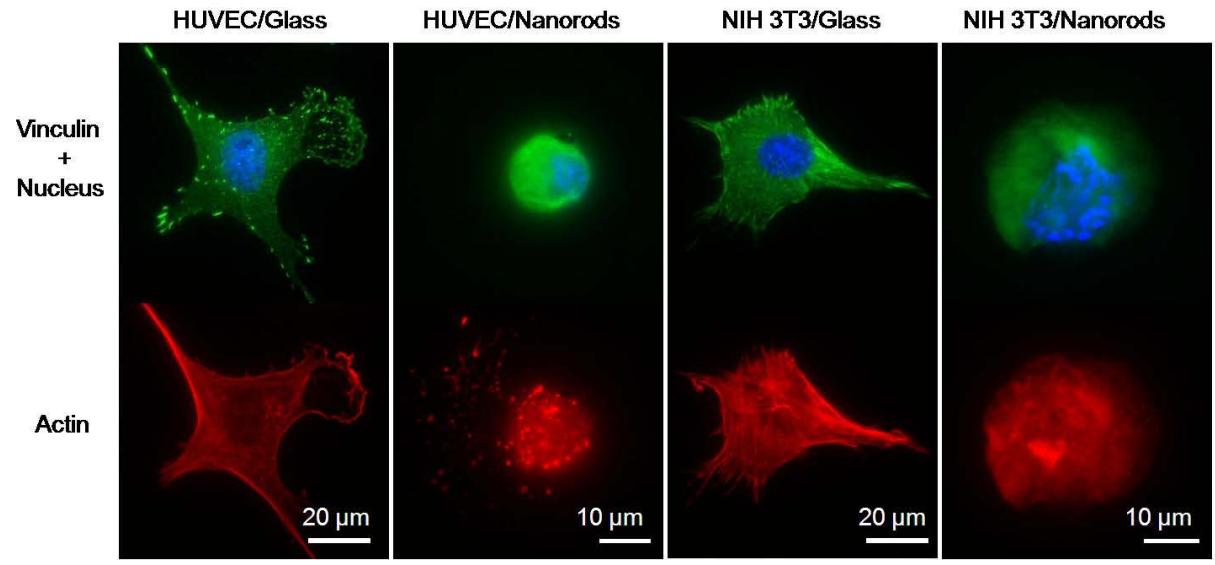

Figure 4-2. Fluorescent microscopic images of HUVEC and NIH 3T3 on glass and nanorods. HUVEC and NIH 3T3 on glass assemble focal adhesions stained with vinculin (green) and actin stress fibers (red). Nuclei were stained with DAPI (blue). HUVEC and NIH 3T3 on nanorods are unable to spread and assemble focal adhesions and stress fibers.

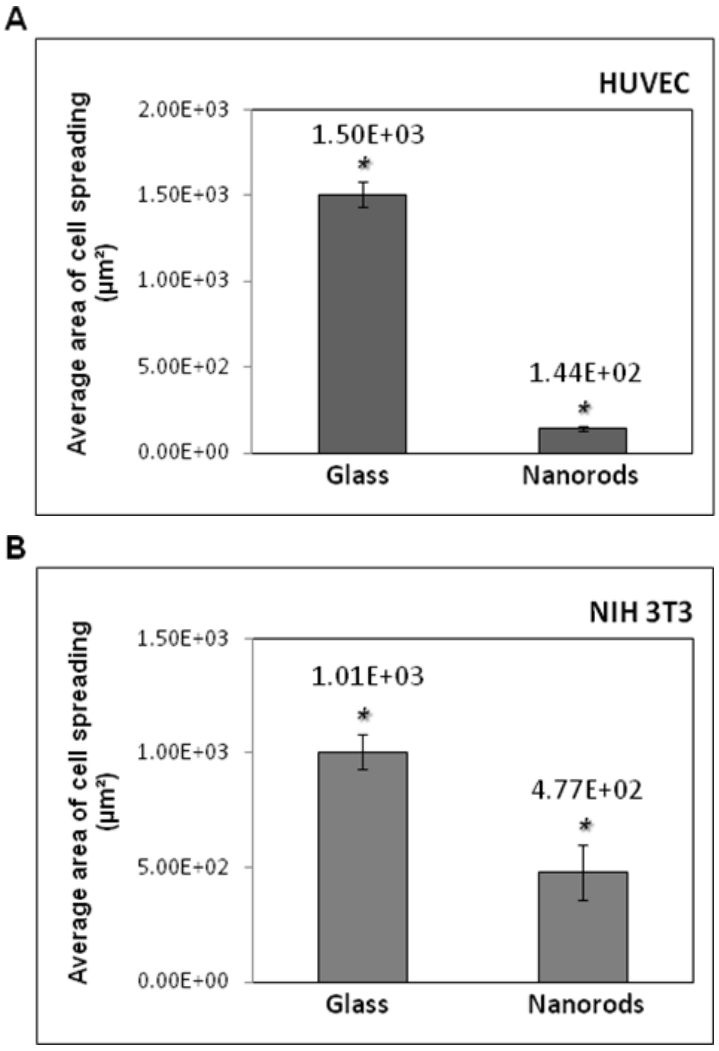

Figure 4-3. The average area of cell spreading on glass and nanorods. A) HUVEC on glass and nanorods (n > 170). B) NIH 3T3 on glass and nanorods (n > 110). * indicates $p < 0.005$. Bar indicates standard error of the mean (SEM). The data were pooled from three independent experiments.

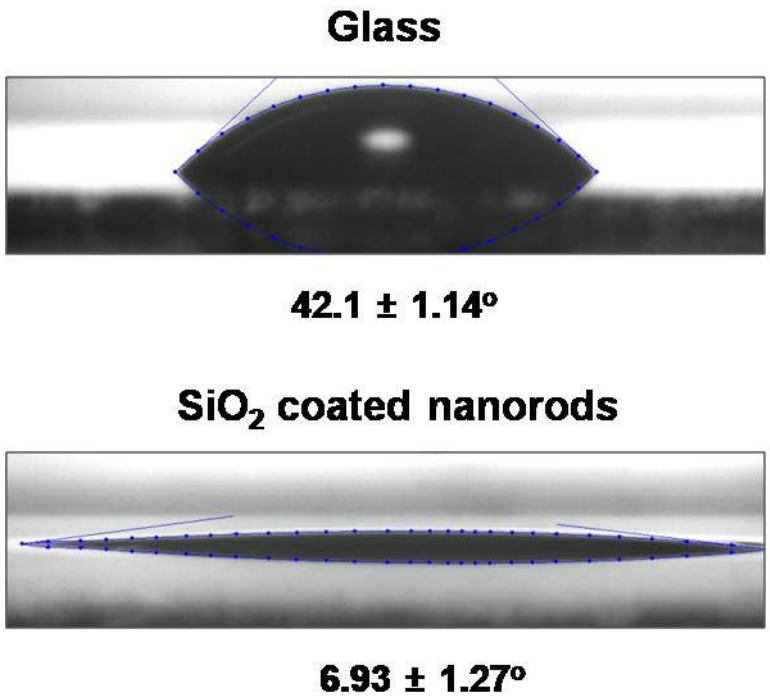

Figure 4-4. Contact angles of water on glass and SiO_2 coated nanorods.

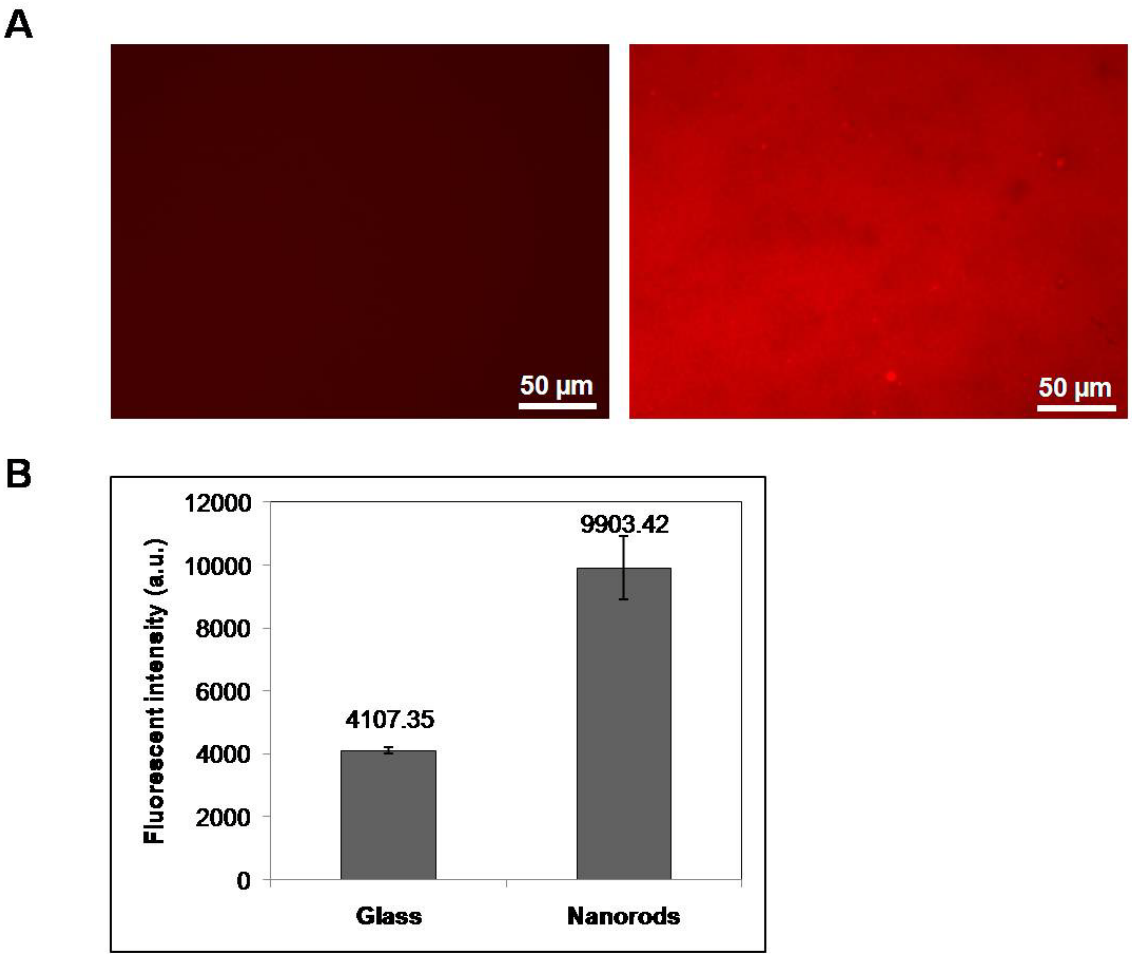

Figure 4-5. Fluorescent images and intensity of rhodamine fibronectin coated glass and nanorods. A) Representative fluorescent images of rhodamine fibronectin on glass and SiO_2 coated nanorods. B) Plots show the average intensity profile pooled from five randomly taken images. Bar indicates the standard deviation (SD).

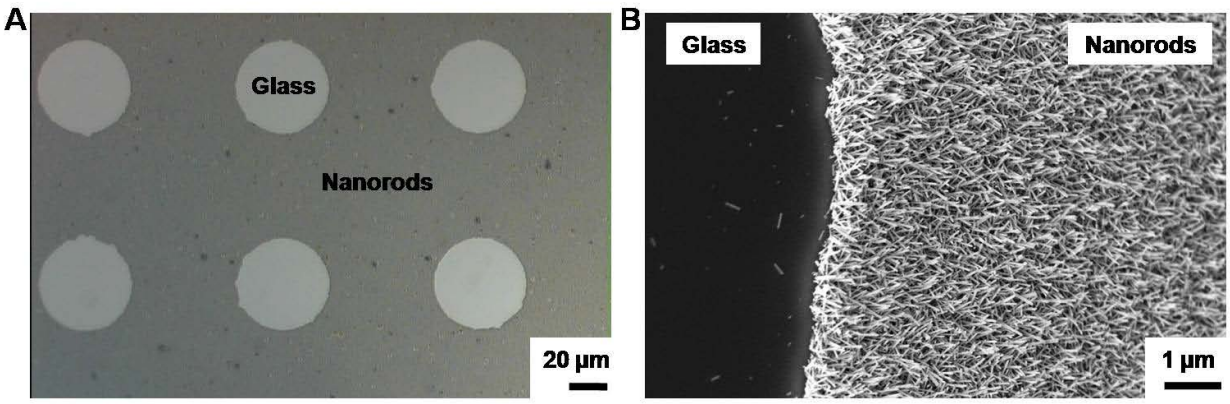

Figure 4-6. SEM images of patterned nanorods. A) Optical microscope image with 400 X objective. B) SEM image.

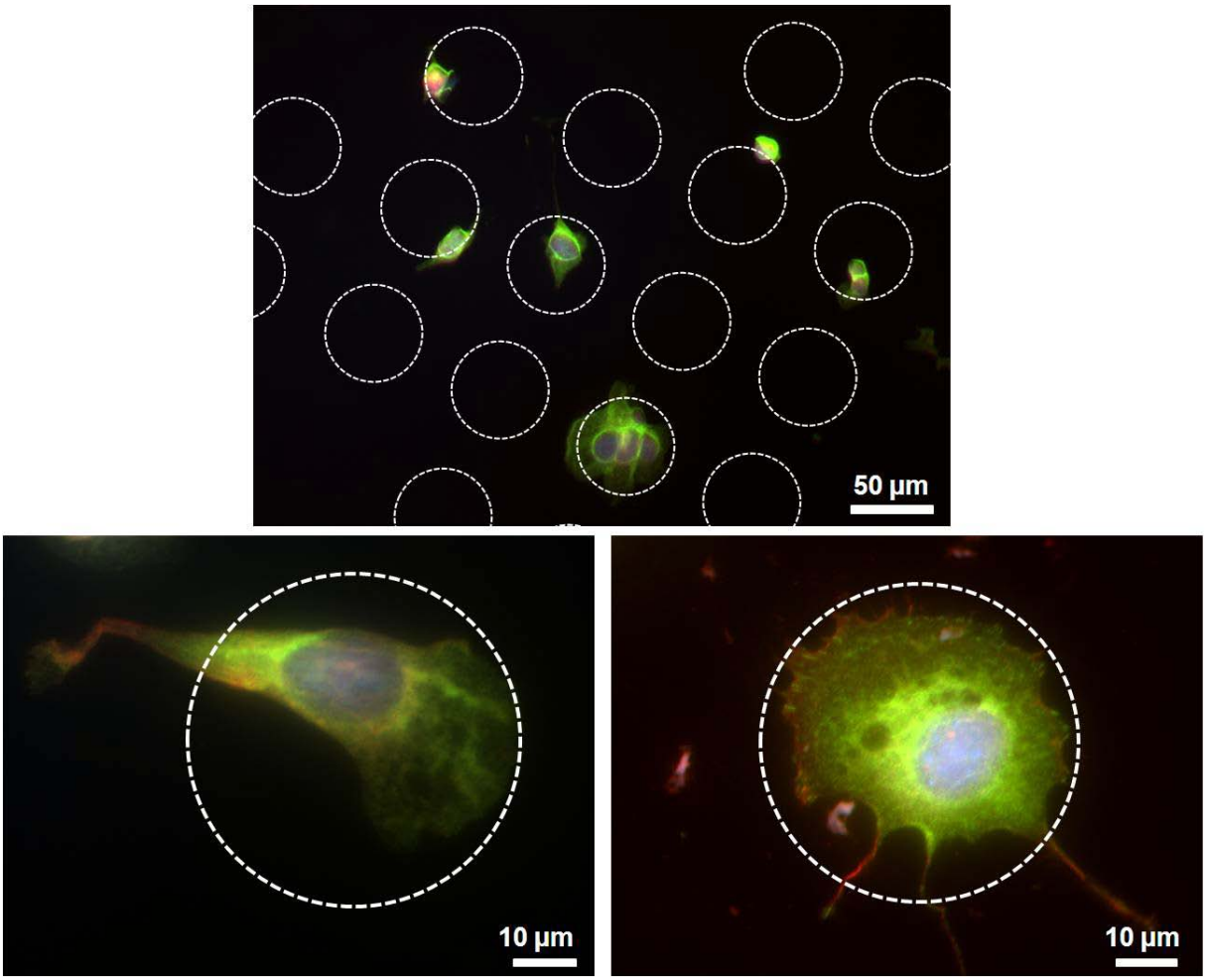

Figure 4-7. NIH 3T3 fibroblasts on patterned SiO_2 coated nanorods. Fluorescent microscopic images showing that NIH 3T3 fibroblasts preferably attached on glass. Cells are stained for actin (red), vinculin (green) and nucleus (blue). Cells were confined on the flat circular regions. Dashed lines indicate the edge of patterns.

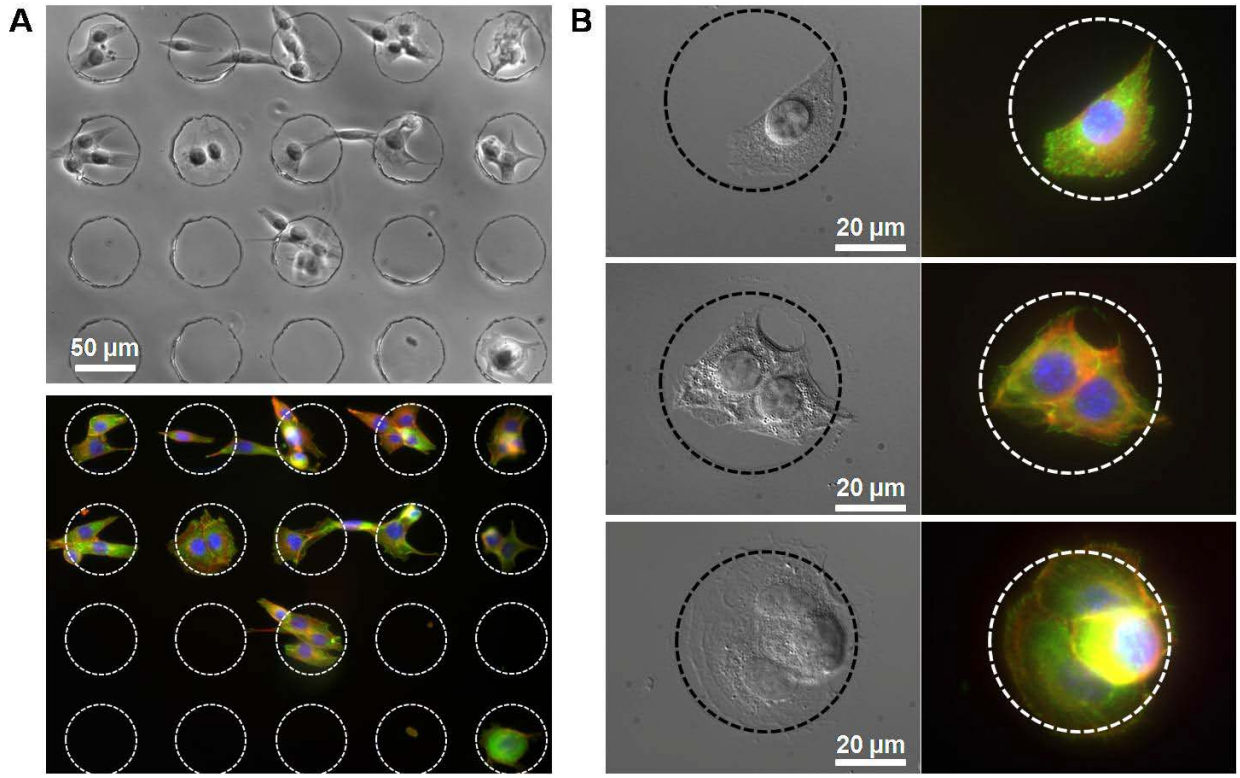

Figure 4-8. NIH 3T3 fibroblasts on patterned ZnO nanorods. A) Phase contrast and fluorescent microscopic images showing that NIH 3T3 fibroblasts preferably attached on glass. Cells are stained for actin (red), vinculin (green) and nucleus (blue). B) Differential interference contrast and fluorescent microscope images. Cells were confined on the flat circular regions. Dashed lines indicate the edge of patterns.

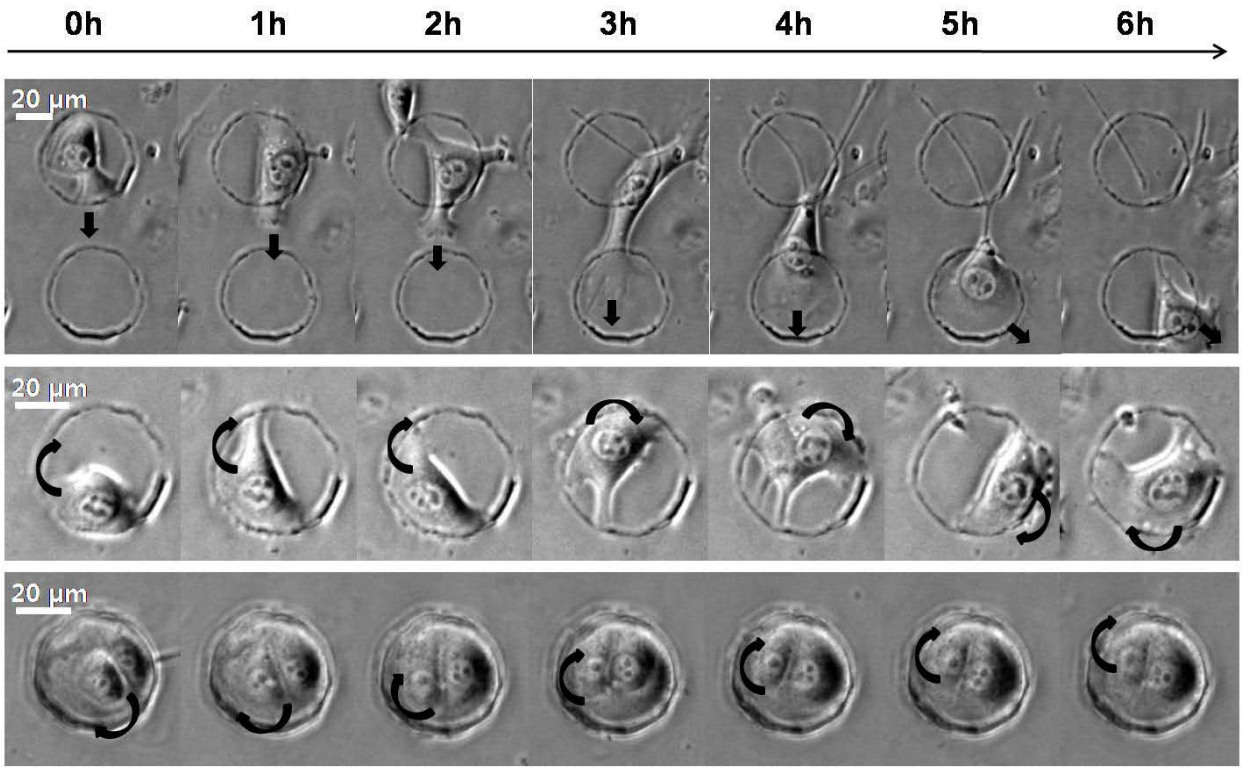

Figure 4-9. Time-lapse phase microscope images of NIH 3T3 on patterned ZnO nanorods. Black arrows indicate the direction of cell motility. Cells are observed to move from glass to glass by spanning intervening nanorods (top panel), or continuously explore the nanorod environment at the edges of the circle (middle and bottom panel). Arrows indicate direction of motion.

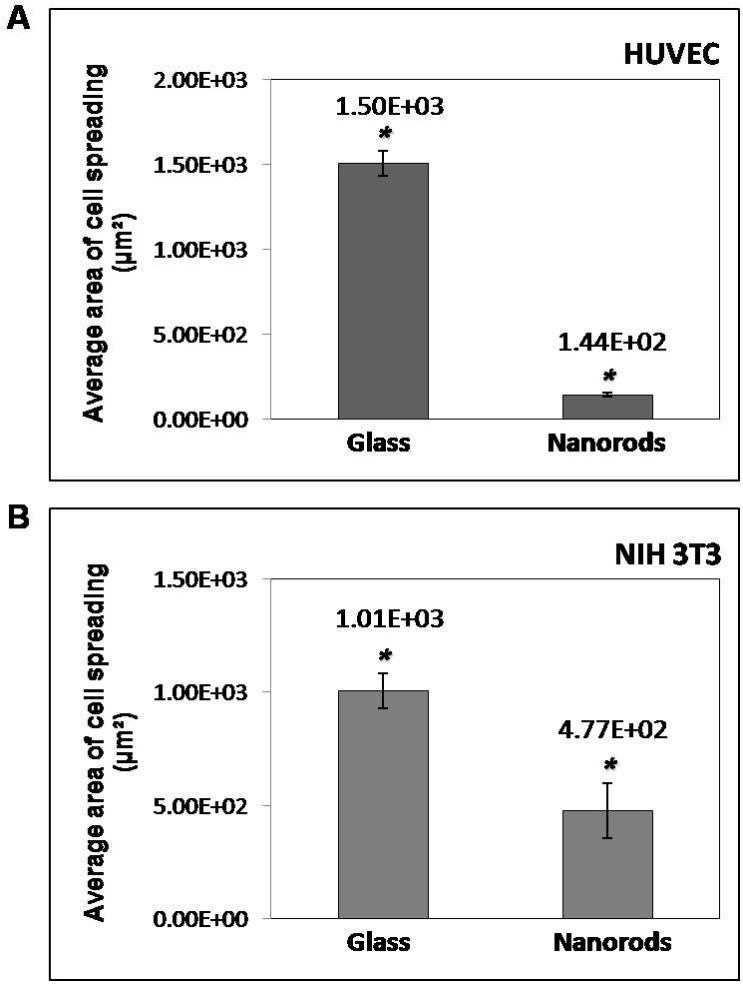

Figure 4-10. Cell attachment and viability on nanorods. A) The ratio of the number of attached cells on nanorods to that on glass. B) The ratio of the number of live cells on nanorods to that on glass. (n > 2500 for HUVECs, n > 1500 for NIH 3T3. Bar indicates SEM. Cells are considerably reduced in numbers on nanorods.

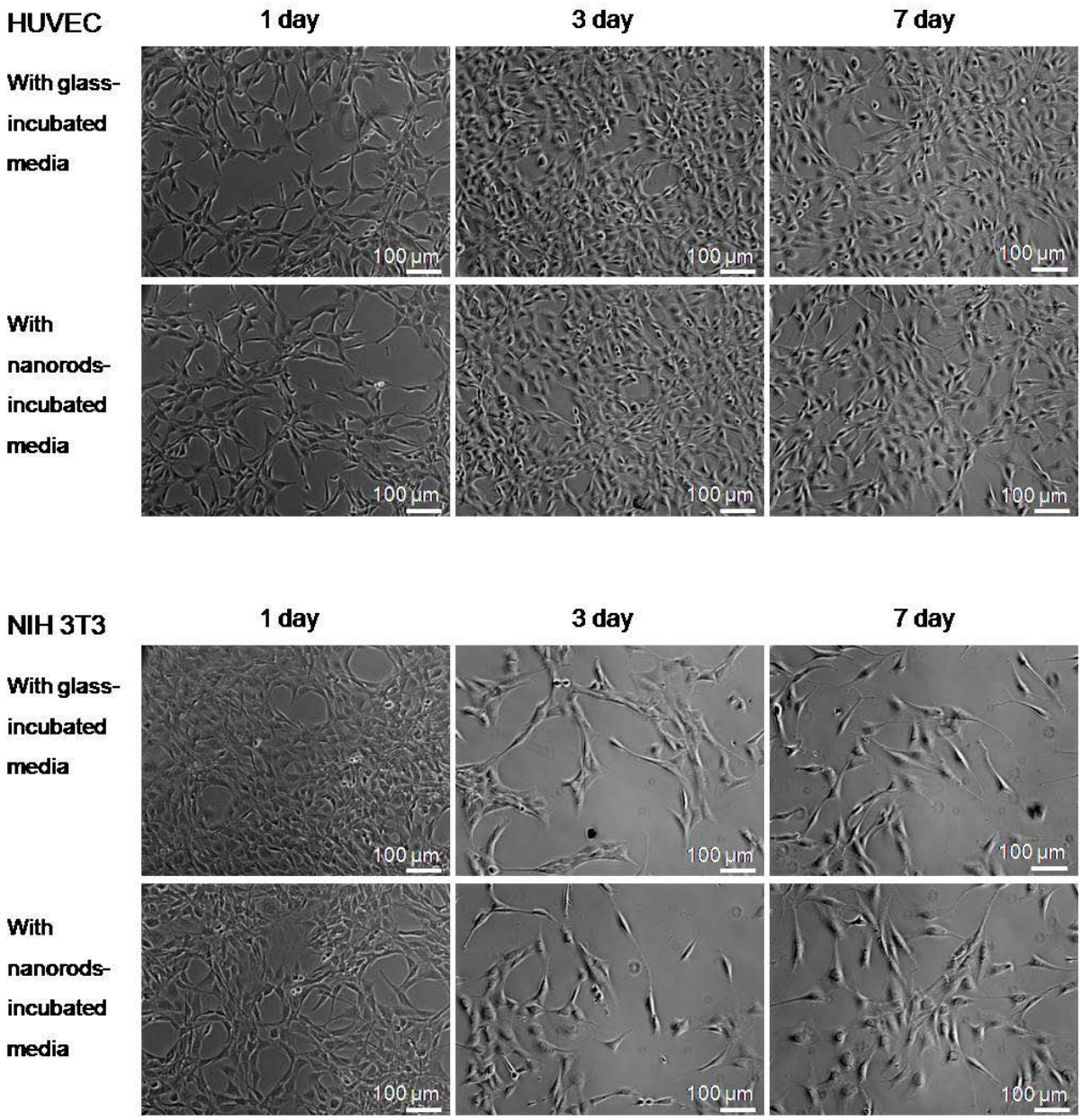

Figure 4-11. Material toxicity test. Media incubated with nanorods (or pure glass) for 1 day, 3 days, and 7 days was added to cells. Cells were cultured in the nanorod treated media for one day. No obvious differences in cell numbers or morphology were observed when cultured with nanorod treated media. This argues against solution toxicity as being responsible for cell death on nanorods day incubated media with nanorods and glass were added to 1 day pre-cultured HUVEC and NIH 3T3 dishes.

CHAPTER 5
MODULATING MALIGNANT EPITHELIAL TUMOR CELL ADHESION, MIGRATION AND MECHANICS WITH NANOROD SURFACES

Introduction

Tumors that occlude the gastrointestinal, pancreatic and biliary ducts are typically surgically removed, and metallic stents are placed in the ducts for preventing subsequent collapse of the injured tissue [1, 104]. However, tumor cell adhesion, migration and proliferation on the installed stents cause stent re-blockage. This requires further surgical interventions for stent removal and causes severe complications in the management of malignancy [105]. To overcome such recurrent problems with metallic stents, plastic-covered stents have been developed [2, 106, 107]. However, plastic-covered stents tend to migrate to other organs [104, 108] and have poor performance compared to metallic stents [108, 109]. Thus, combining the advantages of metal stents with prevention of tumor cell adhesion to the stent surface remains a key challenge [2, 105-109].

One approach to reduce the blockage of stents is to fabricate nanostructured features on the cell surface that will interfere with tumor cell adhesion. A number of studies have shown that cell adhesion [44, 56, 110], assembly [111], and migration [21] are sensitive to the micro- and nano-scale topography of the culture substrate [112]. These studies have been carried out for cells of non-tumor origin, but there are relatively few studies on tumor cell interactions with nanostructured materials. One study showed that the spreading and proliferation of human osteosarcoma cells decreases on micro-grid titatium coated silicon surfaces with increasing surface roughness [113]. Similarly, the adherent human hepatocellular carcinoma cell number on a silicon nanowire surface was decreased by 60.5% compared to a bare silicon

wafer [114]. These studies support the promise of using structured surfaces for controlling tumor cell adhesion.

We recently reported that coating surfaces with dense monolayers of randomly oriented, upright nanorods significantly reduces adhesion and viability of fibroblasts and endothelial cells [45]. Cells on nanorods were unable to assemble focal adhesions and stress fibers, which we hypothesized to be due to disruption of integrin clustering on nanorod substrates [45]. However, it is unclear if a similar approach can be used to modulate the adhesion and viability of tumor cells responsible for stent occlusion.

In this chapter, we investigated the effect of nanorod coatings on the adhesion, motility, and mechanics of malignant, human esophageal epithelial cells. Malignant tumor cells cultured on nanoroad-coated surfaces had significantly decreased non-muscle myosin II activity, decreased stiffness and increased motility. The lack of firm adhesion correlated with an overall decrease in tumor cell number.

Materials and Methods

Growth of Nanorods

A solution-based hydrothermal growth method was used for fabricating ZnO nanorods on the substrates [83]. Briefly, ZnO nanocrystal seed solutions composed with 15 mM zinc acetate dihydrate (Sigma Aldrich, St. Louis, MO) and 30 mM of NaOH (Sigma Aldrich, St. Louis, MO) were prepared at 60ºC for 2 h and spin-coated onto the substrates. Nanorods were grown by placing seed-coated substrates upside down in an aqueous nutrient solution of 20 mM zinc nitrate hexahydrate and 20 mM hexamethylenetriamine (Sigma Aldrich, St. Louis, MO). A Unaxis 790 plasma enhanced chemical vapor deposition (PECVD) system was used to deposit SiO_2 on the ZnO

nanorods at 50ºC using N_2O and 2% SiH_4 balanced by nitrogen as the precursors as reported before [100].

Cell Culture

22 mm square glass cover slips (Corning, Inc., Lowell, MA) were used as control substrates. All of the substrates were sterilized with UV for 5 min, and washed with 70% ethanol and de-ionized water. Before cell culture, the substrates were treated with 5 µg/ml human fibronectin (FN) (BD biosciences, Bedford, MA) at 4ºC overnight. OE33 (human esophageal epithelial tumor cells) cells were cultured in RPMI supplemented with 10% donor bovine serum (DBS) and 200 mM L-Glutamine (Sigma, St. Louis, MO).

Cell Viability Assay

Cells cultured for 24 hours on each substrate were stained with the live/dead viability/cytotoxicity kit for mammalian cells (Invitrogen, Eugene, OR) for quantifying adherent cell viability. The number of OE33 on glass and nanorods was counted from ten fluorescent images taken randomly using a 20 X objective. Three independent experiments of cell viability were performed and the data were pooled. To check for solution toxicity of nanorods, OE33 media was incubated with sterilized nanorods or with glass for 1 day, 3 days and 7 days in incubator. The conditioned media was next used to culture cells for 24 hours. Cell morphology and numbers with nanorod-incubated media was compared to that with glass-incubated media.

BrdU Staining

10 µM 5-bromo-2-deoxyuridine (BrdU) (Sigma Aldrich, St. Louis, MO) was added to cells on glass and nanorods [115]. After 20 hours of incubation, cells were fixed with 4% paraformaldehyde for 20 min and washed several times with PBS. 2 M hydrochloride (HCl) was added to the cells and incubated for 20 min at room

temperature. Cells were permeabilized with 0.2% Triton X-100 supplemented with bovine serum albumin. Cells were stained with primary anti-BrdU IgG (Sigma Aldrich, St. Louis, MO) and goat anti-mouse secondary antibody conjugated with Alexa Fluor 488 (Invitrogen, Eugene, OR). The number of attached and proliferated cells on glass and nanorods was counted with ten randomly taken images using a 20X objective. Three independent experiments were performed, and the data were pooled. A similar fixation and staining protocol was followed for immunostaining of adhesion proteins [45, 46].

Scanning Electron Microscopy (SEM)

After 24 hours of culture, cells were prepared for SEM by fixation with 2% glutaraldehyde buffered in PBS and post-fixed in 1% osmium tetroxide and dehydrated in graded ethanol concentrations. Critical point drying (CPD) was performed on a Bal-Tec 030 instrument (ICBR Electron Microscopy Core Lab, University of Florida) and Au/Pd (50 Å) was deposited on the substrate. SEM was performed on a Hitachi S-4000 FE-SEM (ICBR Electron Microscopy Core Lab, University of Florida). Images of samples were taken at 1.0 -2.0 kX magnifications.

Cell Motility Assay

Phase contrast imaging was performed for 12 hours on a Nikon TE 2000 microscope with a humidified incubator (In Vivo Scientific, St. Louis, MO). Images were collected every 10 minutes using a 10X objective. The images were then analyzed using a Matlab program that tracked the position of the centroid of cells in (x,y) coordinates vs. time. The mean squared displacement was calculated from the data using non-overlapping time intervals [116]. The speed of each cell was determined from the average displacement by the tracking interval 10 min. The persistence time of each

cell was obtained from fit using nonlinear least-square regression with the measured speed to a persistent random walk model for cell migration as reported elsewhere [117].

Cell Stiffness Measurement by Atomic Force Microscopy (AFM)

Cells were cultured on FN-coated glass and nanorods for 20 hours. Detailed method was reported elsewhere [118]. Briefly, Asylum MFP3D AFM (Asylum Research, CA) coupled to a Nikon TE2000U epifluorescence microscope was used for measuring cell stiffness. The pyramid-tip had a spring constant of 60 pN/nm, and tip half-angle was 37 degrees. 122 cells on glass and 87 cells on nanorods were measured from glasses and nanorods. Each profile was fit with a modified Hertzian model.

Western Blotting

Cells cultured on 76.2 mm x 25.4 mm glass and same size of nanorods were washed with cold PBS and lysed with cell lysis buffer (Cell Signaling Technology, Inc., MA) for 10 minutes on ice. Cells were then collected and centrifuged at 10,000 rpm for 10 minutes at 4ºC. The supernatant was then collected and sodium dodecyl sulfate (SDS)-sample buffer was added and stored at -20ºC until used. The samples were separated on 10% SDS polyacrylamide gels and then transferred onto a polyvinylidene fluoride (PVDF) membrane. The membranes were blocked with 5% milk in Tris buffered saline with Tween 20 (TBST) at room temperature for 30 min. The membranes were treated with phosphor-myosin light chain 2 antibody (Cell Signaling Technology, Inc., MA) at 1:1000 dilutions in 5% milk overnight at 4ºC. The membranes were then washed three times in TBST and treated with peroxidase conjugated secondary antibody at 1:10000 in 5% milk in TBST for 2 hours. Blots were developed using SuperSignal West Pico Chemiluminescent reagent (Pierce Biotechnology, IL) and exposed to X-OMAT film (Eastman Kodak Inc., NY).

Results and Discussion

Decrease in Adhesion of Esophageal Epithelial Cells on Nanorods

We used a previously developed method to grow SiO_2 coated nanorods on glass surfaces (Figure 5-1A and 5-1B) [100]. Transmission electron microscopy (TEM) and electrical conductance measurements confirmed that the nanorods were uniformly covered by SiO_2 without any defects [100]. Nanorod surfaces were then coated with fibronectin and tumor epithelial cells were cultured on the substrates. After 24 hours of culture, the number of adherent tumor cells was observed to be nearly 50% lower on nanorod surfaces compared to glass (Figure 5-1C). This decrease was not due to toxicity of materials leached from the nanorods themselves (Figure 5-2). We have also previously shown that the SiO_2 coated nanorod surfaces are hydrophilic, and fibronectin adsorption is unaltered on these surfaces in Chapter 4. This argues against altered matrix protein adsorption as a potential cause of the decrease in tumor cell numbers.

Viability and Proliferation is Unchanged in Tumor Cells on Nanorods

Staining with calcein AM (4 μM) and ethidium homodimer-1 (EthD-1) showed that adherent tumor cells on glass and nanorods were both equally viable (data not shown). BrdU staining revealed that tumor cell proliferation on nanorods was similar to that on glass at 24 hours (Figure 5-1D). Together, these results suggest that the decrease of adherent tumor cells on nanorods is due to weakened adhesion rather than a decrease in proliferation rate or cell viability. The fact the proliferation and viability is unchanged although weak tumor cell adhesion is consistent with the fact that malignant tumor cells lose their dependence on firm adhesion for survival [119, 120].

Tumor Cell Cultured on Nanorods have Decreased Contractility

While tumor cells were able to form colonies on nanorods, individual cells in colonies were rounded on nanorods compared to glass (Figure 5-3). We next stained cells for vinculin and imaged cells with confocal fluorescence microscopy, but clearly defined focal adhesions proved difficult to detect on both glass and nanorods (Figure 5-4). Cells at the periphery of the colonies were observed to form lamellipodial structures on glass, but similar structures were absent on nanorods (Figure 5-3, arrows). These results raised the possibility that nanorods could potentially decrease intracellular tension in the tumor cells. To evaluate this possibility directly, we next measured the levels of phosphorylated non-muscle myosin II as a measure of intracellular contractility in tumor cells. As seen in Figure 5-5, the level of phosphorylated myosin II is significantly decreased in tumor cells adherent to nanorods compared to flat surfaces. These results provide an explanation for the rounded cell morphologies seen in tumor cell colonies on nanorods.

It is known that the levels of phosphorylated non-muscle myosin II correlate with the stiffness of the cortical actomyosin cytoskeleton in adherent cells [121, 122]. We therefore measured stiffness of the adherent tumor cell cortex using atomic force microscopy (AFM) [123, 124]. As cell tension is proportional to cortical stiffness [123], the stiffness can be considered an indirect readout of cell tension. Our measurements revealed that the stiffness of single tumor cells on nanorods was decreased by nearly 50% of that on glass (Figure 5-6). Together, these results suggest that tumor epithelial cells have reduced tension on nanorods compared to glass substrates, which leads to weak adhesion, decreased cell numbers and rounded cell morphologies.

The mechanism of how nanorods alter tumor cell adhesion and mechanics is at least in part due to the nano-scale control of integrin clustering as mentioned in the previous chapters. The clustering of integrins occurs through crosslinking by intracellular proteins like talin [125] which causes the formation of stable adhesions that are physically linked to the intracellular actomyosin cytoskeleton. Interfering with integrin clustering interferes with focal adhesion assembly [8, 59, 94, 126] and feeds back to change actomyosin contractility [6]. Work by Spatz and co-workers has shown that integrin clustering requires that adjacent ligated integrin molecules be at a distance of less than 70 nm [8, 59, 94, 126]. Distances higher than these reduce clustering and focal adhesion formation. A similar mechanism may be responsible for our results because the inter-nanorod spacing is on the order of 50-100 nm [45] which likely interferes with normal integrin clustering.

Single Tumor Cell Motility is Increased on Nanorods

Cell motility has been previously shown to be sensitive to micro- and nano-scale surface topology [127-129]. For example, fibroblasts migrate faster on surfaces with 500 nm nanoholes compared to the corresponding flat glass surface [128]. Similarly, on titanium dioxide (TiO_2) nanotube surfaces, mesenchymal stem cells and fibroblasts moved faster on 15 nm nanotubes compared with the smooth surface [127, 129]. However, it is not clear if tumor cell motility is similarly sensitive to nanostructure. We therefore measured the single tumor cell migration speed and persistence time on nanorods. The average cell speed of single tumor cells and the mean persistence time were both found to be increased on nanorods compared with glass (Figure 5-7A and 5-7B). Given our observation that myosin II based contractility is decreased in tumor cells

on nanorods, (Figure 5-6) it is possible that the observed increase in motility on nanorods is due to weakened adhesion [117, 130].

Conclusions

In summary, our results suggest that it is possible to modulate malignant tumor cell adhesion, migration and mechanics with nanorod surfaces. The weakened adhesion raises the possibility that increased tumor cell detachment may occur under shear forces which are commonly encountered in the body (although not studied here). Our results suggest that nanostructure-based approaches may be a powerful yet simple approach to modulate tumor cell adhesion.

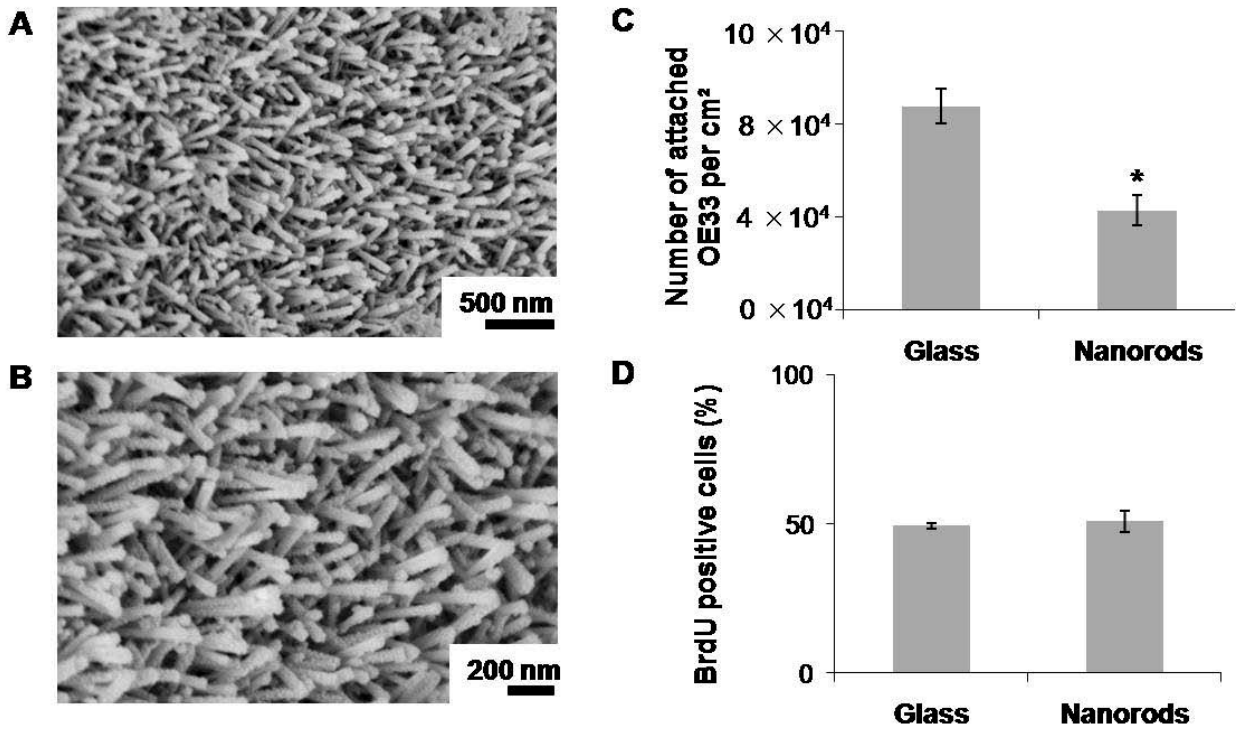

Figure 5-1. Esophageal epithelial tumor cell adhesion was decreased on nanorods. A), B) SEM images of nanorod morphology. Upright nanorods were covered on the underlying glass substrate uniformly. C) Numbers of attached OE33 cells were reduced by 50% on nanorods compared to the flat glass surface after 24 hour culture. D) Cell proliferation is unchanged on nanorods compared to glass as measured by BrdU incorporation. Bars indicate the standard error of the mean (SEM). * indicates statistically significant difference ($p<0.05$).

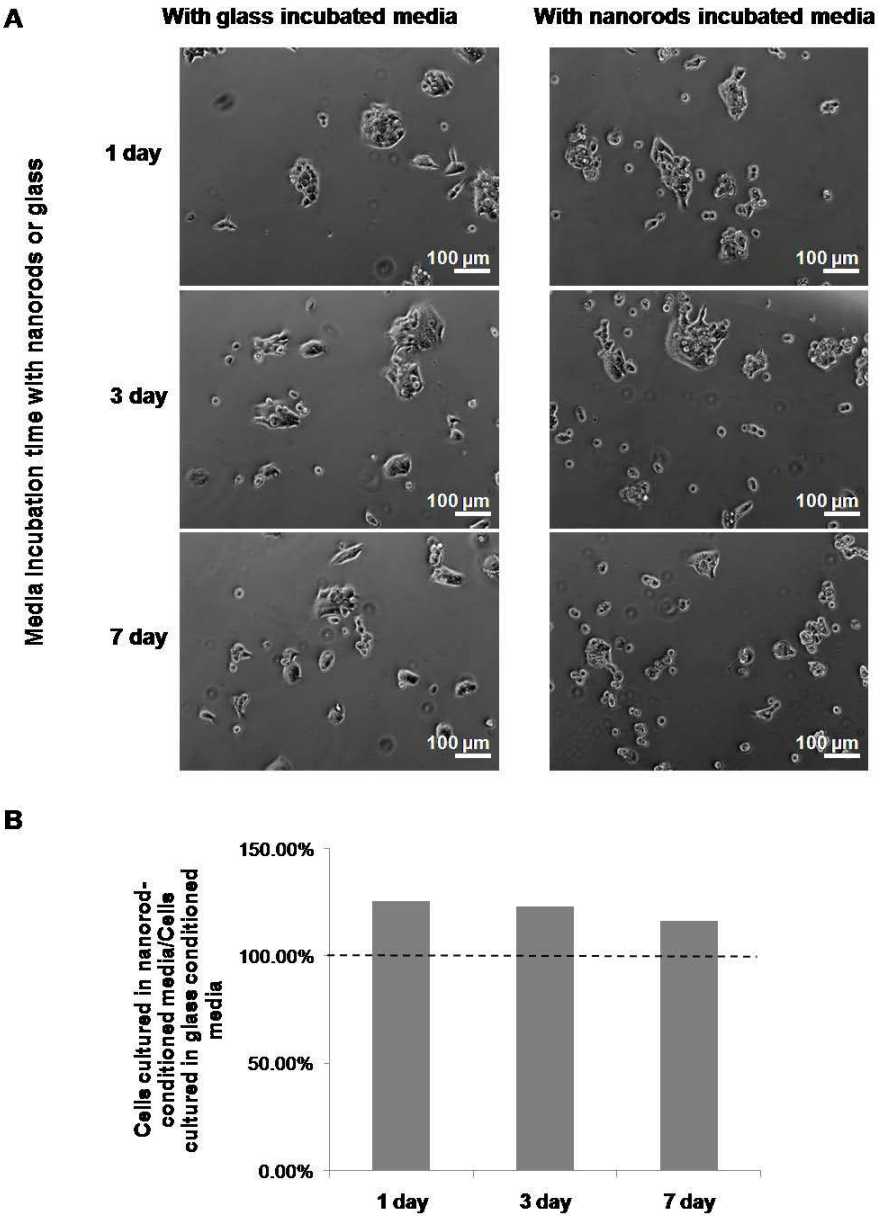

Figure 5-2. Nanorods are not toxic to tumor cells. Media was first incubated with either nanorods or glass for the times indicated. The media was then added to cells cultured at identical seeding densities for 24 hours. A) Phase contrast images of OE33 cells cultured for 24 hours with media incubated either with glass or nanorods for the times indicated. Images show no significant change in the adherent cell number on culturing cells with nanorod or glass incubated media. B) Quantification of data from A suggesting that the nanorod incubated media does not cause a decrease in cell numbers compared to glass incubated media. Number of cells was quantified from five images and divided by the total measured area.

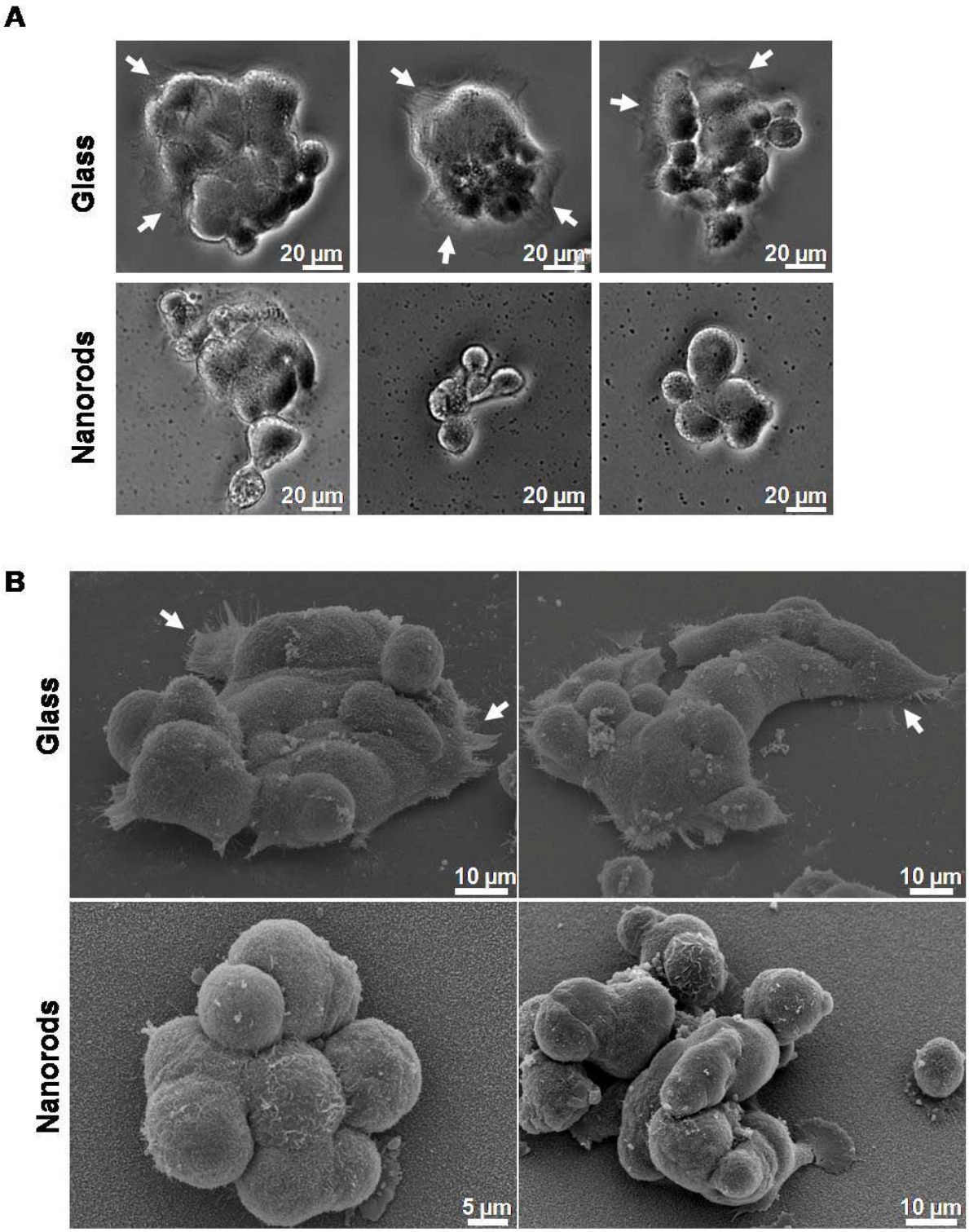

Figure 5-3. Individual tumor cells in colonies were rounded on nanorods unlike cells on glass. A) Phase contrast images of OE33 colony on nanorods and glass. B) SEM images of colony on nanorods and glass. Arrows point to lamellipodial structures on glass surface; similar structures were not detected on nanorods.

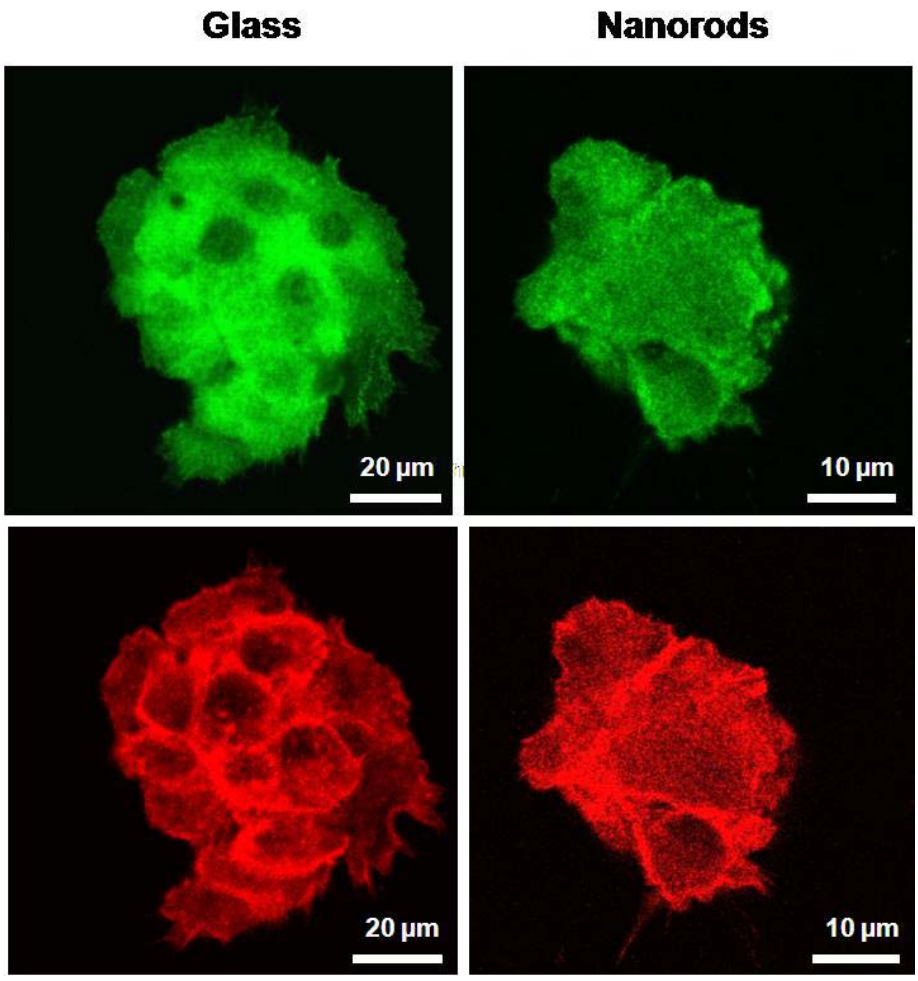

Figure 5-4. Confocal microscopic images of OE33 on glass and nanorods. Cells were stained with vinculin (green), and actin stress fibers (red). Clearly defined focal adhesions are difficult to detect both on glass and on nanorods.

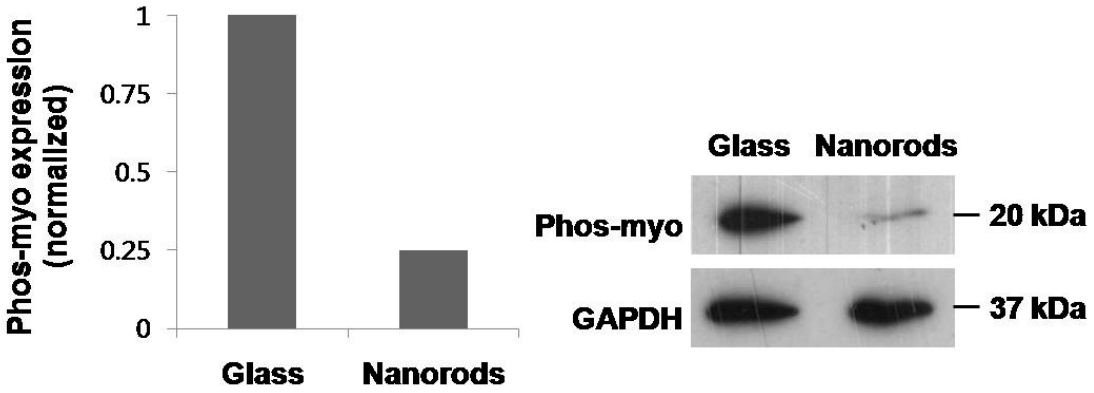

Figure 5-5. Non-muscle myosin II activity is significantly reduced in cells on nanorods compared to cells on glass. Western Blot of phosphorylated myosin shows decreased levels in tumor cells on nanorods. The comparison was made for identical levels of GAPDH to account for the decrease in cell number on nanorods.

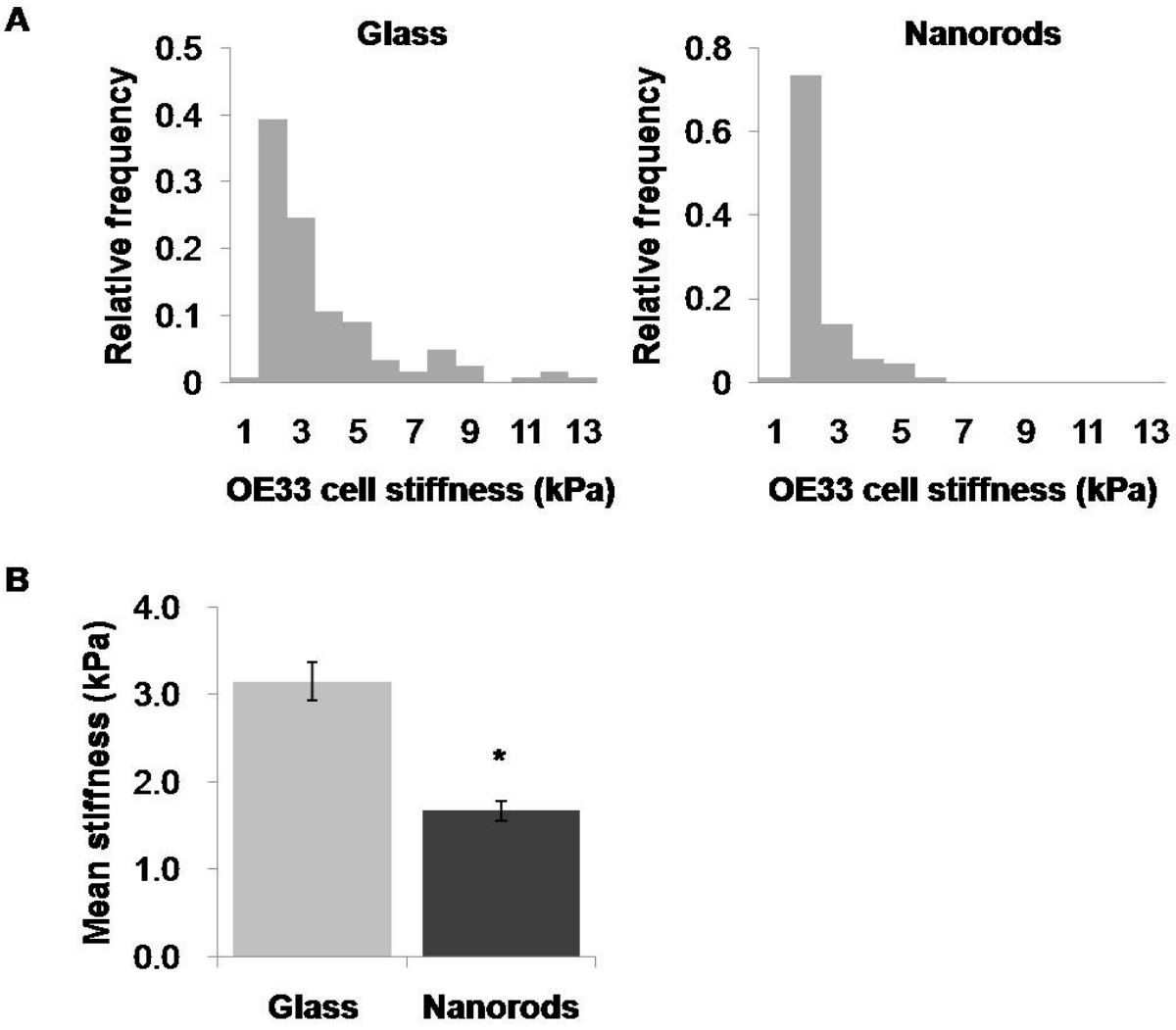

Figure 5-6. Tumor cells are softer on nanorods compared to glass. A) Histograms of single cell stiffnesses measured by AFM on nanorods and glass. B) The mean cell stiffness on nanorods was decreased by 50% compared to that on glass.

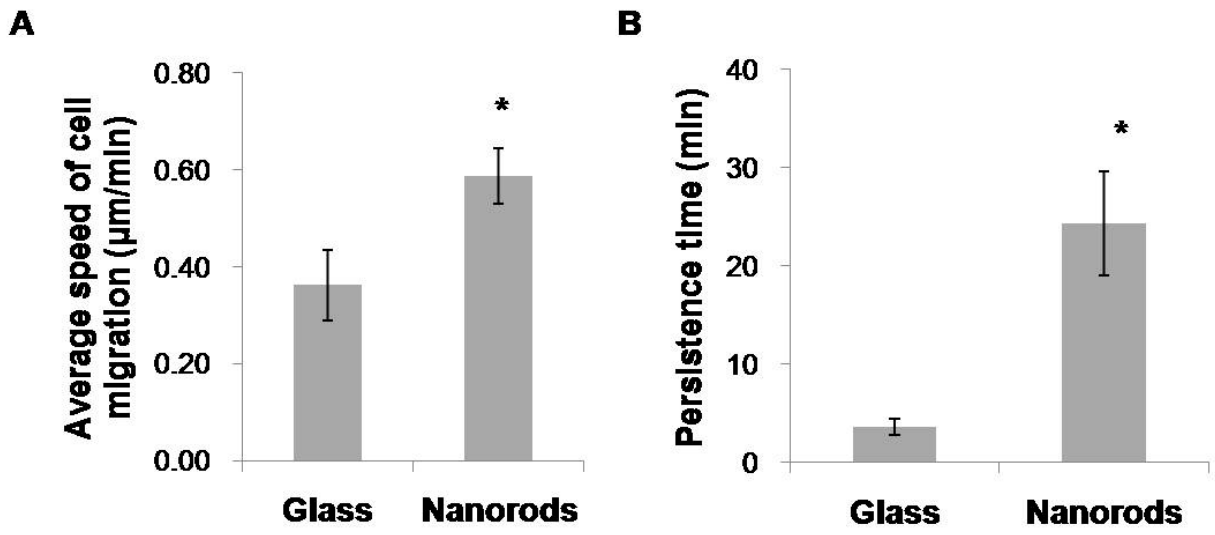

Figure 5-7. OE33 cell motility is altered on nanorods. A) The average speed of OE33 on nanorods was higher than that on glass (n=15 for glass, n=16 for nanorods). B) The mean persistence time is longer on nanorods than on glass (n=9 for glass, n=11 for nanorods). Bars indicate SEM. * indicates a statistically significant difference ($p<0.05$).

CHAPTER 6
THE ROLE OF NUCLEAR-CYTOSKELETAL LINKAGES IN CELL MECHANO-SENSING

Introduction

Recent studies suggest that the physical connection between the nucleus and the actomyosin cytoskeleton may be important in cell sensing of mechanical cues [131-134] . The different proteins that propagate cytoskeletal forces from outside the nucleus to the inside form a complex referred to as the LINC complex (for Linker of Nucleoskeleton to the Cytoskeleton). This complex consists of lamin A/C, a protein that forms a rigid, elastic network under the inner nuclear membrane, SUN family of proteins that bind to lamin A/C and reside in the inner nuclear membrane, and nesprin family of proteins that reside in the outer nuclear membrane. The primary evidence that these proteins are important in cell mechanosensing comes from studies with lamin A/C deficient cells [135-137]. Unlike normal cells, lamin A/C deficient cells exhibit defects in transducing mechanical forces into signaling pathways [135]. Similar effects have been observed in cells lacking other inner nuclear membrane proteins. For example, emerin deficient fibroblasts have irregular nuclear shape, exhibit an increase in cell death in response to mechanical strain and exhibit abnormal mechanotransduction [138]. Even though nesprin-1 is a direct linker between F-actin and the nucleus, the extent to which it influences cell mechanosensing has not been determined.

In addition to sensing externally applied mechanical forces, cells also are sensitive to substrate rigidity. For example, decreasing the stiffness of soft substrate composed of polyacrylamide (PAAm) hydrogel decreased neurite outgrowth and branching of PC12 cells [139]. Depending on the stiffness of substrates, naïve mesenchymal stem cells

(MSCs) specified lineage and committed to phenotypes differently [140]. However, the molecular mechanisms by which cells sense substrate stiffness are unclear.

Recently, Chancellor and co-workers have discovered a novel role for nesprin-1 in endothelial sensing of mechanical forces [141]. They showed that nesprin-1 deficient cells assemble more focal adhesions and exert greater traction on the substrate. The altered traction and adhesion assembly suggests that nesprin-1 may also be necessary for cellular sensing of substrate stiffness. In this chapter, we explored this possibility.

Materials and Methods

Cell Sulture and siRNA Knock Down of Nesprin-1

Human umbilical vascular endothelial cells (HUVECs) were cultured with DMEM-high glucose (Cellgro, Manassa, VA) supplemented with 10% donor bovine serum (DBS) (Gibco, Grand Island, NY). Cells were transfected with 100 nM of smartpool siRNAs (Dharmacon, Lafayette, CO) against human nesprin-1 using siLentFect lipid transfection reagent (BioRad, Hercules, CA) [141]. Non-targeting siRNAs served as controls. After 48-72 hours of transfection, cells were passed onto polyacrylamide substrates and glass.

Fabrication of Polyacrylamide Substrates

Polyacrylamide (PAAm) substrates were fabricated as reported elsewhere [16, 142]. Briefly, 0.1 M NaOH was dropped on the cover glass portion of glass bottomed dishes (MatTek, Ashland, MA) and dried overnight at room temperature. 10% pre-polymerized (3-aminopropyl)trimethoxysilane (APTMS) (Sigma, St. Louis, MO) was added onto the glass portion of dishes and incubated for 5 min. DI water was dropped on top of the APTMS layer and incubated for 10 min. After washing the solution with water, the dishes were shaken for 10 min. 0.5% Glutaraldehyde solution was added to

the dishes for 30 min. The dishes were washed with DI water several times and dried overnight. Four different ratios of acrylamide and bis-acrylamide (Fisher Scientific, Pittsburgh, PA), i.e. 50:1, 40:1, 20:1, and 12.5:1 were chosen to make gels with Young's modulus of 1.0 ± 7.8 kPa, 21.6 ± 6.17 kPa, 45.8 ± 3.31 kPa, and 308.0 ± 14.9 kPa as reported elsewhere [143]. The polyacrylamide solution was degassed, and 10% ammonium persulfate (APS) and tetramethylethylenediamine (TEMED) (Sigma, St. Louis, MO) was added. This solution was dropped on the chemically modified glass portion of glass bottomed dishes. The drop was covered by a cleaned circle cover glass, and allowed to polymerize at room temperature for 10 min. PBS was added before peeling the cover glass with tweezers. The gel surface was treated with 200 mM sulfo-SANPAH (Thermo Fisher Scientific, Waltham, MA) and then incubated with 5 µg/ml fibronectin (FN) overnight. The coverslip glass was treated by FN as a control.

Immunostaining

After 24 hours of cell culture, non-adherent cells were removed by PBS washes. Cells were fixed with 4% paraformaldehyde for 20 min and washed with PBS several times. Then, the samples were permeablized with 0.2% Triton X-100 and treated by mouse monoclonal anti-vinculin antibody (Sigma Aldrich, St. Louis, MO), followed by goat anti-mouse secondary antibody conjugated with Alexa Fluor 488 (Invitrogen, Eugene, OR). Actin was stained with phalloidin (Invitrogen, Eugene, OR) and nucleus was stained with Hoechst 33258 (Sigma Aldrich, St. Louis, MO). Using GFP, Texas Red and DAPI filters on a Nikon TE 2000 microscope, cells were imaged.

Measurement of Cell Spreading Area

1 day cultured cells were stained with phalloidin and Hoechst as reported above. Cell spreading image was taken with a 20X lens. Individual cells which were sufficiently

distant from each other (> 50 μm) were measured using Nikon Element program. The average spreading area of 40 cells for each condition was pooled from two independent experiments.

Cell Motility Assay

Nesprin-1 knockdown siRNA transfected HUVEC (NKHUVEC) and control smartpool siRNAs transfected HUVEC (SHUVEC) were cultured on FN coated PAAms for 6 hours. Cell movement was observed with a 10X phase contrast lens on the Nikon TE 2000 microscope with humidified incubator (In Vivo Scientific, St. Louis, MO). Images were taken every 10 minutes for 10 hours. The images were then analyzed using a Matlab program that tracked the position of the centroid of nuclei in (x, y) coordinates vs. time. The mean square displacement (MSD, $<d^2(t)>$) was calculated from the data using non-overlapping time intervals (t) [144]. The average cell speed (s) was calculated as (displacement in 10 min)/(10 min). The rationale for this calculation is that cells undergo persistent motion at short time intervals of 10 min.

The persistence time (p) and length (p multiplied by s) of each cell were obtained from fitting using nonlinear least-square regression with the measured speed to a persistent random walk model for cell migration as reported elsewhere [145].

$$< d^2(t) >= 2s^2 p[t - p(1 - e^{-t/p})] \quad (6\text{-}1)$$

Results

The Rigidity Dependence of Cell Spreading is Altered in Nesprin-1 Deficient Cells

A simple method to quantify rigidity sensing in cells is to measure the area of cell spreading on substrates of varying rigidities. Typically, cells on soft substrates are poorly spread, while cells on stiff substrates are well-spread. NKHUVEC and SHUVEC were cultured on PAAms with varying Young's modulus (1 kPa (1.0 ± 7.8 kPa), 22 kPa (21.6 ± 6.17 kPa), 46 kPa (45.8 ± 3.31 kPa), and 308 kPa (308.0 ± 14.9 kPa) [143]) for 1 day. Figure 6-1 shows average cell spreading area pooled from two independent experiments. The spreading area of SHUVEC increased with increasing stiffness in agreement with previous reports [143, 146, 147]. However, NKHUVEC spreading area did not increase from 22 kPa to 46 kPa, and increased much less on 308 kPa compared to SKHUVEC. Also, the spreading area between SHUVEC and NKHUVEC was significantly different on 1 kPa, 22 kPa and 308 kPa. This suggests that there is at least some disruption of cell sensing of substrate rigidity.

Focal Adhesion and Stress Fiber Assembly on PAAms

Focal adhesion assembly and stress fiber formation was next explored. It has been previously shown for normal rat kidney epithelial cells that focal adhesions appear as irregular punctuate structures on the soft PAAm surface (Young's modulus is approximately 15 kPa), but cells formed stable focal adhesions at the high stiffness PAAm (Young's modulus is approximately 70 kPa) [142]. As seen in Figure 6-2, stress fibers and adhesions are visible in SHUVECs on 46 kPa and 308 kPa PAAms, while these structures are less clear in NKHUVECs on all stiffnesses.

NKHUVECs have Altered Single Cell Motility

Next, the single cell motility of NKHUVEC and SHUVEC was monitored every 10 minutes for 10 hours. The centroid of nuclei in (x, y) coordinates was tracked in time. Non-overlapping MSD using x, y positions was quantified and fit to a random walk model [144, 145]. Figure 6-3 show the model fits to representative time-dependent MSD.

Cell speed has been to shown to depend on stiffness in a bimodal fashion [143]. We observed a very small peak for SHUVECs on 22 kPa and a bigger peak for NKHUVECs (arrows in Figure 6-4A). It is possible that the HUVECs exhibit a bimodal dependence; however, we do not have data on PAAm gels with intermediate stiffnesses between 0, 22 and 46 kPa to be conclusive. Qualitatively the speed-dependence on stiffness is not significantly different between NKHUVEC and SHUVEC. What is surprising is that the dependence of persistence length on stiffness of NKHUVECs is bell shaped compared to the monotonic increase for SHUVECs (Figure 6-4B and 6-4C). This may be due to the drastic decrease in the persistence length (or time) in NKHUVECs on high stiffnesses, a finding that is already supported by the results of Chancellor et al on glass surfaces [141]. Together, these results suggest that nesprin-1 may play a key role in cellular sensing of matrix rigidity.

Discussion

Recent research by Chancellor et al has shown an important role for nesprin-1 in endothelial mechanosensing [141]. This study proposed that actomyosin tension normally balanced by the nucleus is balanced in nesprin-1 deficient cells by the substrate. As a consequence, in the absence of nesprin-1, cells formed more focal adhesions and exerted increased traction on the substrate. Interestingly, there was no change in non-muscle myosin II activity.

The decrease in directional persistence observed in our experiments on 308 kPa is similar to the observation made by Chancellor et al on glass surfaces [141]. One possible explanation for this observation is the fact that nesprin-1 deficient cells form more adhesions on 308 kPa, leading to decreased frequency of detachment. Our images of focal adhesions on 308 kPa do not support this explanation as adhesions were less visible with nesprin-1 deficient cells on 308 kPa. Another possible explanation is that actin polymerization is inhibited in nesprin-1 deficient cells on 308 kPa. This possibility is supported by our observation that cell spreading area is significantly decreased on 308 kPa in nesprin-1 deficient cells. Actin polymerization is known to decrease on soft substrates and this has been shown to correlate with decreased spreading [148, 149]. More experiments with live cell imaging are needed to quantify the rates of actin polymerization in cells on different stiffnesses to support this preliminary conclusion. It is possible that Rho pathways that control actin polymerization are altered in nesprin-1 deficient cells- these include Rac and Cdc42 signaling. Western blotting to assay for differences in GTPase activity of these proteins in cells on different stiffnesses would greatly aid in better understanding the mechanisms that cause altered stiffness sensing in nesprin-1 deficient cells.

Conclusion

Endothelial sensing of substrate rigidity is altered in the absence of nuclear-cytoskeletal connections mediated by nesprin-1. The relationships most influenced by nesprin-1 deficiency are stiffness dependence of cell spreading area and stiffness dependence of directional persistence. More experiments that measure the rates of actin polymerization and the levels of Rac/Cdc42 signaling pathways are needed to understand the mechanism for our observations.

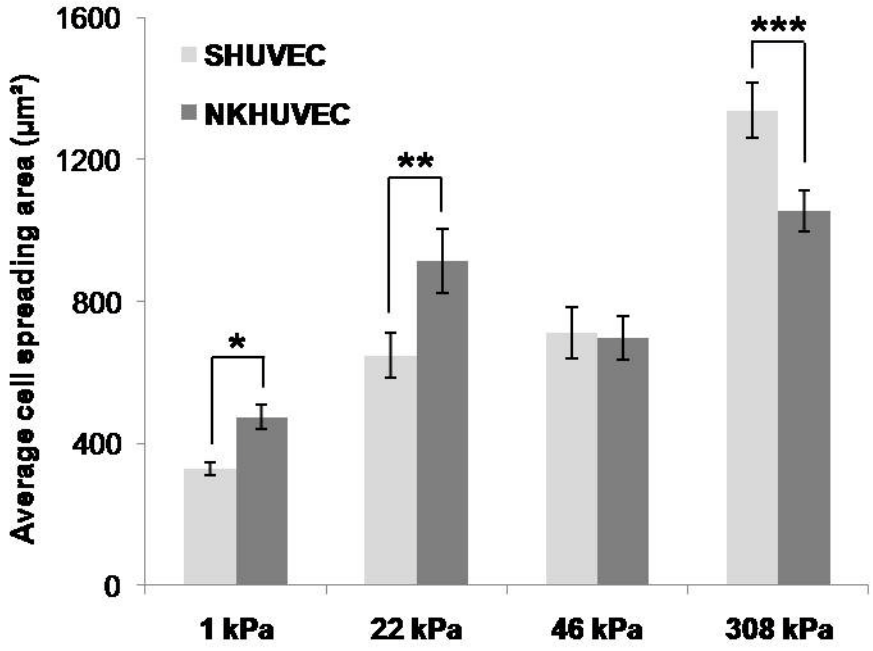

Figure 6-1. Average cell spreading area. Error bars represent the standard error of the mean (SEM) from two different experiments and *, **, *** indicate $p<0.05$.

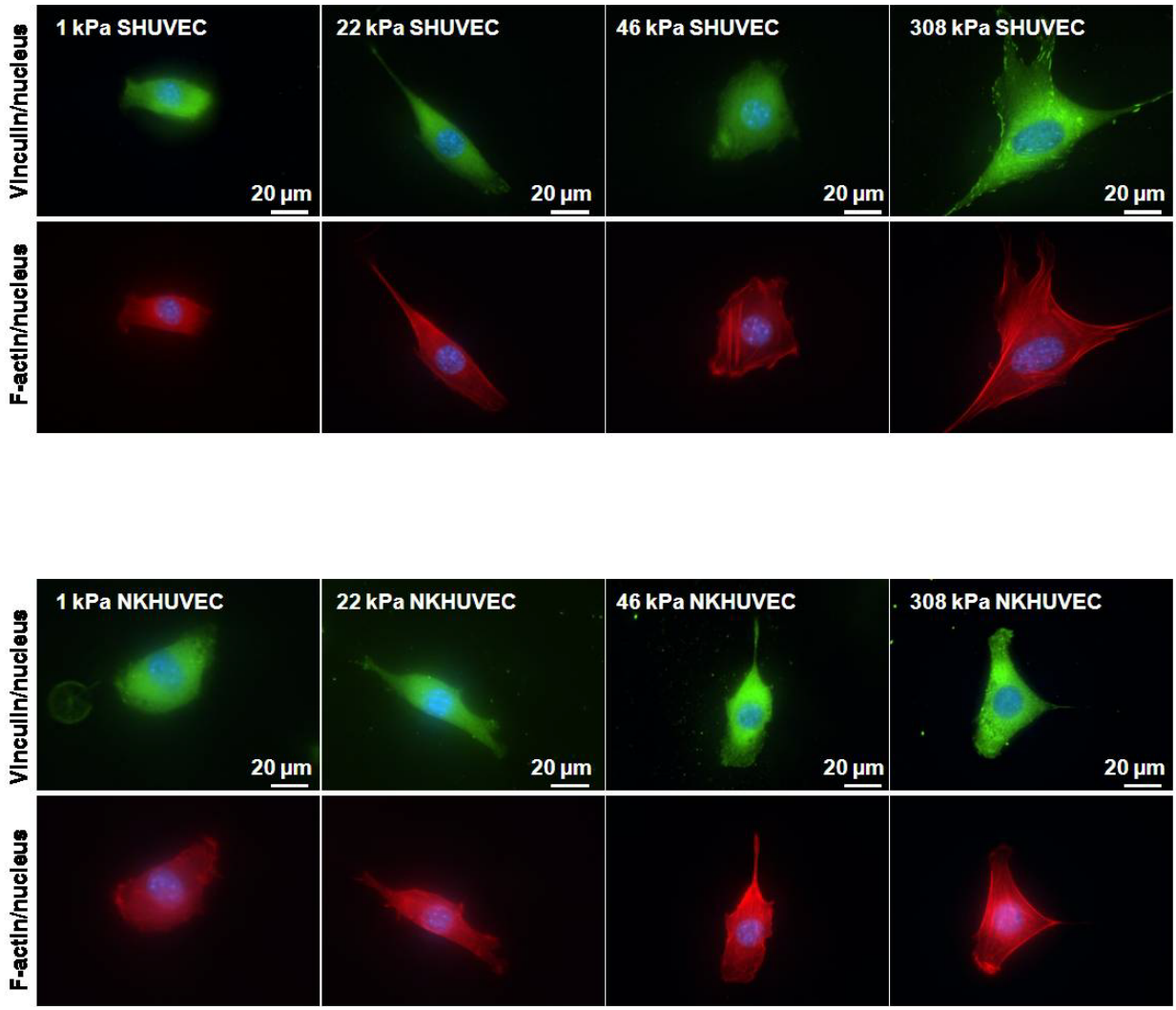

Figure 6-2. Fluorescent microscopy images of vinculin and F-actin.

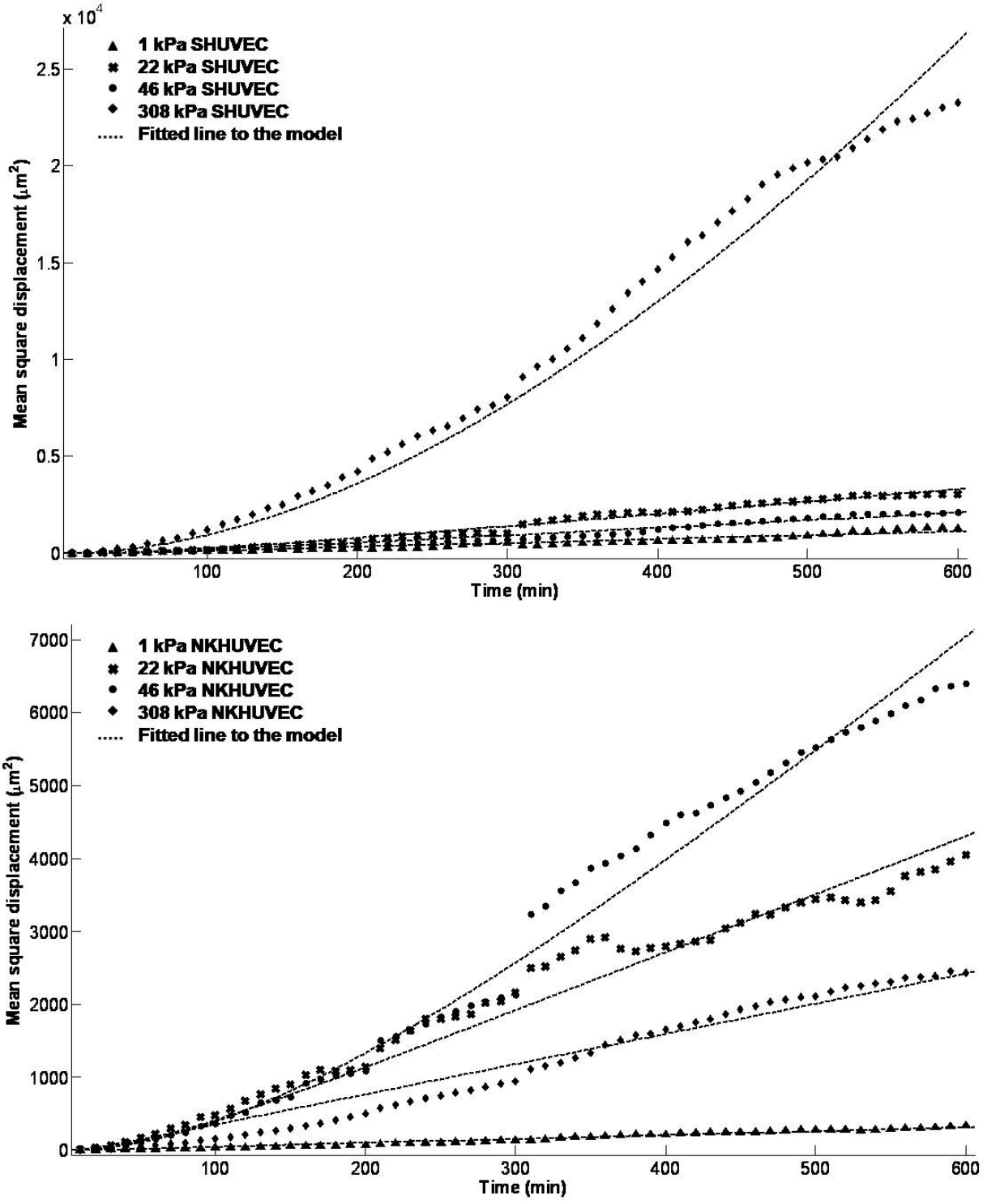

Figure 6-3. Representative mean square displacement (MSD) calculated for SHUVEC and NKHUVEC on PAAms of varying stiffness and model fits.

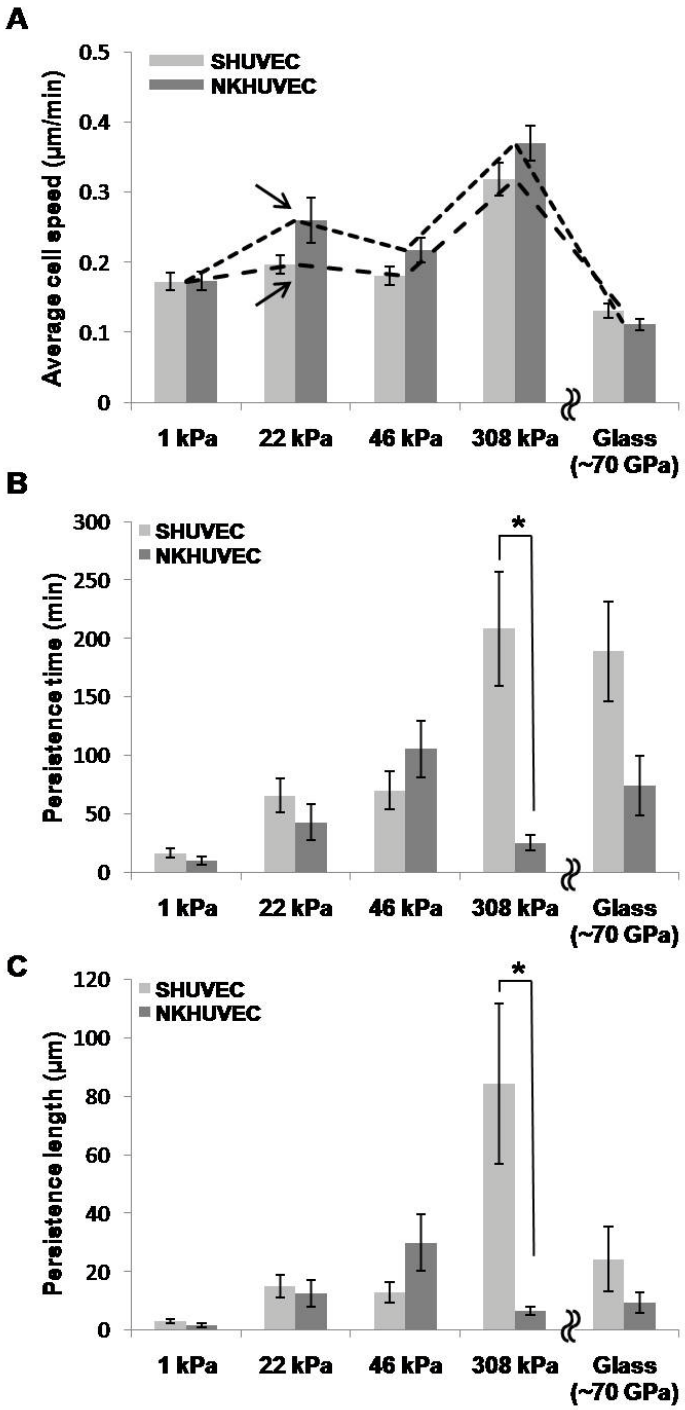

Figure 6-4. Cell speed, persistence time and persistence length of NKHUVEC and SHUVEC on PAAms. A) Arrows indicate an apparent peak in speed on 22 kPa PAAm. B) Persistence time and C) persistence length increase with stiffness for SHUVEC, whereas a bell shaped trend of persistence time and length is observed for NKHUVEC. Error bars represent SEM and * indicates $p<0.05$ (n=17~34 for PAAm, n=6~9 for glass).

CHAPTER 7
A STAMP-WOUND ASSAY TO STUDY COUPLED CELL PEELING AND MIGRATION: TOWARD A REALISTIC WOUND HEALING ASSAY

Introduction

Wound healing is a complex process that is critical for preserving the integrity of multicellular organisms and tissue homeostasis [150]. Wound healing involves the migration of cells of different types directed by chemotactic signals into the wound. *In vitro* models of wound healing traditionally [151-153] involve scratching a confluent cell monolayer with a microneedle or micropipette tip, and capturing the time dependent closure of the wound with microscopy. Such studies have allowed the discovery of key signaling pathways that control the migration of cells during wound closure [154-156]. One limitation of the scratch wound assay is that it lacks precision for creating a controlled wound. Alternative assays to create wounds have been recently reported that use laser photoablation [157] or masks to prevent cell adhesion to defined 'wound' areas [158-160]. While these traditional techniques offer more reliable models to study wound healing, they all share the common feature that the wound area is devoid of any cells. However, wound healing in the body involves not only the migration of cells into the wound, but also the simultaneous clearing of cell debris by the process of phagocytosis [161-165]. Assays that allow study of the coupled process of wound healing and phagocytosis are therefore desirable for realizing realistic *in vitro* wound healing assays.

Here, we report a new technique to make more wounds on epithelial cell monolayer using a stamping technique. The method involves the physical contact of a soft mold with raised features onto confluent epithelial cells. With this method, we successfully created well-defined wounds with dead cell debris in the wound area.

Imaging over several hours showed that the cells migrate into the wound after first clearing the wound area of cell debris. The rate of wound closure was found to be faster than the scratch wound assay. Interestingly, the inhibition of non-muscle myosin II with blebbistatin interfered with the healing of the wound in the presence of cell debris, but was unable to inhibit wound healing without dead cells. These results suggest that the proposed stamp-wound assay can be used to provide novel insight into the mechanisms of wound healing.

Materials and Methods

Fabrication of Poly(dimethyl)siloxane (PDMS) Molds

A master mold was fabricated by a conventional photolithography method. Prepolymers of soft PDMS (Sylgard 184, Dow Corning, MI) were poured over the photoresist master mold and degassed for 20 min in a vacuum, then cured at 60 °C in an oven for 2 hours. After peel off, the PDMS mold was sterilized by 70% ethanol and washed several times with sterilized DI water. For removing any remaining solvent and prepolymer, the PDMS mold attached to a glass slide was baked at 120 °C in an oven for 2 hours.

Cell Culture and Soft Imprinting with the PDMS Mold

Human esophageal epithelial cells (Het1A) were cultured in LHC-9 Medium (Invitrogen, Eugene, OR) supplemented with 5% donor bovine serum (DBS) (Gibco, Grand Island, NY). Cells were passed to glass bottom dishes (MatTek, Ashland, MA) or normal petri dishes, and cultured. When cells were confluent, fabricated PDMS mold was placed on the top of cell monolayer with an 86.3 g weight. After 20 min, the weight and the PDMS mold was carefully removed from the cell culture dish.

Time-Lapse Microscopy

After imprinting the cell monolayer with a PDMS mold, cell culture dishes were washed with PBS once for removing non-adherent cells and new media was added to the dish. Phase contrast imaging was performed for 18 hours on the Nikon TE 2000 microscope with humidified incubator (In Vivo Scientific, St. Louis, MO). Images were collected every 5 min or 10 min using 10x, 20x, and 60x objectives.

Cell Viability Assay

The live/dead viability/cytotoxicity kit for mammalian cells (Invitrogen, Eugene, OR) was used for observing live and dead cells. Imprinted cells were washed with PBS once and incubated with 4 μM calcein AM and 4 μM ethidium homodimer-1 (EthD-1) for 30-45 min. After washing with PBS, new media was added to the dish. Cells were imaged with time lapse microscopy using phase contrast, GFP and Texas Red filters as mentioned above.

Blebbistatin Assay

Imprinted cells were washed with PBS once, and 5 μM blebbistatin (Calbiochem, San Diego, CA) in cell media was added to the dishes. Images were collected every 10 min using a 10x objective for 18 hours on the Nikon TE 2000 microscope. The area of wound was measured with Image J, and the time-dependent wound closure ratio was pooled and averaged.

Results

We utilized the soft imprint technology to stamp a wound on a confluent monolayer of cultured cells. Figure 7-1 shows the experimental scheme. Briefly, PDMS prepolymers were poured on the photoresist master mold and then cured. After PDMS mold was carefully peeled off, they were sterilized and baked again at 120°C to remove

any remaining solvent and prepolymer. The raised features on the PDMS were square in shape with a size of 250 μm. Imprinting the PDMS mold on the confluent human epithelial cell monolayer caused cells to have a flattened morphology in the stamped area (Figure 7-2A). The flattened cells were completely replaced by normal cells after 15 hours (Figure 7-2A). When the PDMS mold was shifted laterally before peeling it off from the confluent cells, the flattened cells were removed and 'clean' wounds could be created (Figure 7-2B). Interestingly, the rate of wound closure in this 'cleaned wound' without dead cells was faster than that measured in the 'stamped wound' with dead cells (Figure 7-3).

We next stained cells to test viability of the stamped cells. All the cells in the stamped area were found to be dead with predominant nuclei, suggesting that the stamping caused substantial damage to the cell (Figure 7-4A). Time lapse images further revealed that the dead cell debris was 'cleaned' by inwardly migrating cells (Figure 7-4B). Cells were observed to efficiently peel off dead cell debris first and then migrated further into the wound (Figure 7-4B). Overlaid images of phase contrast and fluorescent images shows that peeled off dead cells were engulfed by neighboring live cells (white arrows in Figure 7-4C).

Given that wound closure in the stamp-wound assay requires the peeling off of dead cell debris, we hypothesized that this process may require contractile forces generated by migrating cells. We therefore inhibited non-muscle myosin II using blebbistatin (5 μM). During the experiment, blebbistatin was not washed out to prevent possible recovery of myosin II activity during the slow healing process. Interestingly, cells were not peeled off after blebbistatin treatment even after 15 hours (Figure 7-5A).

However, wound healing was only slightly slowed in the presence of blebbistatin without dead cells in the ‘cleaned wound’ suggesting a fundamental requirement for actomyosin contractility in wound closure in the ‘stamped wound’ (Figure 7-5B and 7-6).

Discussion

Soft imprinting technology is widely used for fabricating patterns at the nano and micron scale [166]. This method has been used to pattern extracellular matrix proteins (such as fibronectin) on the substrate and confining cell adhesion on the individual protein islands [167-169]. Here, we used a similar soft imprinting method to create wounds with dead cell debris. This stamping wound assay can be used to study both the migration of cells into the wound and simultaneous phagocytosis in the wound site. Alternative methods to achieve dead cells surrounded by live cells include electric pulses to kill cells locally [170].

We showed that the rate of wound closure in the ‘stamped wound’ without dead cells was slower than that measured in the ‘cleaned wound’ with dead cells. This is probably due to the fact that migrating cells were observed to first peel off dead cells before moving forward. One interesting finding in our study is that the wound closure rate with non-muscle myosin II inhibition is faster when no dead cells or debris remain at the site of wound. We attribute this to the fact that cells cannot phagocytose the dead cell debris in the absence of myosin activity [171-173]. Due to the inability of cells to peel off debris, cells are unable to migrate inward due to the presence of cell debris resulting in decreased rates of wound healing.

The fact that this assay allows us to study wound healing in the presence of cell debris is significant because local necrosis of cells causes the release of chemotactic factors locally that influence the directionality of cell migration [174-176]. Therefore

wound healing occurs not only because of the disruption of cell-cell junctions due to the generation of a ‘clean’ surface but also because of a local burst in chemotactic factors. As a result, this assay can be used to quantify the extent to which local chemotactic factors influence cell migration during wound healing. The mechanism for migration involves a complex interplay between chemotaxis, migration due to disruption of cell-cell junctions and myosin-dependent cell peel-off. The efficiency with which cells peel off cells is surprising- no structures are evident on the dish surface once peel off occurs. The peeling process itself appears similar to phagocytosis but with important differences. Our confocal images demonstrate that the debris is not internalized entirely (data not shown here), which is intriguing given that cells continue to migrate with this extra ‘payload’ without any noticeable decrease in speed.

Conclusions

A new method for creating realistic wounds in adherent cell monolayers was proposed. Successful removal of migration of healthy cells toward dead cells was observed, and the partial engulfment of dead cells by live cells was shown. The migration of cells into the wound was shown to require myosin activity only in the presence of debris. Collectively, this novel wound assay is expected to result in better understanding of the process of wound healing.

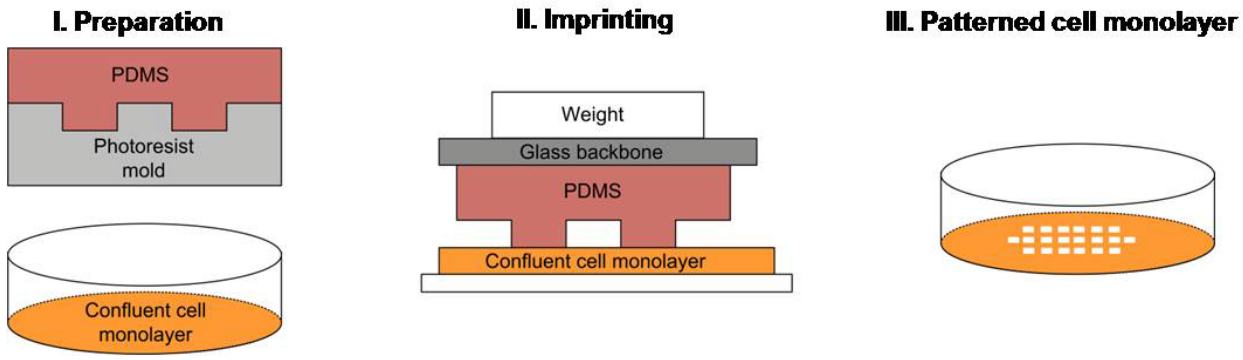

Figure 7-1. Schematic diagram of stamping wound assay.

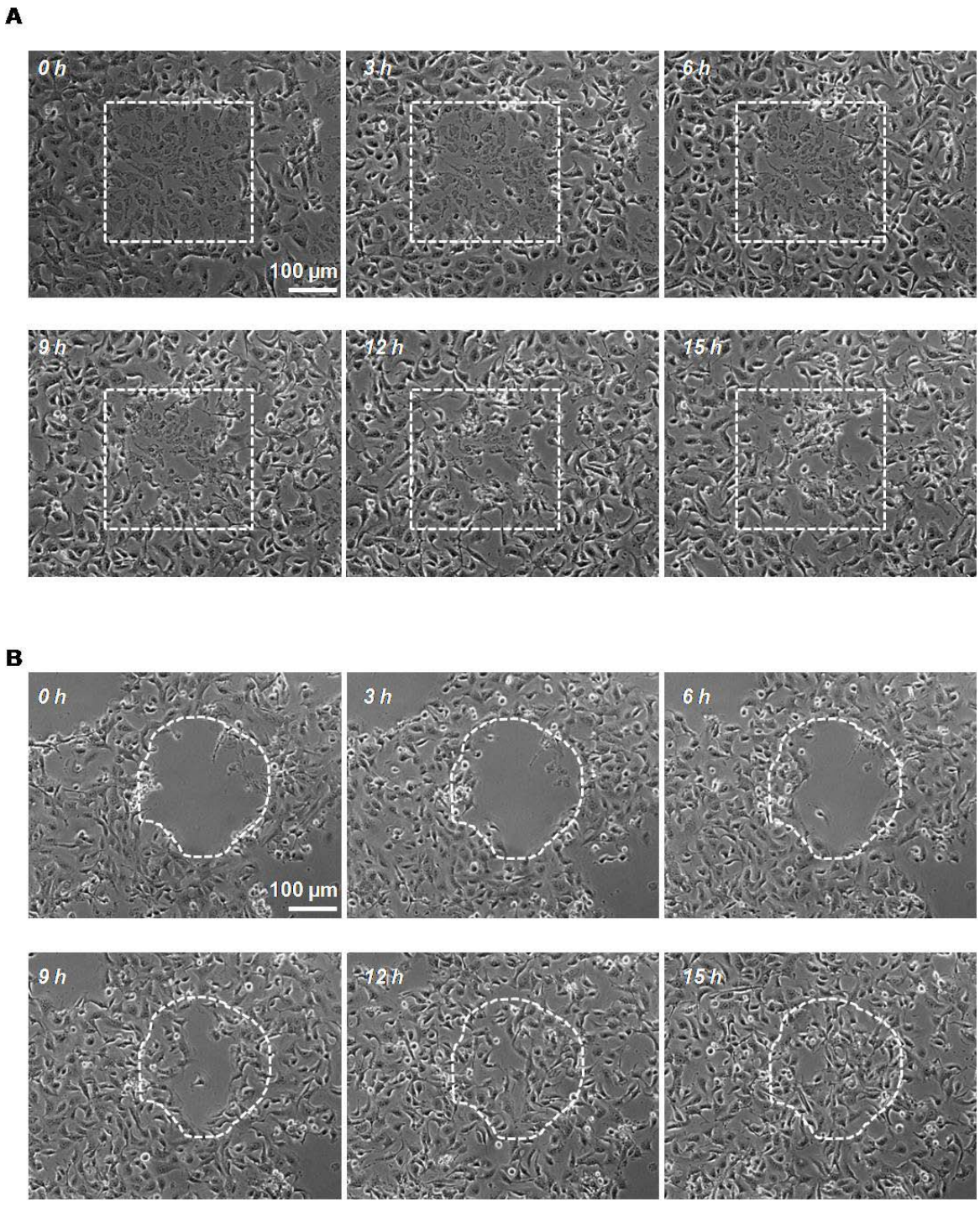

Figure 7-2. Time lapse microscope images of stamped Het1A cells. Neighboring cells (outside of dashed line) started migrating into patterned cells (inside of dashed line) after removing the stamp. A) Stamping caused flattened cells (stamped wound). B) Shifting the stamp created a 'clean wound'. After 15 hours, neighboring cells occupied the wound site.

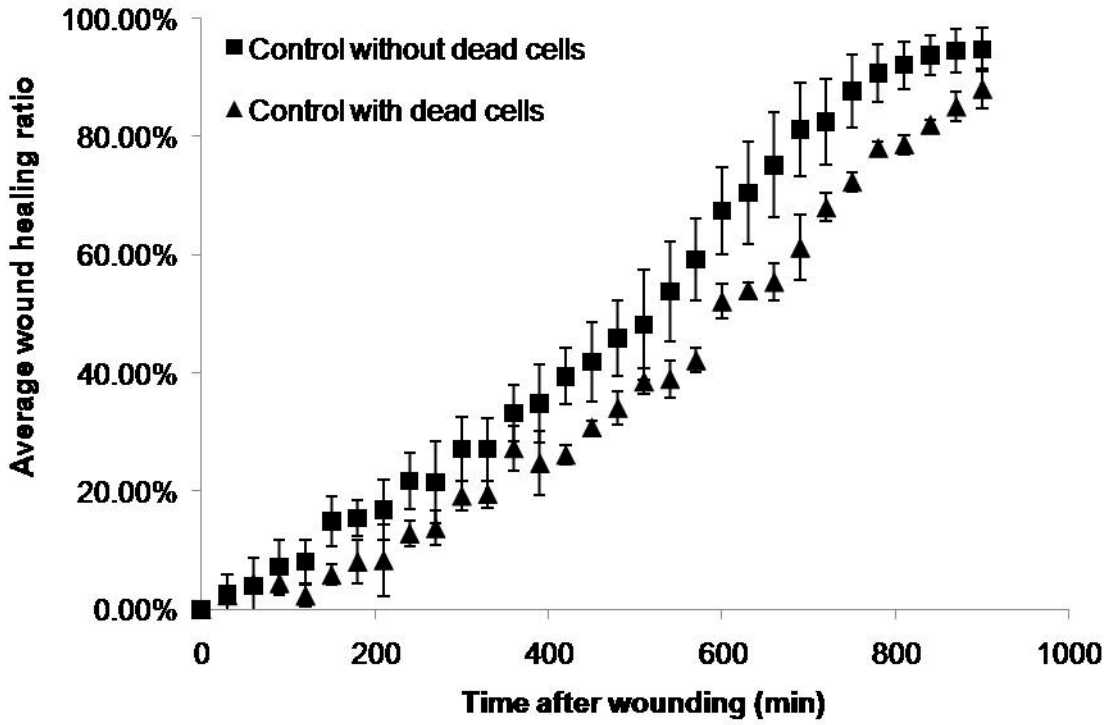

Figure 7-3. Wound healing ratio with Het1A cells. Average wound healing ratio of control (not treated by any drug) cells with dead cells (stamped wound) and without dead cells (cleaned wound). Wound healing rate without dead cells was a little bit faster than that with dead cells, but both of wounds were completely closed in both of cases after 15 hours. Bars indicate the standard error of the mean (SEM) (n=3 for each condition).

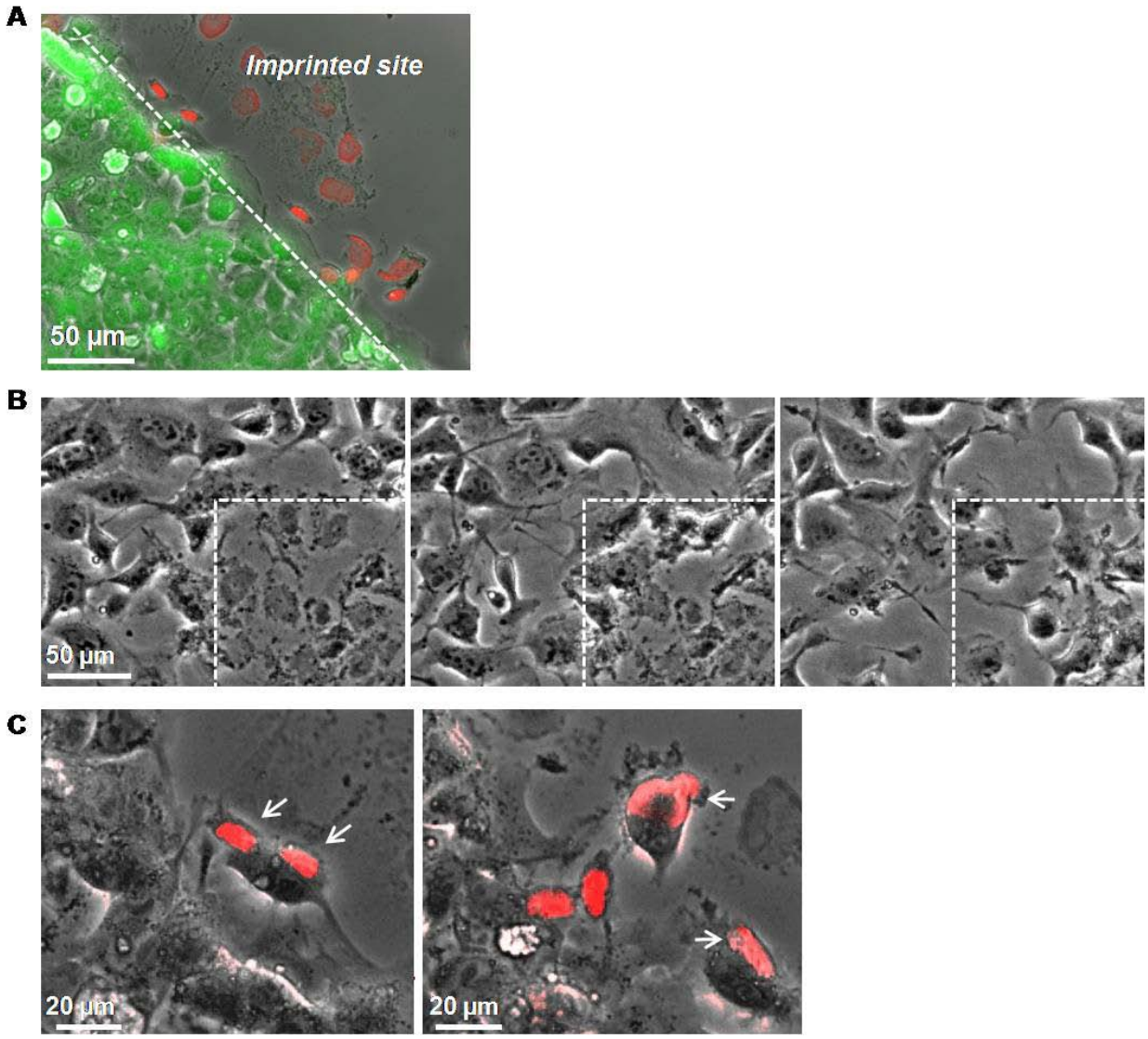

Figure 7-4. Epithelial cell migrates to the wound after peeling off dead cells. A) Overlaid image of phase contrast and fluorescent microscope. Stamped cells were dead (red fluorescent), whereas neighboring cells were live (green fluorescent). B) Phase contrast images of stamped Het1A cells by time. Dead cells were peeled off by neighboring live cells. Dashed line indicates the boundary of stamped cells. C) Overlaid images of phase contrast and fluorescent microscope. White arrows show live cell ingest dead cell debris (red fluorescent).

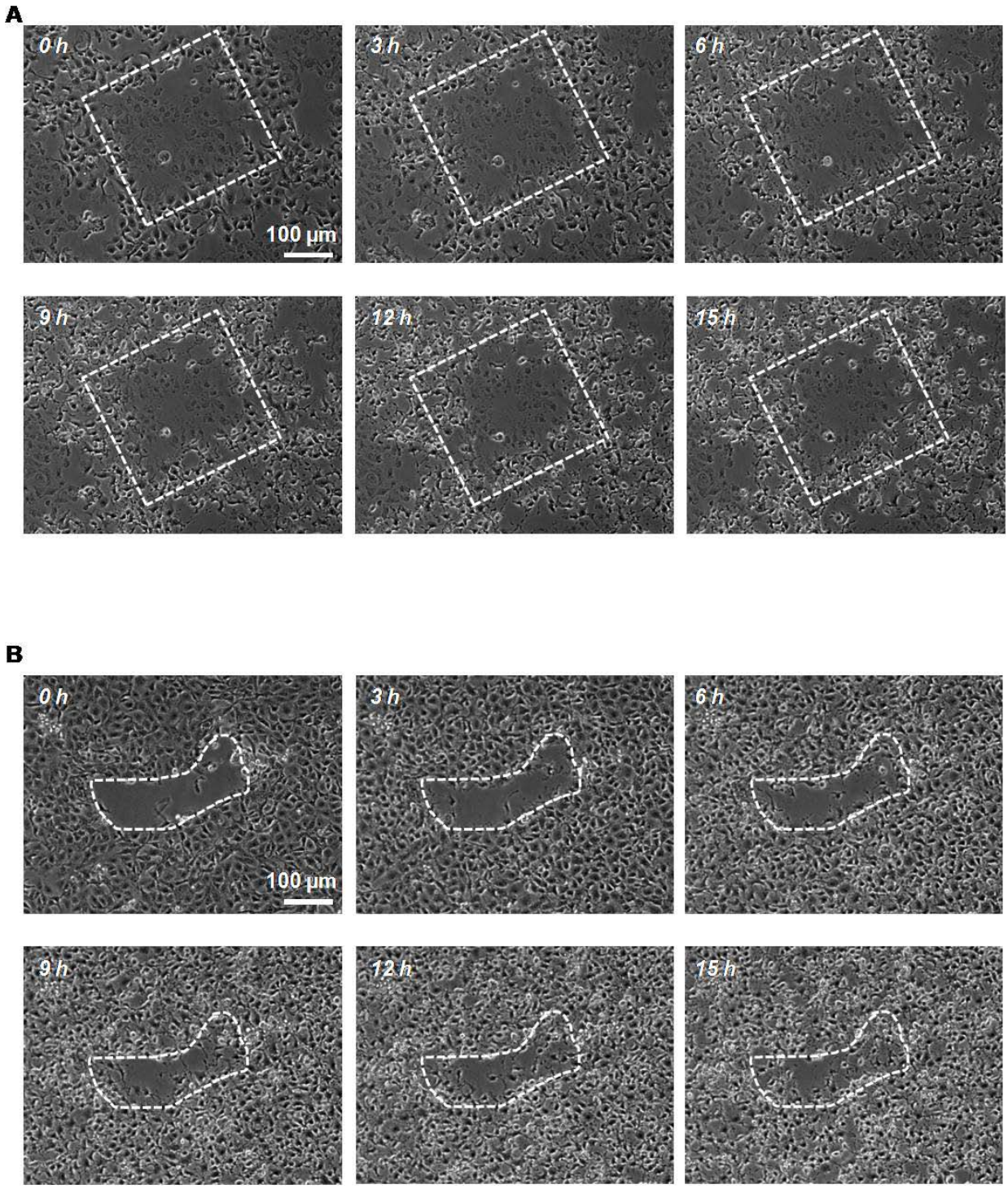

Figure 7-5. Time lapse images of stamped Het1A cells with blebbistatin treatment. A) Stamped wound closure was not completed even after 15 hours. B) Approximately 70% of cleaned wound was closed after 15 hours.

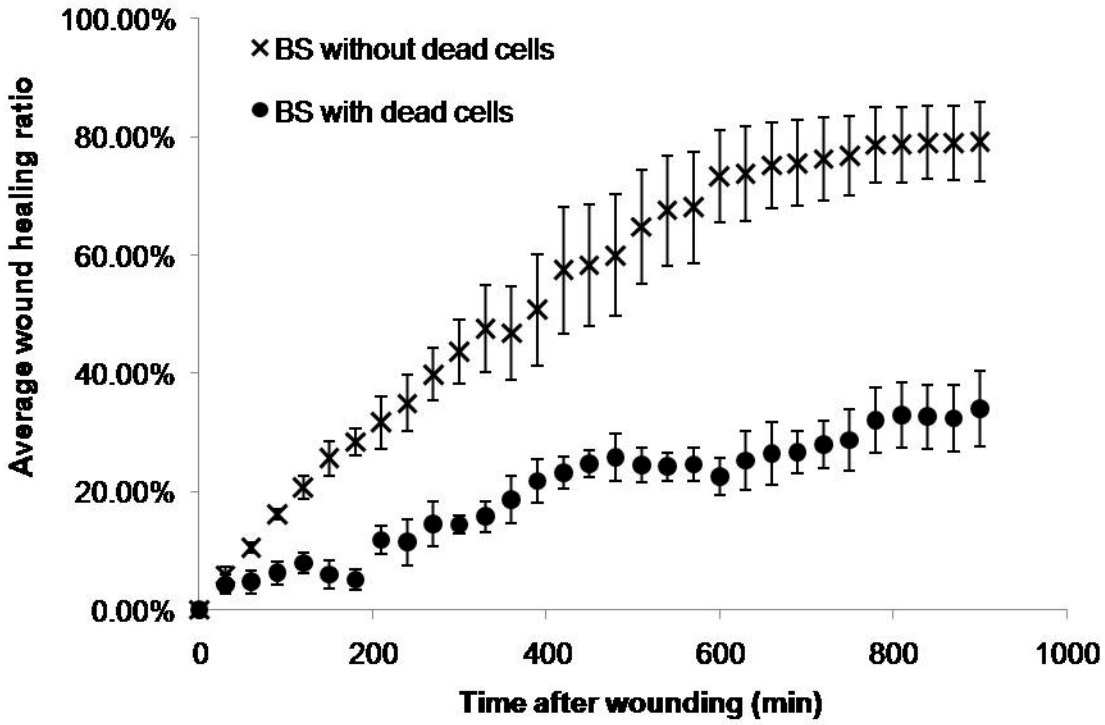

Figure 7-6. Wound healing ratio with non-muscle myosin II inhibition. Average wound healing ratio of blebbistatin (BS) treated cells with dead cells (stamped wound) and without dead cells (cleaned wound). After 15 hours, BS treated cells with dead cells did not close wound entirely (only 30%), while BS treated cells without dead cells completed 80% of wound healing. Bars indicate SEM (n=4 for each condition).

CHAPTER 8
CONCLUSIONS

Cell interactions with nanostructured biomaterials have received increasing attention because of applications in controlling tissue response to biomedical implants. Biomedical implants such as stents that are designed to keep lumenal organs open (e.g. cardiovascular stents or tumor stents) are frequently blocked and require removal and replacement. This increases morbidity and mortality and is a serious challenge to the success of therapies. The blockage occurs in part due to mammalian cell adhesion and proliferation on the implanted stent surface. Because fundamental cell behaviors such as adhesion, proliferation, and migration are exquisitely sensitive to nano-scale topography, we investigated the potential of upright randomly oriented monolayers of nanorods for anti-fouling. This work resulted in the following contributions.

1. NIH 3T3 fibroblasts, human umbilical vein endothelial cells, and bovine capillary endothelial cells were found to adhere far less to ZnO nanorods than the corresponding ZnO flat substrate. The decrease in numbers was associated with a lack of focal adhesion and stress fibers assembly, decrease in spreading area and a lack of lamellipodia formation.

2. To account for potential toxicity issues due to ZnO leaching, the above experiments were repeated with SiO_2 coated ZnO nanorods. The SiO_2 coating was confirmed to be conformal and solution toxicity assays showed that chemical dissolved material from the nanorods did not reduce cell number. Cell adhesion in NIH 3T3 fibroblasts and endothelial cells was dramatically decreased on SiO_2 coated nanorods. The lack of adhesion was not due to a decrease in matrix protein adsorption on the nanostructures (as confirmed by fibronectin adsorption), but rather an inability of cells to assemble focal adhesions.

3. The adhesion of esophageal epithelial tumor cells to SiO_2 coated nanorod monolayers was next investigated. The morphology of tumor epithelial cells cultured on nanorods was rounded compared to flat surfaces and was associated with decreased cellular stiffness and non-muscle myosin II phosphorylation. Single tumor cell motility was significantly increased on nanorods compared to flat surfaces while cell adhesion was reduced. Tumor cell number was decreased by nearly 50%, although proliferation and survival in adherent cells was unchanged. Collectively, these results supported the conclusion that tumor epithelial cells are unable to adhere firmly to nanorod monolayers.

4. A new ‘stamp wound’ healing assay was developed that allowed the quantification of wound healing rates in the presence of cell debris in the wound area. Significant differences were found between wound healing rates with and without cell debris in the wound area. The wound healing was found to depend on myosin activity only when cell debris was present. Finally, the role of nesprin-1 in cell sensing of substrate stiffness was investigated. Nesprin-1 depletion abolished cellular response to stiffness, suggesting a new role for nuclear-cytoskeletal connections in intracellular tension generation.

Together, the experiments with four different cell types on nanorods of two different materials support a model in which interfering with the nano-scale spacing of ligated integrins results in reduced cell adhesion and, for the case of normal cells, cell death. These findings are significant because they suggest a novel approach to interfere with cell adhesion based on surface topology. The key advantage is that the surface topology is permanent compared to other strategies that rely on coating with soluble chemicals.

The work in this dissertation clearly indicates the promise of upright nanorods for modulating cell adhesion and behavior. However, much work needs to be done before the technology can be tested for clinical applications. First, the mechanism underlying cell-nanorod interactions needs further investigation. Our initial conclusion that the cell adhesion is decreased on nanorods owing to the spacing between neighboring nanorods is based on the observations that (1) adhesion assembly and initial cell spreading are disrupted on nanorods; (2) fibronectin adsorption is unchanged; and (3) decreased cell numbers are not due to the leaching of toxic chemicals from the nanorods. The conclusion is supported by findings in the literature [58, 59, 177] that the critical spacing for integrin clustering is ~70 nm, which is comparable to than the average inter-nanorod spacing (~80-100 nm). Finally, cells spread well on electrospun

nanofibers [74, 178] which are horizontal, thereby providing a mesh like continuous surface for integrin ligation. However, this conclusion has not yet been directly tested in our experiments. Systematic experiments that will control the inter-nanorod spacing while at the same time preventing adhesion in between the nanorods are necessary to unequivocally answer this question.

We showed that more fibronectin was adsorbed on nanorods than glass. However, it is not clear if fibronectin conformation on the nanorods is conducive to cell adhesion [179]. Protein adsorption is a dynamic process relating to hydrophobic interactions, electrostatic forces, hydrogen bonding, and van der Waals forces [180] and hence protein parameters such as primary structure, size, stability, and conformation can be altered by surface energy, roughness, and chemistry [181]. Currently, protein adsorption and its partial unfolding structure on the surface can be determined by surface analysis measurements including Fourier transform infrared (FTIR) spectroscopy, nuclear magnetic resonance (NMR), AFM, and total internal reflectance fluorescence (TIRF) spectroscopy [182-185]. Analyzing unfolding fibronectin conformation on nanorods using these surface analysis measurements is required for better understanding the mechanism.

In this work, we investigated two different materials ZnO and SiO_2 coated ZnO. Similar studies need to be repeated with other materials with similar geometries to firmly establish the observed effect as well as to establish feasibility with a broad spectrum of materials. Gold, titanium, and silicon have been used as biocompatible materials [52, 79, 177] which do not induce an activation of the immune system and are non-toxic. Further experiments with these materials could promote other possible applications of upright

nanorods structures, such as bone prostheses and biosensors. Another potential application is the delivery of drugs immobilized on the nanorods into the cell. Silicon nanowires have been recently used to deliver genes into cells [82].

For successful use of nanorod coated substrates in tumor stents, a number of questions need to be addressed. First, strategies are needed to decrease tumor cell numbers to values lower than the 50% reduction reported here. One strategy is to coat the nanorods with protein-resistant polymers- this would be a synergistic approach that incorporates both topology and chemistry into the stent surface. Also, our results suggest that the tumor cells adhere only weakly to the nanorods. Based on these results, mechanical forces as are commonly seen in the body could detach the tumor cells and further reduce their numbers. Therefore, studies that include hydrodynamic flows are crucial. Also, the nanorods need to be very resistant to mechanical forces- tests based on hydrodynamic shear flow or frictional forces due to solid abrasion need to be performed and strategies to increase the adhesive strength between the nanorods and the underlying surface need to be explored. While nanorods have recently been coated on curved surfaces [186], it remains to be seen if the nanorods can withstand the expansion-compression that inevitably occurs with pre-expanding stents. If locally, the nanorods get removed, this could allow cells to adhere and more importantly, the removed nanorods could cause wear to surrounding tissue or cause toxicity, which is highly undesirable. Finally, the adhesion of other cell types (particularly macrophages) to nanorods should be studied, as this will help understand the inflammatory response that the body could potentially have to implanted nanorod-coated devices. Also,

nanorods may be useful for preventing bacterial adhesion- this could be an inexpensive approach for maintaining sterility of surfaces.

LIST OF REFERENCES

[1] Dormann A, Meisner S, Verin N, Lang AW. Self-expanding metal stents for gastroduodenal malignancies: Systematic review of their clinical effectiveness. Endoscopy 2004;36(6):543-550.

[2] Togawa O, Kawabe T, Isayama H, Nakai Y, Sasaki T, Arizumi T, et al. Management of occluded uncovered metallic stents in patients with malignant distal biliary obstructions using covered metallic stents. Journal of Clinical Gastroenterology 2008;42(5):546-549.

[3] Refai AK, Textor M, Brunette DM, Waterfield JD. Effect of titanium surface topography on macrophage activation and secretion of proinflammatory cytokines and chemokines. J Biomed Mater Res A 2004;70(2):194-205.

[4] Sun T, Tan H, Han D, Fu Q, Jiang L. No platelet can adhere--largely improved blood compatibility on nanostructured superhydrophobic surfaces. Small 2005;1(10):959-963.

[5] Peppas NA, Langer R. New challenges in biomaterials. Science 1994;263(5154):1715-1720.

[6] Ingber DE. Cellular mechanotransduction: putting all the pieces together again. FASEB J 2006;20(7):811-827.

[7] Benzeev A, Farmer SR, Penman S. Protein-Synthesis Requires Cell-Surface Contact While Nuclear Events Respond to Cell-Shape in Anchorage-Dependent Fibroblasts. Cell 1980;21(2):365-372.

[8] Girard PP, Cavalcanti-Adam EA, Kemkemer R, Spatz JP. Cellular chemomechanics at interfaces: sensing, integration and response. Soft Matter 2007;3(3):307-326.

[9] Re F, Zanetti A, Sironi M, Polentarutti N, Lanfrancone L, Dejana E, et al. Inhibition of anchorage-dependent cell spreading triggers apoptosis in cultured human endothelial cells. J Cell Biol 1994;127(2):537-546.

[10] Vakonakis I, Campbell ID. Extracellular matrix: from atomic resolution to ultrastructure. Curr Opin Cell Biol 2007;19(5):578-583.

[11] Stevens MM, George JH. Exploring and engineering the cell surface interface. Science 2005;310(5751):1135-1138.

[12] Ingber DE. Fibronectin controls capillary endothelial cell growth by modulating cell shape. Proc Natl Acad Sci U S A 1990;87(9):3579-3583.

[13] Schnell E, Klinkhammer K, Balzer S, Brook G, Klee D, Dalton P, et al. Guidance of glial cell. migration and axonal growth on electrospun nanofibers of poly-epsilon-caprolactone and a collagen/poly-epsilon-caprolactone blend. Biomaterials 2007;28(19):3012-3025.

[14] Clark P, Connolly P, Curtis AS, Dow JA, Wilkinson CD. Topographical control of cell behaviour: II. Multiple grooved substrata. Development 1990;108(4):635-644.

[15] Flemming RG, Murphy CJ, Abrams GA, Goodman SL, Nealey PF. Effects of synthetic micro- and nano-structured surfaces on cell behavior. Biomaterials 1999;20(6):573-588.

[16] Lo CM, Wang HB, Dembo M, Wang YL. Cell movement is guided by the rigidity of the substrate. Biophys J 2000;79(1):144-152.

[17] Chen CS, Mrksich M, Huang S, Whitesides GM, Ingber DE. Geometric control of cell life and death. Science 1997;276(5317):1425-1428.

[18] Webster TJ, Ergun C, Doremus RH, Siegel RW, Bizios R. Specific proteins mediate enhanced osteoblast adhesion on nanophase ceramics. J Biomed Mater Res 2000;51(3):475-483.

[19] Zhang L, Chen Y, Rodriguez J, Fenniri H, Webster TJ. Biomimetic helical rosette nanotubes and nanocrystalline hydroxyapatite coatings on titanium for improving orthopedic implants. Int J Nanomedicine 2008;3(3):323-333.

[20] Dalby MJ, Gadegaard N, Wilkinson CD. The response of fibroblasts to hexagonal nanotopography fabricated by electron beam lithography. J Biomed Mater Res A 2008;84(4):973-979.

[21] Yim EK, Reano RM, Pang SW, Yee AF, Chen CS, Leong KW. Nanopattern-induced changes in morphology and motility of smooth muscle cells. Biomaterials 2005;26(26):5405-5413.

[22] Liliensiek SJ, Campbell S, Nealey PF, Murphy CJ. The scale of substratum topographic features modulates proliferation of corneal epithelial cells and corneal fibroblasts. J Biomed Mater Res A 2006;79(1):185-192.

[23] Sniadecki NJ, Desai RA, Ruiz SA, Chen CS. Nanotechnology for cell-substrate interactions. Ann Biomed Eng 2006;34(1):59-74.

[24] Teixeira AI, McKie GA, Foley JD, Bertics PJ, Nealey PF, Murphy CJ. The effect of environmental factors on the response of human corneal epithelial cells to nanoscale substrate topography. Biomaterials 2006;27(21):3945-3954.

[25] Giancotti FG, Ruoslahti E. Transduction - Integrin signaling. Science 1999;285(5430):1028-1032.

[26] Hynes RO. Integrins - Versatility, Modulation, and Signaling in Cell-Adhesion. Cell 1992;69(1):11-25.

[27] Hynes RO. Integrins: Bidirectional, allosteric signaling machines. Cell 2002;110(6):673-687.

[28] Luo BH, Carman CV, Springer TA. Structural basis of integrin regulation and signaling. Annu Rev Immunol 2007;25:619-647.

[29] Nayal A, Webb DJ, Horwitz AF. Talin: an emerging focal point of adhesion dynamics. Curr Opin Cell Biol 2004;16(1):94-98.

[30] Schlaepfer DD, Hanks SK, Hunter T, van der Geer P. Integrin-mediated signal transduction linked to Ras pathway by GRB2 binding to focal adhesion kinase. Nature 1994;372(6508):786-791.

[31] Brown MC, Turner CE. Paxillin: adapting to change. Physiol Rev 2004;84(4):1315-1339.

[32] Otey CA, Carpen O. Alpha-actinin revisited: a fresh look at an old player. Cell Motil Cytoskeleton 2004;58(2):104-111.

[33] Burridge K, ChrzanowskaWodnicka M, Zhong CL. Focal adhesion assembly. Trends in Cell Biology 1997;7(9):342-347.

[34] Franz CM, Muller DJ. Analyzing focal adhesion structure by atomic force microscopy. J Cell Sci 2005;118(Pt 22):5315-5323.

[35] Hall A, Nobes CD. Rho GTPases: molecular switches that control the organization and dynamics of the actin cytoskeleton. Philosophical Transactions of the Royal Society B-Biological Sciences 2000;355(1399):965-970.

[36] Kitamura K, Tokunaga M, Iwane AH, Yanagida T. A single myosin head moves along an actin filament with regular steps of 5.3 nanometres. Nature 1999;397(6715):129-134.

[37] Choquet D, Felsenfeld DP, Sheetz MP. Extracellular matrix rigidity causes strengthening of integrin-cytoskeleton linkages. Cell 1997;88(1):39-48.

[38] Wang N, Butler JP, Ingber DE. Mechanotransduction across the cell surface and through the cytoskeleton. Science 1993;260(5111):1124-1127.

[39] Zamir E, Geiger B. Molecular complexity and dynamics of cell-matrix adhesions. J Cell Sci 2001;114(Pt 20):3583-3590.

[40] Zaidel-Bar R, Cohen M, Addadi L, Geiger B. Hierarchical assembly of cell-matrix adhesion complexes. Biochem Soc Trans 2004;32(Pt3):416-420.

[41] Zimerman B, Volberg T, Geiger B. Early molecular events in the assembly of the focal adhesion-stress fiber complex during fibroblast spreading. Cell Motil Cytoskeleton 2004;58(3):143-159.

[42] DeMali KA, Wennerberg K, Burridge K. Integrin signaling to the actin cytoskeleton. Current Opinion in Cell Biology 2003;15(5):572-582.

[43] Huang S, Ingber DE. The structural and mechanical complexity of cell-growth control. Nat Cell Biol 1999;1(5):E131-138.

[44] Choi CH, Hagvall SH, Wu BM, Dunn JCY, Beygui RE, Kim CJ. Cell interaction with three-dimensional sharp-tip nanotopography. Biomaterials 2007;28(9):1672-1679.

[45] Lee J, Chu BH, Chen KH, Ren F, Lele TP. Randomly oriented, upright SiO2 coated nanorods for reduced adhesion of mammalian cells. Biomaterials 2009;30(27):4488-4493.

[46] Lee J, Kang BS, Hicks B, Chancellor TF, Jr., Chu BH, Wang HT, et al. The control of cell adhesion and viability by zinc oxide nanorods. Biomaterials 2008;29(27):3743-3749.

[47] Dalby MJ, McCloy D, Robertson M, Agheli H, Sutherland D, Affrossman S, et al. Osteoprogenitor response to semi-ordered and random nanotopographies. Biomaterials 2006;27(15):2980-2987.

[48] Dalby MJ, Riehle MO, Sutherland DS, Agheli H, Curtis AS. Morphological and microarray analysis of human fibroblasts cultured on nanocolumns produced by colloidal lithography. Eur Cell Mater 2005;9:1-8; discussion 8.

[49] Lim JY, Hansen JC, Siedlecki CA, Runt J, Donahue HJ. Human foetal osteoblastic cell response to polymer-demixed nanotopographic interfaces. J R Soc Interface 2005;2(2):97-108.

[50] Chen QM, Kinch MS, Lin TH, Burridge K, Juliano RL. Integrin-Mediated Cell-Adhesion Activates Mitogen-Activated Protein-Kinases. Journal of Biological Chemistry 1994;269(43):26602-26605.

[51] Dalby MJ, Gadegaard N, Wilkinson CDW. The response of fibroblasts to hexagonal nanotopography fabricated by electron beam lithography. J Biomed Mater Res A 2008;84A(4):973-979.

[52] Choi CH, Hagvall SH, Wu BM, Dunn JC, Beygui RE, CJ CJK. Cell interaction with three-dimensional sharp-tip nanotopography. Biomaterials 2007;28(9):1672-1679.

[53] Zhu XY, Mills KL, Peters PR, Bahng JH, Liu EH, Shim J, et al. Fabrication of reconfigurable protein matrices by cracking. Nature Materials 2005;4(5):403-406.

[54] Garibaldi S, Brunelli C, Bavastrello V, Ghigliotti G, Nicolini C. Carbon nanotube biocompatibility with cardiac muscle cells. Nanotechnol 2006;17(2):391-397.

[55] Dalby MJ, Riehle MO, Johnstone H, Affrossman S, Curtis AS. In vitro reaction of endothelial cells to polymer demixed nanotopography. Biomaterials 2002;23(14):2945-2954.

[56] Arnold M, Cavalcanti-Adam EA, Glass R, Blummel J, Eck W, Kantlehner M, et al. Activation of integrin function by nanopatterned adhesive interfaces. Chemphyschem 2004;5(3):383-388.

[57] Walter N, Selhuber C, Kessler H, Spatz JP. Cellular unbinding forces of initial adhesion processes on nanopatterned surfaces probed with magnetic tweezers. Nano Letters 2006;6(3):398-402.

[58] Cavalcanti-Adam EA, Micoulet A, Blummel J, Auernheimer J, Kessler H, Spatz JP. Lateral spacing of integrin ligands influences cell spreading and focal adhesion assembly. European Journal of Cell Biology 2006;85(3-4):219-224.

[59] Cavalcanti-Adam EA, Volberg T, Micoulet A, Kessler H, Geiger B, Spatz JP. Cell spreading and focal adhesion dynamics are regulated by spacing of integrin ligands. Biophys J 2007;92(8):2964-2974.

[60] Huang JH, Grater SV, Corbellinl F, Rinck S, Bock E, Kemkemer R, et al. Impact of Order and Disorder in RGD Nanopatterns on Cell Adhesion. Nano Letters 2009;9(3):1111-1116.

[61] Xiong JP, Stehle T, Diefenbach B, Zhang R, Dunker R, Scott DL, et al. Crystal structure of the extracellular segment of integrin alpha Vbeta3. Science 2001;294(5541):339-345.

[62] Erb EM, Tangemann K, Bohrmann B, Muller B, Engel J. Integrin alphaIIb beta3 reconstituted into lipid bilayers is nonclustered in its activated state but clusters after fibrinogen binding. Biochemistry 1997;36(24):7395-7402.

[63] Martines E, Seunarine K, Morgan H, Gadegaard N, Wilkinson CDW, Riehle MO. Superhydrophobicity and superhydrophilicity of regular nanopatterns. Nano Letters 2005;5(10):2097-2103.

[64] Abdelsalam ME, Bartlett PN, Kelf T, Baumberg J. Wetting of regularly structured gold surfaces. Langmuir 2005;21(5):1753-1757.

[65] Lau KKS, Bico J, Teo KBK, Chhowalla M, Amaratunga GAJ, Milne WI, et al. Superhydrophobic carbon nanotube forests. Nano Letters 2003;3(12):1701-1705.

[66] Suh KY, Jon S. Control over wettability of polyethylene glycol surfaces using capillary lithography. Langmuir 2005;21(15):6836-6841.

[67] Webster TJ, Schadler LS, Siegel RW, Bizios R. Mechanisms of enhanced osteoblast adhesion on nanophase alumina involve vitronectin. Tissue Eng 2001;7(3):291-301.

[68] Khang D, Kim SY, Liu-Snyder P, Palmore GT, Durbin SM, Webster TJ. Enhanced fibronectin adsorption on carbon nanotube/poly(carbonate) urethane: independent role of surface nano-roughness and associated surface energy. Biomaterials 2007;28(32):4756-4768.

[69] Pegueroles M, Aparicio C, Bosio M, Engel E, Gil FJ, Planell JA, et al. Spatial organization of osteoblast fibronectin matrix on titanium surfaces: Effects of roughness, chemical heterogeneity and surface energy. Acta Biomater 2009.

[70] Ainslie KM, Sharma G, Dyer MA, Grimes CA, Pishko MV. Attenuation of protein adsorption on static and oscillating magnetostrictive nanowires. Nano Lett 2005;5(9):1852-1856.

[71] Teixeira AI, Abrams GA, Bertics PJ, Murphy CJ, Nealey PF. Epithelial contact guidance on well-defined micro- and nanostructured substrates. Journal of Cell Science 2003;116(10):1881-1892.

[72] Loesberg WA, te Riet J, van Delft FCMJM, Schon P, Figdor CG, Speller S, et al. The threshold at which substrate nanogroove dimensions may influence fibroblast alignment and adhesion. Biomaterials 2007;28(27):3944-3951.

[73] van Delft FCMJ, van den Heuvel FC, Loesberg WA, te Riet J, Schon P, Figdor CG, et al. Manufacturing substrate nano-grooves for studying cell alignment and adhesion. Microelectronic Engineering 2008;85(5-6):1362-1366.

[74] Chew SY, Mi R, Hoke A, Leong KW. The effect of the alignment of electrospun fibrous scaffolds on Schwann cell maturation. Biomaterials 2008;29(6):653-661.

[75] Lee CH, Shin HJ, Cho IH, Kang YM, Kim IA, Park KD, et al. Nanofiber alignment and direction of mechanical strain affect the ECM production of human ACL fibroblast. Biomaterials 2005;26(11):1261-1270.

[76] Dalby MJ, Riehle MO, Sutherland DS, Agheli H, Curtis AS. Morphological and microarray analysis of human fibroblasts cultured on nanocolumns produced by colloidal lithography. Eur Cell Mater 2005;9:1-8.

[77] Karuri NW, Liliensiek S, Teixeira AI, Abrams G, Campbell S, Nealey PF, et al. Biological length scale topography enhances cell-substratum adhesion of human corneal epithelial cells. J Cell Sci 2004;117(Pt 15):3153-3164.

[78] Yim EKF, Reano RM, Pang SW, Yee AF, Chen CS, Leong KW. Nanopattern-induced changes in morphology and motility of smooth muscle cells. Biomaterials 2005;26(26):5405-5413.

[79] Khang D, Lu J, Yao C, Haberstroh KM, Webster TJ. The role of nanometer and sub-micron surface features on vascular and bone cell adhesion on titanium. Biomaterials 2008;29(8):970-983.

[80] Spatz JP, Geiger B. Molecular engineering of cellular environments: cell adhesion to nano-digital surfaces. Methods Cell Biol 2007;83:89-111.

[81] Washburn NR, Yamada KM, Simon CG, Jr., Kennedy SB, Amis EJ. High-throughput investigation of osteoblast response to polymer crystallinity: influence of nanometer-scale roughness on proliferation. Biomaterials 2004;25(7-8):1215-1224.

[82] Kim W, Ng JK, Kunitake ME, Conklin BR, Yang P. Interfacing silicon nanowires with mammalian cells. J Am Chem Soc 2007;129(23):7228-7229.

[83] Kang BS, Pearton SJ, Ren F. Low temperature (< 100 degrees C) patterned growth of ZnO nanorod arrays on Si. Applied Physics Letters 2007;90(8):-.

[84] Lele TP, Pendse J, Kumar S, Salanga M, Karavitis J, Ingber DE. Mechanical forces alter zyxin unbinding kinetics within focal adhesions of living cells. J Cell Physiol 2006;207(1):187-194.

[85] Parker KK, Brock AL, Brangwynne C, Mannix RJ, Wang N, Ostuni E, et al. Directional control of lamellipodia extension by constraining cell shape and orienting cell tractional forces. FASEB J 2002;16(10):1195-1204.

[86] Michikawa M, Yanagisawa K. Apolipoprotein E4 induces neuronal cell death under conditions of suppressed de novo cholesterol synthesis. J Neurosci Res 1998;54(1):58-67.

[87] Lele TP, Pendse J, Kumar S, Salanga M, Karavitis J, Ingber DE. Mechanical forces alter zyxin unbinding kinetics within focal adhesions of living cells. J Cell Physiol 2006;207(1):187-194.

[88] Al-Hilli SM, Willander M, Ost A, Stralfors P. ZnO nanorods as an intracellular sensor for pH measurements. J Appl Phys 2007;102(8):084304.

[89] Kang BS, Ren F, Heo YW, Tien LC, Norton DP, Pearton SJ. pH measurements with single ZnO nanorods integrated with a microchannel. Appl Phys Lett 2005;86(11):112105.

[90] Sun XW, Kwok HS. Optical properties of epitaxially grown zinc oxide films on sapphire by pulsed laser deposition. J Appl Phys 1999;86(1):408-411.

[91] Dorfman A, Kumar N, Hahm J. Nanoscale ZnO-enhanced fluorescence detection of protein interactions. Adv Mater 2006;18(20):2685-2690.

[92] Dorfman A, Kumar N, Hahm JI. Highly sensitive biomolecular fluorescence detection using nanoscale ZnO platforms. Langmuir 2006;22(11):4890-4895.

[93] Greene LE, Law M, Goldberger J, Kim F, Johnson JC, Zhang Y, et al. Low-temperature wafer-scale production of ZnO nanowire arrays. Angew Chem Int Ed Engl 2003;42(26):3031-3034.

[94] Arnold M, Cavalcanti-Adam EA, Glass R, Blummel J, Eck W, Kantlehner M, et al. Activation of integrin function by nanopatterned adhesive interfaces. Chemphyschem 2004;5(3):383-388.

[95] Xia N, Thodeti CK, Hunt TP, Xu Q, Ho M, Whitesides GM, et al. Directional control of cell motility through focal adhesion positioning and spatial control of Rac activation. Faseb J 2008.

[96] Gojova A, Guo B, Kota RS, Rutledge JC, Kennedy IM, Barakat AI. Induction of inflammation in vascular endothelial cells by metal oxide nanoparticles: effect of particle composition. Environ Health Perspect 2007;115(3):403-409.

[97] Brinkman SF, Johnston WD. Acute toxicity of aqueous copper, cadmium, and zinc to the mayfly Rhithrogena hageni. Archives of Environmental Contamination and Toxicology 2008;54(3):466-472.

[98] Gojova A, Guo B, Kota RS, Rutledge JC, Kennedy IM, Barakat AI. Induction of inflammation in vascular endothelial cells by metal oxide nanoparticles: Effect of particle composition. Environmental Health Perspectives 2007;115(3):403-409.

[99] Lin WS, Xu Y, Huang CC, Ma YF, Shannon KB, Chen DR, et al. Toxicity of nano- and micro-sized ZnO particles in human lung epithelial cells. Journal of Nanoparticle Research 2009;11(1):25-39.

[100] Chu BH, Leu, L. C., Chang, C. Y., Lugo, F., Norton, D., Lele, T., Keselowsky, B., Pearton, S. J., Ren, F. Conformable coating of SiO2 on hydrothermally grown ZnO nanorods. Applied Physics Letters 2008;93:233111.

[101] Bershadsky A, Kozlov M, Geiger B. Adhesion-mediated mechanosensitivity: a time to experiment, and a time to theorize. Curr Opin Cell Biol 2006;18(5):472-481.

[102] Feng X, Feng L, Jin M, Zhai J, Jiang L, Zhu D. Reversible super-hydrophobicity to super-hydrophilicity transition of aligned ZnO nanorod films. J Am Chem Soc 2004;126(1):62-63.

[103] Grinnell F, Feld MK. Fibronectin adsorption on hydrophilic and hydrophobic surfaces detected by antibody binding and analyzed during cell adhesion in serum-containing medium. J Biol Chem 1982;257(9):4888-4893.

[104] McLoughlin MT, Byrne MF. Endoscopic stenting: where are we now and where can we go? World J Gastroenterol 2008;14(24):3798-3803.

[105] Siersema PD. Treatment options for esophageal strictures. Nat Clin Pract Gastroenterol Hepatol 2008;5(3):142-152.

[106] Han YM, Jin GY, Lee SO, Kwak HS, Chung GH. Flared polyurethane-covered self-expandable nitinol stent for malignant biliary obstruction. J Vasc Interv Radiol 2003;14(10):1291-1301.

[107] Isayama H, Komatsu Y, Tsujino T, Yoshida H, Tada M, Shiratori Y, et al. Polyurethane-covered metal stent for management of distal malignant biliary obstruction. Gastrointest Endosc 2002;55(3):366-370.

[108] Costamagna G, Marchese M, Iacopini F. Self-expanding stents in oesophageal cancer. Eur J Gastroenterol Hepatol 2006;18(11):1177-1180.

[109] Perdue DG, Freeman ML, DiSario JA, Nelson DB, Fennerty MB, Lee JG, et al. Plastic versus self-expanding metallic stents for malignant hilar biliary obstruction: a prospective multicenter observational cohort study. J Clin Gastroenterol 2008;42(9):1040-1046.

[110] Milner KR, Siedlecki CA. Fibroblast response is enhanced by poly(L-lactic acid) nanotopography edge density and proximity. Int J Nanomedicine 2007;2(2):201-211.

[111] Karuri NW, Nealey PF, Murphy CJ, Albrecht RM. Structural organization of the cytoskeleton in SV40 human corneal epithelial cells cultured on nano- and microscale grooves. Scanning 2008;30(5):405-413.

[112] Patel AA, Thakar RG, Chown M, Ayala P, Desai TA, Kumar S. Biophysical mechanisms of single-cell interactions with microtopographical cues. Biomed Microdevices 2009.

[113] Mwenifumbo S, Li M, Chen J, Beye A, Soboyejo W. Cell/surface interactions on laser micro-textured titanium-coated silicon surfaces. J Mater Sci Mater Med 2007;18(1):9-23.

[114] Qi S, Yi C, Chen W, Fong CC, Lee ST, Yang M. Effects of silicon nanowires on HepG2 cell adhesion and spreading. Chembiochem 2007;8(10):1115-1118.

[115] Ammoun S, Lindholm D, Wootz H, Akerman KE, Kukkonen JP. G-protein-coupled OX1 orexin/hcrtr-1 hypocretin receptors induce caspase-dependent and -independent cell death through p38 mitogen-/stress-activated protein kinase. J Biol Chem 2006;281(2):834-842.

[116] Dickinson RB, Tranquillo RT. Optimal Estimation of Cell-Movement Indexes from the Statistical-Analysis of Cell Tracking Data. Aiche J 1993;39(12):1995-2010.

[117] Harms BD, Bassi GM, Horwitz AR, Lauffenburger DA. Directional persistence of EGF-Induced cell migration is associated with stabilization of lamellipodial protrusions. Biophysical Journal 2005;88(2):1479-1488.

[118] Sen S, Kumar S. Cell-Matrix De-Adhesion Dynamics Reflect Contractile Mechanics. Cell Mol Bioeng 2009;2(2):218-230.

[119] Paszek MJ, Zahir N, Johnson KR, Lakins JN, Rozenberg GI, Gefen A, et al. Tensional homeostasis and the malignant phenotype. Cancer Cell 2005;8(3):241-254.

[120] Tilghman RW, Parsons JT. Focal adhesion kinase as a regulator of cell tension in the progression of cancer. Semin Cancer Biol 2008;18(1):45-52.

[121] Clark K, Langeslag M, Figdor CG, van Leeuwen FN. Myosin II and mechanotransduction: a balancing act. Trends Cell Biol 2007;17(4):178-186.

[122] Hale CM, Sun SX, Wirtz D. Resolving the role of actoymyosin contractility in cell microrheology. PLoS One 2009;4(9):e7054.

[123] Rotsch C, Jacobson K, Radmacher M. Dimensional and mechanical dynamics of active and stable edges in motile fibroblasts investigated by using atomic force microscopy. Proc Natl Acad Sci U S A 1999;96(3):921-926.

[124] Sen S, Subramanian S, Discher DE. Indentation and adhesive probing of a cell membrane with AFM: theoretical model and experiments. Biophys J 2005;89(5):3203-3213.

[125] Ye F, Hu G, Taylor D, Ratnikov B, Bobkov AA, McLean MA, et al. Recreation of the terminal events in physiological integrin activation. J Cell Biol 2010;188(1):157-173.

[126] Cavalcanti-Adam EA, Micoulet A, Blummel J, Auernheimer J, Kessler H, Spatz JP. Lateral spacing of integrin ligands influences cell spreading and focal adhesion assembly. Eur J Cell Biol 2006;85(3-4):219-224.

[127] Park J, Bauer S, Schmuki P, von der Mark K. Narrow window in nanoscale dependent activation of endothelial cell growth and differentiation on TiO2 nanotube surfaces. Nano Lett 2009;9(9):3157-3164.

[128] Westcott NP, Lou Y, Muth JF, Yousaf MN. Patterned hybrid nanohole array surfaces for cell adhesion and migration. Langmuir 2009;25(19):11236-11238.

[129] Park J, Bauer S, von der Mark K, Schmuki P. Nanosize and vitality: TiO2 nanotube diameter directs cell fate. Nano Letters 2007;7(6):1686-1691.

[130] Palecek SP. Integrin-ligand binding properties govern cell migration speed through cell-substratum adhesiveness (vol 385, pg 537, 1997). Nature 1997;388(6638):210-210.

[131] Maniotis AJ, Chen CS, Ingber DE. Demonstration of mechanical connections between integrins, cytoskeletal filaments, and nucleoplasm that stabilize nuclear structure. Proc Natl Acad Sci U S A 1997;94(3):849-854.

[132] Crisp M, Liu Q, Roux K, Rattner JB, Shanahan C, Burke B, et al. Coupling of the nucleus and cytoplasm: role of the LINC complex. J Cell Biol 2006;172(1):41-53.

[133] Worman HJ, Gundersen GG. Here come the SUNs: a nucleocytoskeletal missing link. Trends Cell Biol 2006;16(2):67-69.

[134] Warren DT, Zhang Q, Weissberg PL, Shanahan CM. Nesprins: intracellular scaffolds that maintain cell architecture and coordinate cell function? Expert Rev Mol Med 2005;7(11):1-15.

[135] Lammerding J, Schulze PC, Takahashi T, Kozlov S, Sullivan T, Kamm RD, et al. Lamin A/C deficiency causes defective nuclear mechanics and mechanotransduction. J Clin Invest 2004;113(3):370-378.

[136] Broers JL, Peeters EA, Kuijpers HJ, Endert J, Bouten CV, Oomens CW, et al. Decreased mechanical stiffness in LMNA-/- cells is caused by defective nucleo-cytoskeletal integrity: implications for the development of laminopathies. Hum Mol Genet 2004;13(21):2567-2580.

[137] Stewart-Hutchinson PJ, Hale CM, Wirtz D, Hodzic D. Structural requirements for the assembly of LINC complexes and their function in cellular mechanical stiffness. Exp Cell Res 2008;314(8):1892-1905.

[138] Lammerding J, Hsiao J, Schulze PC, Kozlov S, Stewart CL, Lee RT. Abnormal nuclear shape and impaired mechanotransduction in emerin-deficient cells. J Cell Biol 2005;170(5):781-791.

[139] Leach JB, Brown XQ, Jacot JG, Dimilla PA, Wong JY. Neurite outgrowth and branching of PC12 cells on very soft substrates sharply decreases below a threshold of substrate rigidity. J Neural Eng 2007;4(2):26-34.

[140] Engler AJ, Sen S, Sweeney HL, Discher DE. Matrix elasticity directs stem cell lineage specification. Cell 2006;126(4):677-689.

[141] Chancellor T, Lee J, Thodeti C, Lele TP. Nesprin-1 is required for endothelial mechanotransduction, polarization and motility. Biophysical Journal 2009;In review.

[142] Pelham RJ, Jr., Wang Y. Cell locomotion and focal adhesions are regulated by substrate flexibility. Proc Natl Acad Sci U S A 1997;94(25):13661-13665.

[143] Peyton SR, Putnam AJ. Extracellular matrix rigidity governs smooth muscle cell motility in a biphasic fashion. J Cell Physiol 2005;204(1):198-209.

[144] Burgess BT, Myles JL, Dickinson RB. Quantitative analysis of adhesion-mediated cell migration in three-dimensional gels of RGD-grafted collagen. Ann Biomed Eng 2000;28(1):110-118.

[145] Harms BD, Bassi GM, Horwitz AR, Lauffenburger DA. Directional persistence of EGF-induced cell migration is associated with stabilization of lamellipodial protrusions. Biophys J 2005;88(2):1479-1488.

[146] Engler A, Bacakova L, Newman C, Hategan A, Griffin M, Discher D. Substrate compliance versus ligand density in cell on gel responses. Biophys J 2004;86(1 Pt 1):617-628.

[147] Polte TR, Eichler GS, Wang N, Ingber DE. Extracellular matrix controls myosin light chain phosphorylation and cell contractility through modulation of cell shape and cytoskeletal prestress. Am J Physiol Cell Physiol 2004;286(3):C518-528.

[148] Solon J, Levental I, Sengupta K, Georges PC, Janmey PA. Fibroblast adaptation and stiffness matching to soft elastic substrates. Biophys J 2007;93(12):4453-4461.

[149] Yeung T, Georges PC, Flanagan LA, Marg B, Ortiz M, Funaki M, et al. Effects of substrate stiffness on cell morphology, cytoskeletal structure, and adhesion. Cell Motil Cytoskeleton 2005;60(1):24-34.

[150] Shaw TJ, Martin P. Wound repair at a glance. J Cell Sci 2009;122(Pt 18):3209-3213.

[151] Pinco KA, He W, Yang JT. alpha4beta1 integrin regulates lamellipodia protrusion via a focal complex/focal adhesion-independent mechanism. Mol Biol Cell 2002;13(9):3203-3217.

[152] Yarrow JC, Perlman ZE, Westwood NJ, Mitchison TJ. A high-throughput cell migration assay using scratch wound healing, a comparison of image-based readout methods. BMC Biotechnol 2004;4:21.

[153] Wang E, Zhao M, Forrester JV, McCaig CD. Electric fields and MAP kinase signaling can regulate early wound healing in lens epithelium. Invest Ophthalmol Vis Sci 2003;44(1):244-249.

[154] Rodriguez LG, Wu X, Guan JL. Wound-healing assay. Methods Mol Biol 2005;294:23-29.

[155] Lo CM, Keese CR, Giaever I. Monitoring motion of confluent cells in tissue culture. Exp Cell Res 1993;204(1):102-109.

[156] van der Meer AD, Vermeul K, Poot AA, Feijen J, Vermes I. A microfluidic wound-healing assay for quantifying endothelial cell migration. Am J Physiol Heart Circ Physiol 298(2):H719-725.

[157] Tamada M, Perez TD, Nelson WJ, Sheetz MP. Two distinct modes of myosin assembly and dynamics during epithelial wound closure. J Cell Biol 2007;176(1):27-33.

[158] Block ER, Matela AR, SundarRaj N, Iszkula ER, Klarlund JK. Wounding induces motility in sheets of corneal epithelial cells through loss of spatial constraints: role of heparin-binding epidermal growth factor-like growth factor signaling. J Biol Chem 2004;279(23):24307-24312.

[159] van Horssen R, Galjart N, Rens JA, Eggermont AM, ten Hagen TL. Differential effects of matrix and growth factors on endothelial and fibroblast motility: application of a modified cell migration assay. J Cell Biochem 2006;99(6):1536-1552.

[160] Poujade M, Grasland-Mongrain E, Hertzog A, Jouanneau J, Chavrier P, Ladoux B, et al. Collective migration of an epithelial monolayer in response to a model wound. Proc Natl Acad Sci U S A 2007;104(41):15988-15993.

[161] Martin P. Wound healing--aiming for perfect skin regeneration. Science 1997;276(5309):75-81.

[162] Giulian D, Chen J, Ingeman JE, George JK, Noponen M. The role of mononuclear phagocytes in wound healing after traumatic injury to adult mammalian brain. J Neurosci 1989;9(12):4416-4429.

[163] Kovalchin JT, Wang R, Wagh MS, Azoulay J, Sanders M, Chandawarkar RY. In vivo delivery of heat shock protein 70 accelerates wound healing by up-regulating macrophage-mediated phagocytosis. Wound Repair Regen 2006;14(2):129-137.

[164] Hopkinson-Woolley J, Hughes D, Gordon S, Martin P. Macrophage recruitment during limb development and wound healing in the embryonic and foetal mouse. J Cell Sci 1994;107 (Pt 5):1159-1167.

[165] Witte MB, Barbul A. General principles of wound healing. Surg Clin North Am 1997;77(3):509-528.

[166] Xia YN, Whitesides GM. Soft lithography. Angew Chem Int Edit 1998;37(5):551-575.

[167] Brock A, Chang E, Ho CC, LeDuc P, Jiang XY, Whitesides GM, et al. Geometric determinants of directional cell motility revealed using microcontact printing. Langmuir 2003;19(5):1611-1617.

[168] Kane RS, Takayama S, Ostuni E, Ingber DE, Whitesides GM. Patterning proteins and cells using soft lithography. Biomaterials 1999;20(23-24):2363-2376.

[169] Whitesides GM, Ostuni E, Takayama S, Jiang X, Ingber DE. Soft lithography in biology and biochemistry. Annu Rev Biomed Eng 2001;3:335-373.

[170] Keese CR, Wegener J, Walker SR, Giaever I. Electrical wound-healing assay for cells in vitro. Proc Natl Acad Sci U S A 2004;101(6):1554-1559.

[171] Swanson JA, Johnson MT, Beningo K, Post P, Mooseker M, Araki N. A contractile activity that closes phagosomes in macrophages. J Cell Sci 1999;112 (Pt 3):307-316.

[172] Tsai RK, Discher DE. Inhibition of "self" engulfment through deactivation of myosin-II at the phagocytic synapse between human cells. Journal of Cell Biology 2008;180(5):989-1003.

[173] Arora PD, Conti MA, Ravid S, Sacks DB, Kapus A, Adelstein RS, et al. Rap1 Activation in Collagen Phagocytosis Is Dependent on Nonmuscle Myosin II-A. Molecular Biology of the Cell 2008;19(12):5032-5046.

[174] Hebda PA. Stimulatory effects of transforming growth factor-beta and epidermal growth factor on epidermal cell outgrowth from porcine skin explant cultures. J Invest Dermatol 1988;91(5):440-445.

[175] Schor SL, Ellis IR, Harada K, Motegi K, Anderson AR, Chaplain MA, et al. A novel 'sandwich' assay for quantifying chemo-regulated cell migration within 3-dimensional matrices: wound healing cytokines exhibit distinct motogenic activities compared to the transmembrane assay. Cell Motil Cytoskeleton 2006;63(5):287-300.

[176] Coussens LM, Werb Z. Inflammation and cancer. Nature 2002;420(6917):860-867.

[177] Arnold M, Schwieder M, Blummel J, Cavalcanti-Adam EA, Lopez-Garcia M, Kessler H, et al. Cell interactions with hierarchically structured nano-patterned adhesive surfaces. Soft Matter 2009;5(1):72-77.

[178] Ma Z, He W, Yong T, Ramakrishna S. Grafting of gelatin on electrospun poly(caprolactone) nanofibers to improve endothelial cell spreading and proliferation and to control cell Orientation. Tissue Eng 2005;11(7-8):1149-1158.

[179] Miller T, Boettiger D. Control of intracellular signaling by modulation of fibronectin conformation at the cell-materials interface. Langmuir 2003;19(5):1723-1729.

[180] Michael KE, Vernekar VN, Keselowsky BG, Meredith JC, Latour RA, Garcia AJ. Adsorption-induced conformational changes in fibronectin due to interactions with well-defined surface chemistries. Langmuir 2003;19(19):8033-8040.

[181] Shen M, Horbett TA. The effects of surface chemistry and adsorbed proteins on monocyte/macrophage adhesion to chemically modified polystyrene surfaces. J Biomed Mater Res 2001;57(3):336-345.

[182] Xia N, May CJ, McArthur SL, Castner DG. Time-of-flight secondary ion mass spectrometry analysis of conformational changes in adsorbed protein films. Langmuir 2002;18(10):4090-4097.

[183] Wertz CF, Santore MM. Effect of surface hydrophobicity on adsorption and relaxation kinetics of albumin and fibrinogen: Single-species and competitive behavior. Langmuir 2001;17(10):3006-3016.

[184] Raghavachari M, Tsai HM, Kottke-Marchant K, Marchant RE. Surface dependent structures of von Willebrand factor observed by AFM under aqueous conditions. Colloid Surface B 2000;19(4):315-324.

[185] Buijs J, Norde W, Lichtenbelt JWT. Changes in the secondary structure of adsorbed IgG and F(ab')(2) studied by FTIR spectroscopy. Langmuir 1996;12(6):1605-1613.

[186] Chu BH, Lee J, Chang CY, Jiang P, Tseng Y, Pearton SJ, et al. The study of low temperature hydrothermal growth of ZnO nanorods on stents and its applications of cell adhesion and viability. Appl Surf Sci 2009;255(20):8309-8312.

BIOGRAPHICAL SKETCH

Jiyeon Lee was born in Sokcho City, Gangwon Province, South Korea, in 1981. She graduated from Chuncheon Girls' High School in Chuncheon City, Gangwon Province, South Korea, in 2000. In 2004, she received a Bachelor of Science in chemical engineering from Seoul National University with honors. She joined Dr. Hong H. Lee's research group in 2004 and studied nano-patterning, electronic materials and organic devices, specifically studying modification and application of electronic materials for two years. In 2006, she received a Master of Science in chemical and biological engineering from Seoul National University. She started her Ph.D course at the University of Florida in chemical Engineering in 2006 and joined Dr. Tanmay Lele's group in 2007. She obtained her Doctor of Philosophy in chemical engineering from University of Florida in 2010.